Administrative unit: **University of Padova**

Department: **Land, Environment, Agriculture and Forestry (LEAF)**

PhD Program: **Land, Environment, Resources and Health (LERH)**

Batch: XXXII

INTEGRATION OF CLIMATE-RELATED ENERGY SOURCES ACROSS AN ALPINE TRANSECT

Thesis financially supported by LPDP Indonesia Endowment Fund for Education

PhD Program Coordinator: Prof. Davide Matteo Pettenella

Supervisor: Prof. Marco Borga

Co-supervisor: Dr. Baptiste Francois
(University of Massachusetts Amherst, Civil & Environmental Engineering, Amherst, MA, United States)

PhD candidate: Handriyanti Diah Puspitarini

Università degli Studi di Padova

Sede Amministrativa: Università degli Studi di Padova

Dipartimento Territorio e Sistemi Agro-Forestali (TESAF)

CORSO DI DOTTORATO DI RICERCA: **Land, Environment, Resources, Health (LERH)**

Ciclo: XXXII

INTEGRAZIONE DELLE FONTI ENERGETICHE DI ORIGINE CLIMATICA: ANALISI SU UN TRANSETTO ALPINO

Tesi redatta con il contributo finanziario di LPDP Indonesia Endowment Fund for Education

Coordinatore: Prof. Davide Matteo Pettenella

Supervisore: Prof. Marco Borga

Co-Supervisore: Dr. Baptiste Francois
(University of Massachusetts Amherst, Civil & Environmental Engineering, Amherst, MA, United States)

Dottorando: Handriyanti Diah Puspitarini

Table of Contents

List of Figures

List of Tables

Acknowledgements

My PhD journey was an interesting part of my life. The subject that I chose, which is renewable energy, is something that I wanted to learn since I started my MSc 6 years ago. In the last three years, I acquired new knowledge and at the same time I struggled a lot during the learning process. During this journey, I found lots of people supporting and helping me throughout the various stages of the PhD. Therefore, in these few lines I would like to thank all of them for their great support they gave me.

First of all, I would like to express my grateful to my supervisor, Marco Borga, who taught me how to be a researcher who can produce good results and write properly, and who reminded me to stay focused on my work. I started my journey with a small knowledge about renewable energy and hydrological modelling, but I learnt more and more on these topics under Borga's guidance. He also gave me many chances to join several conferences and collaborations that increased my knowledge and network. All the comments from him were the most meaningful comments assisting me during these years. I also feel thankful to my co-supervisor, Baptiste François who taught me how to write an efficient code that can run faster, how to write a scientific paper in a nice way, and many other things. I also thank him for his supervision during my visit at University of Massachusetts (Amherst, USA). The 4 months I spent there were very fruitful for networking, discussing the results of my data analyses and paper writing, and meeting new people.

I am deeply grateful to Davide Zoccatelli and Mattia Zaramella. Davide taught me how to perform analyses using ICHYMOD, MySQL and ArcGIS. Mattia taught me some hacks to increase the analyses performance in Matlab and Heidi. I consider them as my brothers in Italy.

I cannot miss to thank my close friends in Padova, Echo, Ylenia, and Eros, who reminded me to have a break and be happy, so I could keep a fresh and good motivation during my PhD. Many thanks also go to my psychologist in Padova, Francesca, who was angry when I did not go to my therapy session and kept telling me that I have an amazing life.

A great pleasure for me to meet gorgeous colleagues in Laboratorio IDEA and colleagues of PhD 32nd cycle. The coffee and lunch time with them were the precious moment every day to talk about lame yet funny things. I will definitely miss their high-fives too. Thank you very much Martino, Massimo, Giulia Roder, Giulia Zuecco, Roberta, Francesco, Loris, Tommaso, Luca, Daniele, Anam, and others. My Indonesian friends, Berto, Iqbal, Janet, Jo, Eko, Alfa, Elissa, and Fira were also people who supported me to finish this PhD and pursue a happy life. Our moments helped me reducing my homesick feeling. My roommates and my hangout friends in Padova (Nicola, Laura, Linda, Alice, Debora, Federica, and Dorin) also kept my high motivation in these years.

My greatest thanks to my Umik, Abi, and Ocid. Thank you very much for keeping your pray for me and your advice to keep remembering my life goals. Although I am a bad daughter sometimes, you always keep mentioning my name during your pray. Thank you to Ocid who sent me funny videos whenever I told him that I was stressful with all the works. My big thanks to Marco Parcianello for always being next to me. He is the one who told me to focus on my issues one-by-one, so I could solve them nicely, who kept telling me to remember Allah S.W.T and pushing me to meet Francesca, and many more that I cannot write in here. My three years spent far away from home would not finish nicely without their prays and reminders.

This research could not be done without any help from Indonesia Endowment Fund for Education that provided me a full scholarship named LPDP Scholarship. The fast and efficient responses from their staff to my questions was also remarkable.

I also would like to thank the external reviewers, Marco Baratieri and David Moser, who gave some suggestions to improve my thesis manuscript.

Beyond everything, I must acknowledge the strength given by the Almighty Allah S.W.T. He had given me a great opportunity to take this PhD in “Land, Environment, Resources and Health” at the University of Padova and meet nice people in Padova. Without His blessings, this achievement would have not been possible.

Summary

The key challenge to satisfy electricity demand using a high share VREs is to deal with the variability of their weather variables, such as solar radiation for solar power, precipitation for hydropower, and wind velocity for wind power. The low production of VREs may lead to the imbalance between demand and supply, and shortfall risk. Accounting for climatic variability in this concern is highly important, because the shortfall risk may be enhanced by climatic change and variability, but also because climatic variability in the district area can make more robust the complementarity between VREs.

This thesis aims to identify the climatic control on the structure of the complementarity between different VREs, analyzing the balance between energy demand and energy generation along a geographical transect across the Italian Alps. A transect from mountainous area in the Alps to plain area in Veneto region, where runoff generation is snow-controlled in the North and rain-controlled in the lower portions, is used as a study area for analyzing the impact of climate change and variability on VREs complementarity. This transect is also a good example for small communities that depend on the production of Run-of-River (RoR) hydropower and solar Photovoltaic (PV) for matching their electricity demand. In addition, this study area has high potential of Combined Heat and Power (CHP) fueled by biomass. In this study we examine PV, RoR, and CHP energy sources.

Our results show that glacier shrinkage affects the increase of spring runoff and thus decrease the hydropower production because of the increase of inactive rate of power plant. The changes in hydropower production cause the changes in future demand satisfaction. Disregarding glacier shrinkage leads to an underestimation of future RoR generation and demand satisfaction from the combination of RoR and PV. We also highlight the ability of CHP to increase demand satisfaction and change the complementarity of PV and RoR, especially in the areas with snow-controlled runoff regime. The optimization of VRE production is not only for increasing the demand satisfaction, but also for reducing the energy drought events. We find that increasing the PV percentage in the PV-RoR energy mix leads to decrease the mean values of energy drought

duration and severity and to increase the mean values of energy drought peak. Climate change may therefore be viewed as both a risk and an opportunity for power system performance, depending on one's estimation of damage and ability to adjust operations and complementarity in relation to shortfall duration and magnitude.

Chapter 1

Introduction

The Intergovernmental Panel on Climate Change (IPCC, 2018) has reported that human-induced global warming has already reached 1°C above preindustrial levels and is increasing at approximately 0.2°C per decade. Without stepping up international climate action, the global average temperature increase could reach 2°C soon after 2060 and continue rising afterward. Such unconstrained climate change has the potential to make large-scale irreversible climate impacts more likely.

The European Union (EU), who responsible for 16% of global greenhouse gas (GHG) emissions from fuel combustion (IEA, 2018a), is a global leader in the transition towards a net-zero-GHG emissions economy (IEA, 2018b). EU has set its objective to reduce emissions by 80-95% below 1990 in 2050 and has launched its strategy to improve the EU's energy efficiency by at least 32.5% and to increase renewable energy to at least 32% of the EU's final energy consumption by 2030 (European Commission, 2018). This clean energy transition would result in an energy system where primary energy supply would largely come from renewable energy sources. Variable energy sources (called VRE hereafter), such as solar photovoltaic power (PV hereafter), hydropower from small plants and run-of-river (called RoR hereafter), and wind power, play a key role in this strategy (IEA, 2018c).

Driving the decarbonization of the European electricity system is a complex process. On the one hand, this process is embedded in demographic growth, multi-level legislations, market rules, economic and technological constraints, private initiatives and public interests (Biesbroek et al., 2010; Lin and Ouyang, 2014; Urry, 2015; Aguiar et al., 2018). On the other hand, it must also consider the multiscale climate and environmental variability governing VRE resources. The easiness of VRE integration in the energy mix potentially conflicts with regard to land and water use as well as environmental regulation (Rasul and Sharma, 2016; Scott, 2011; Scott et al., 2011). From a European policy perspective, how to fully supply the demand using renewable energies

is critical questions. Answers to these questions need to be guided by a robust knowledge that informs where and how climate-related energy is available in regard to supply energy demand.

The VRE availability depends on several climatic variables, including solar radiation, wind velocity, air temperature, precipitation and river runoff (Gaudard et al., 2018; Kahl et al., 2019; Nawri et al., 2014; Troccoli et al., 2014). These variables fluctuate in space and time, exhibit correlations and, in turn, control the intermittency of VRE sources (Engeland et al., 2017). The combined variability of VRE production and demand leads to periods of so-called positive "residual load", when VRE production does not meet the demand, and other periods of negative residual load with VRE surplus generation. Therefore, the space-time variability of CRE production challenges one of the primary goals of electric utilities, which is to balance supply and demand. The terms stability (or sometimes regulation), balancing (or sometimes load following) and adequacy designate the supply-demand balance over, respectively, high (less than seconds), medium (minutes to days) and low (month to years) frequency, which characterize the "flexibility" of electricity systems (IEA, 2011) and also evolves with consumption patterns under the influence of market mechanisms and smart grids (e.g. Blaabjerg and Guerrero, 2011; Palensky and Kupzog, 2013; Siano, 2014). The adequacy of VRE production depends, among others, on long term climate variations and hence on climate change.

Balancing at time scales from minutes to days responds to meteorological processes ranging from meso- to synoptic-scale, including diurnal and orographic local circulations as well as larger scale perturbations as described by Orlanski (1975). Connecting VRE production utilities to transport grids smooths such medium frequency variations, as long as their space-time co-variability is weak enough over the connected domain (e.g. Heide et al., 2010). Wind and solar energy production may experience large and sudden variations called "ramps" linked, respectively, to wind turbulence and cloud circulation (Engeland et al., 2017; Ferreira et al., 2010; Renné, 2014). Demand response programs, schedulable power production and energy storage are used to level out the residual load that is not smoothed by grid transport (Albadi and El-Saadany, 2008; Barton and Infield, 2004; Wood et al., 1984). Among the schedulable power means for balancing residual load, reservoir-type hydropower is the most commonly used (Huertas-Hernando et al., 2017). Biomass can also provide an important back up resource.

Biomass is a renewable carbon source and can be used for provision of a wide range of bioenergy carriers and substitute fossil fuels in the power sector. Additionally, biomass and the produced bioenergy carriers are storable and can provide energy on demand in principle. This quality is especially relevant in energy systems with high shares of fluctuating renewables like wind and solar power (Blaschke et al., 2013). The dimension of the challenge related to the contrasting variability of VREs availability and of the demand is described by *Figure 1.1* for the European case. The figure, based on data from François et al. (2016b), compares at the daily time step the variability of the electricity demand (X-axis) to the variability of the potential production (Y-axis) of wind (green), solar (yellow) and river (blue) energy in 12 regions – 200 km side square spread over Europe. Renewable production appears to vary broadly 4 times more than consumption. The figure show that dispersion between regions and sources is substantial (circles), and wind power has the largest fluctuations in every region. At continental scale (squares), the variability of wind and hydro are smaller than solar power. Merging wind and solar energies (crosses) also significantly smooth the variability. As shown by several past studies over Europe (Heide et al., 2011, 2010), this is due to the seasonal characteristics of wind and solar power patterns, which are remarkably anti-correlated.

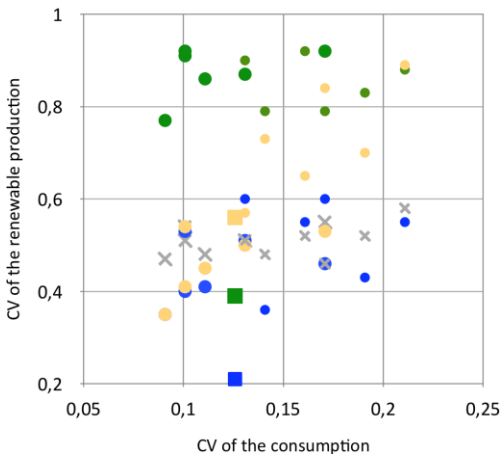

Figure 1.1 Comparison of variability of demand and VREs for different energy sources and different regions in Europe. Green symbols are for wind power, yellow is solar power, and blue is hydropower. Circles represent the values of each region. The northern regions (Finland, Norway, Belarus, England, Germany, and France) have smaller circle size than the southern regions (Italy, Romania, Greece, Galicia, Andalucía, and Tunisia). Squares represent the averaged values over Europe. Crosses are the CV values obtained from the combination of wind and solar power.

Figure 1.1 shows the benefit of mixing together different sources of VREs. The potential of a mixing of these renewable energies to cover the temporal variability of the energy load is termed complementarity (e.g., François et al., 2016a) in this work. Complementarity depends primarily on the co-variability between renewable energy sources, for two main reasons. Energy sources must vary within the same order of magnitude to be efficiently combined and satisfy the energy load (e.g., François et al., 2016b). Moreover, complementarity depends also on the correlation between the renewable energies themselves and increases by decreasing their temporal correlation, because only in this case the mixing may significantly smooth their temporal variability.

In a power system, hydropower is a useful complement to wind and solar power because of its flexibility (Huertas-Hernando et al., 2017). Rivers integrate the weather variability through their basin and branching structure. Natural river flows are less variable and more predictable than their meteorological drivers – precipitation and temperature essentially. With its ability to produce and store energy, hydropower holds a specific status in the context of energy transition and renewable energy targets. Indeed, large hydropower storage is used for balancing production and load mismatches. In this sense, the term of 'blue battery' is used when referring to the huge energy storage capacity provided by Scandinavian or Alpine reservoirs (Piria and Junge, 2013) . Less attention is paid to small RoR power, even if the amount of energy produced is important in several places. In Italy for instance, small RoR plants (i.e. with a power capacity lower than 3 MW) provide 22% of the annual hydropower energy which reached 45,823 GWh in 2011, i.e. about 24% of the electricity consumption (GSE, 2011). However, the scientific literature dealing with the use of RoR in complementarity with solar- and/or wind-power is still limited, despite the fact that they share common driving meteorological and climatological phenomena, and they are supposed to be the three masterpieces of a 100% renewable energy scenario. Nevertheless, based on 33 years of daily data (1980-2012) for a set of 12 European regions, François et al. (2016b) provides estimates of the optimal mix when wild RoR energy is included in the solar/wind mix. This is found to be highly region-dependent but the highest shares are

often obtained for RoR, ranging from 35% to 65%. For all regions, including RoR in the mix allows increasing the penetration rate of VREs.

1.1 Research gaps and research questions

Given the background reported above, different research gaps were identified, and research questions were formulated accordingly. The complementarity among the various VREs in a given region strongly depends on the climatic setting of the region, and therefore it is likely to be modified with climatic change. Several investigations assessed future hydropower (e.g., Schaefli, 2015), solar power (e.g., Jerez et al., 2015) and wind power generations (e.g., Tobin et al., 2016) under climate change. However, to our knowledge, limited knowledge is available on the effects of climate change on the combination between hydropower and other renewable energy sources. François et al. (2016b) investigated the effect of rising temperatures on complementarity between solar power and RoR power generation in several catchments in the Italian Alps. They found that these energy sources fluctuate more than the load at all temporal scales, and that the correlation between solar and hydropower generation increases with increasing the ratio of solid to liquid annual mean precipitation. Higher temperature is likely to change this ratio and, consequently, change the hydrological regime and the complementarity between these two energy sources. However, the effects of glacier shrinkage on VREs complementarity has been not assessed so far, at the best of our knowledge. This effect may be important in mountainous areas where ice melt drives the seasonal changes of runoff and RoR is an important energy source.

Combined Heat and Power systems (CHP) produce heat and electricity simultaneously. Their resulting high efficiency makes them more attractive from the energy managers' perspective than other conventional thermal systems. Although heat is a by-product of the electricity generation process, system operators usually operate CHP systems to satisfy heat demand. Electricity generation from CHP is thus driven by the heat demand, which follows the variability of seasonal temperature, and thus is not always correlated with the fluctuation of electricity demand. Several studies investigated the potential of CHP plants to serve as back-up electricity generation for the VRE sources. For example, Söder et al. (2018) reviewed the power

production within the Nordic electricity market. They highlight that in 2015 Denmark supplied 70% of its electricity demand by using a combination of wind power and CHP generation, the remaining being covered by buying from the Nordic electricity market, mainly from Norway and Sweden. Romero Rodríguez et al. (2016) shown in various climate areas in Spain that a combination of electricity generation from PV panels and CHP is a tangible solution for reducing the emission of GHG. However, to the best of our knowledge no studies are available which explicitly investigate the role of climatic variability on the integration of CHP in combination with other VRE sources at the district level.

Statistical characterization of the periods, ranging in duration from minutes to days, when the electrical energy availability from VREs is lower than energy demand has been attempted in a number of studies with focus on specific sources of VRE. This is the case of wind, with a large number of studies focused on the characterization of these conditions in terms of occurrence, durations and severity from local to continental (Fisher et al., 2013; Handschy et al., 2017; Leahy and McKeogh, 2013) . Similar investigations have been also focused on solar energy (Köhler et al., 2017; Pelland et al., 2013; Rieger et al., 2017) . These efforts brought to the concept of energy drought, i.e. a period with an uninterrupted energy production/demand mismatch (Raynaud et al., 2018). However, no studies are available which explore how the characteristics of energy droughts also depend on the climatic spatial variability at fine temporal resolution (hourly, for instance).

The abovementioned research gaps lead to the identification of the following main research objective of this work, i.e.

to identify the climatic control on the structure of the complementarity between different VREs, analyzing the balance between energy demand and energy generation along a geographical transect across the Italian Alps.

The research will thus investigate the complementarity along a climate transect going from the Alpine crest to the Veneto plain, with a focus on relatively small, rural communities (Figure 1.2). This transect provides a range of climatic, environmental and ecological variability and it is of interest from four main viewpoints. First, it includes runoff regimes that gradually

move from snow-melt dominated to rainfall dominated, with a ratio of solid to liquid precipitation decreasing from 0.6 in the northern part to almost 0 in the Veneto plain. François et al. (2014) highlighted that this ratio controls the monthly correlation between RoR and solar power generation within this area, and thus the complementarity between those VREs. This climatic gradient is obviously linked to the elevation above sea level, but it also illustrates expected climate change effects like a temperature rise in the region. Second, this region is characterized by a relatively high level of small RoR hydropower stations related to the initiatives of private actors or small communities. Third, the rate of PV equipment is rather high thanks both to public subsidies and easiness of installation (GSE, 2018). Fourth, the transect includes also a range of institutional and normative settings. This ranges from the adoption of the KLIMALAND energy policy in the Alto Adige region (Moser et al., 2014) to the high penetration of biomass energy and PV in the Veneto region (GSE, 2018).

The main research question is approached by means of three specific objectives:

i) To assess the impacts of glacier shrinkage and climate change to the modification of RoR production in glacierized basins and its complementarity with PV production,
ii) To analyze the benefit of combining electricity generation from biomasses through CHP plants, with electricity generation from RoR and PV production, in different climatic conditions along the climatic transect, and
iii) To evaluate the main statistical characteristics of energy droughts from the combination of PV and RoR, by considering different climatic conditions along the climatic transect.

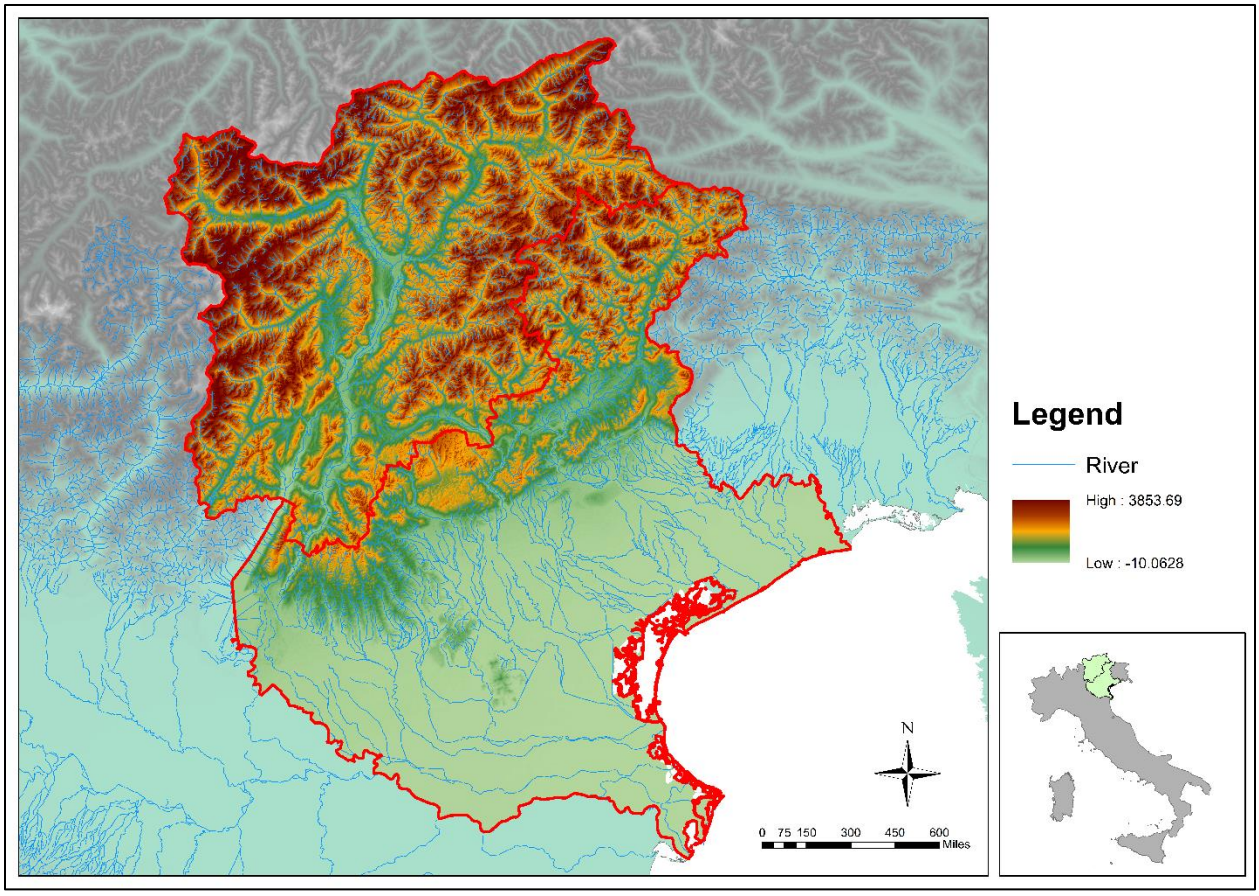

Figure 1.2 The geographical transect chosen as a study area

VREs considered in this thesis include PV, RoR, and biomass CHP. Wind power is not considered, given the limited potential for this energy source in the area covered by the transect due to topographic conditions (Monforti et al., 2014).

The work is based on two main assumptions. We consider that the communities considered in the transect are “autonomous”, i.e. that there are no energy exchanges with the neighboring regions. We further consider that all the regional production comes from the studied VREs, and that the long-term mean regional VRE production equals the mean regional electricity demand. This configuration corresponds to the so-called 100% renewable scenario considered in a number of recent works (e.g. (François et al., 2016b; Raynaud et al., 2018; von Bremen, 2010). We also assume that there is no energy transmission limitation within the region and there are no energy losses when energy is being distributed in the area (e.g. Bett and Thornton, 2016;

François et al., 2018; Raynaud et al., 2018; Ueckerdt et al., 2017). Analyses done in this thesis estimate the potential use of high share renewables in electricity supply sector, and do not apply the further analysis in energy coupling, such as electricity for heating – cooling, and mobility sectors.

The analyses for addressing the specific objectives are carried out at hourly time resolution. Hydrological modelling is carried out by the Integrated Catchment Hydrological Model (ICHYMOD, Norbiato et al., 2009), which is a conceptual and semi-distributed rainfall-runoff model that simulates potential evapotranspiration, soil moisture, and snow and ice accumulation and melt (Zaramella et al., 2018). RoR generation is simulated based on ICHYMOD by taking into account typical environmental and operational constraints (Hänggi and Weingartner, 2012). PV model is simulated based on the global horizontal irradiance and temperature (Perpiñan et al., 2007). PV generation model in this thesis does not consider the azimuth and tilt angle definition of the solar cells because we focus more to the impact of sub-daily fluctuation of solar irradiance and temperature to PV system performance. We also do not consider the future seasonal changes in solar radiation for modelling solar PV generation. There is no solar radiation data for basins located in our transect. We thus use the reanalysis data from EXPRESS-Hydro database, which is available at hourly scale and 0.037 degree of spatial resolution (4 km) (Silvestro et al., 2018). In addition, there is no available electricity demand data in study area of this thesis. National electricity demand from European Network of Transmission System Operators for Electricity (ENTSO-E, https://www.entsoe.eu/) is then used and downscaled to hourly time step based on GDP and temperature data of the transect. This approach is described by François et al. (2016a).

Three research papers, illustrated in the following chapters, have been produced to address the specific research objectives. The methodology and the results concerning the first specific objective are presented in Chapter 2, which is originally from the article titled “The impact of glacier shrinkage on energy production from solar-hydropower complementarity in alpine river basins”. This article has been submitted and still under review in Journal of Science of Total Environment. The analyses concerning the integration of CHP with PV and RoR sources, which represents the second specific objective, are presented in Chapter 3. This Chapter is from

the article titled “Complementarity between Combined Heat and Power systems, solar PV and hydropower at a district level: application to the North Eastern Alps”, which is ready to be submitted to Energies. The third specific objective is analyzed in Chapter 4, which is from article “Statistical analysis of energy supply droughts from renewable energy sources across an Alpine transect”. This article is still in the process of authors review. Main conclusions and suggestions for further research are reported in Chapter 5. Appendix A provides the details of ICHYMOD. Appendix B provides the results obtained in Chapter 2 for the basin of Plima.

Chapter 2

The impact of glacier shrinkage on energy production from hydropower-solar complementarity in alpine river basins[1]

[1]This chapter is based on a paper that has been submitted as: **Puspitarini, H.D.**, François, B. Zaramella, M., Brown, C., Borga, M. 2019. The impact of glacier shrinkage on energy production from hydropower-solar complementarity in alpine river basins. Science of Total Environment. Manuscript submitted for publication. Conditionally accepted

2.1 Introduction

Hydropower plays a key role in our electricity systems. Although hydropower contribution to total global electricity supply remains below 20% (IEA, 2018), its inherent flexibility is often critical for the electricity grid (e.g., Engeland et al., 2017; François et al., 2017a; Huertas-Hernando et al., 2017). Run-of-the River (RoR) power plants with small poundage play an important role in this regard (e.g., Jurasz and Ciapała, 2017). The current temperature rises and changes in precipitation patterns and variability due to climate change are expected to modify the spatial and temporal distribution of streamflow (IPCC, 2014a), and subsequently hydropower generation. In mountainous areas, specifically, the rise in temperature alters both snow (e.g., Gobiet et al., 2014) and ice (e.g., Pellicciotti et al., 2014) accumulation and melt processes, which may lead to further changes of hydropower generation mean and seasonality (e.g., Gaudard, et al., 2018). While the effects of altered snowpack on hydropower seasonality is well characterized (e.g., Schaefli, et al., 2007; Vicuna et al., 2008; François, et al., 2014a), recent literature shed light on the potential effects of glacier shrinkage on hydropower generation (e.g., Finger et al., 2012; Gaudard, et al., 2018; Schaefli et al., 2019). The literature mainly agrees on: i) an increased variability in hydropower generation for the next decades (higher temperatures enhancing ice melt and subsequently runoff, especially during spring), and ii) a decrease in hydropower generation toward the end of the century (i.e., once glacier volume has been significantly shrunk). Maran, et al. (2014) also noticed that glacier shrinkage would increase the percentage of days when streamflow conditions do not allow power generation (i.e., flows are either too low or too high).

In mountainous areas, the growing competition between water demand for electricity and for other uses (e.g., ecological services, irrigation), together with an increased concern about greenhouse gas emissions, promote more diversity in the electricity mix. This is currently achieved by combining hydropower with other renewable energy sources such as wind and solar (François, et al., 2014b; Kougias et al., 2016; Huertas-Hernando et al., 2017, Ming et al., 2018). The potential of a mixing of these renewable energies to cover the temporal variability of the energy load is termed complementarity (e.g., François et al., 2016a). Complementarity depends primarily on the co-variability between renewable energy sources as generation must vary within

the same order of magnitude to be efficiently combined and satisfy the energy load, which is well-known to vary much less than any renewable energy source taken alone (e.g., François et al., 2016b). Complementarity depends also on the correlation between the renewable energies themselves and increases by decreasing the correlation. Climate change is expected to modify the distribution of weather variables that drive hydro, wind and solar power generations, and as such, it may impact on the complementarity of the energy sources.

Several analysis frameworks are available for the assessment of future hydropower (e.g., Schaefli, 2015), solar power (e.g., Jerez et al., 2015) and wind power generations (e.g., Tobin et al., 2016) under climate change. However, to our knowledge, only few studies examined the effects of climate change on the combination between hydropower and other renewable energy sources. François et al. (2014b; 2016a) investigated the complementarity between solar power and Run-of-the River power generation in several catchments in the Italian Alps. They found that these energy sources fluctuate more than the load at all temporal scales, and that the correlation between solar and hydropower generation increases with increasing the ratio of solid to liquid annual mean precipitation. Higher temperature is likely to change this ratio and, consequently, change the hydrological regime and the complementarity between these two energy sources. François et al. (2018) explicitly analyzed the effects of climate change on the complementarity between solar and RoR power generation in Northern Italy. They showed that complementarity is likely to increase, leading to higher satisfaction of the electricity consumption in this region. However, to our knowledge, the impact of changes in glacier area and volume on the complementarity of energy sources has not been considered so far, although glacier melt contribution can be significant for glacierized catchments, especially during summer when precipitation is often low (Pellicciotti et al., 2014).

The objective of this study is to investigate to what extent glacier alteration due to climate change modifies the energy production from RoR hydropower plants in glacierized basins and eventually its complementarity with solar power. Two catchments located in the upper Adige River basin (Eastern Italian Alps) are considered for the study. By considering nested sub-catchments, we investigate the basin scale control on the contribution of ice melt to total runoff. In this study we extend the Decision Scaling approach (Brown et al., 2012) by considering climate

change effects not only in the weather conditions but also in the extension of the glacier coverage. Decision Scaling uses a sensitivity analysis, termed as 'climate stress test', to reveal vulnerabilities and/or opportunities for the considered system regarding several set of plausible future states. In this study, the sensitivity analyses are obtained by applying multiple time series of precipitation and temperature that are obtained by perturbing the observed weather time series following the change factor method and by using various fixed glacier coverage, which are considered to represent the possible future states of the glaciers. Projections from Regional Climate Models (RCMs) are used to infer the likelihood of the future climate states and subsequently changes in complementarity.

The article is organized as follow. Section 2 presents the study area and the considered database. Section 3 presents the modeling framework, which includes the modeling of solar and RoR power generation, the modeling of the electricity demand and the combination of solar and RoR hydropower. It also presents the use of climate change scenarios within the Decision Scaling approach. Section 4 gives an outlook of the electricity balance under current climate conditions and Section 5 discusses the impact of climate and glacier change on the complementarity between solar and RoR hydropower. Section 5 concludes and gives insights for future research work.

2.2 Study area and data

The study area is located in the upper Adige river basin (Figure 2.1) (Adige at Ponte Adige), where we focus on two high elevation catchments: the Plima (160.7 km^2) and the Saldura (99.8 km^2) river basins. The basins range in altitude from 654 m asl to 3,719 m asl (Plima) and from 894 m asl to 3,725 m asl (Saldura). Glaciers cover 12.4 km^2 (7.7% of the basin area) and 4.08 km^2 (4.4% of the basin area) for the Plima and the Saldura, respectively (Knoll and Kerschner, 2009). Plima river flows are regulated by a hydropower reservoir (Gioveretto Lake) with a direct drainage area of 77.1 km^2. Over the Plima river basin, mean annual precipitation (computed based on data available for the period 1956-2017) increases from 810 mm at the basin outlet to around 1,400 mm at 2,000 m asl. The spatially averaged mean annual precipitation is around 1,290 mm. The Saldura river basin is located in a drier portion of the main Adige river basin, and mean annual precipitation increases from 480 mm at the basin outlet to around 1,000 mm at

2,000 m asl. The spatially averaged mean annual precipitation amounts to 690 mm. Mean annual air temperature at the mean basin altitude amounts to 2.2° and to 2.0° for Plima and Saldura, respectively. Precipitation in the upper Adige river basin is mainly concentrated during the summer and autumn seasons (e.g. Norbiato et al., 2009; Laiti et al., 2018). In both basins, the hydrological regime is ice melt and snowmelt dominated with high flows during spring and low flows during winter. Summer flows are mainly supported by glacier melt.

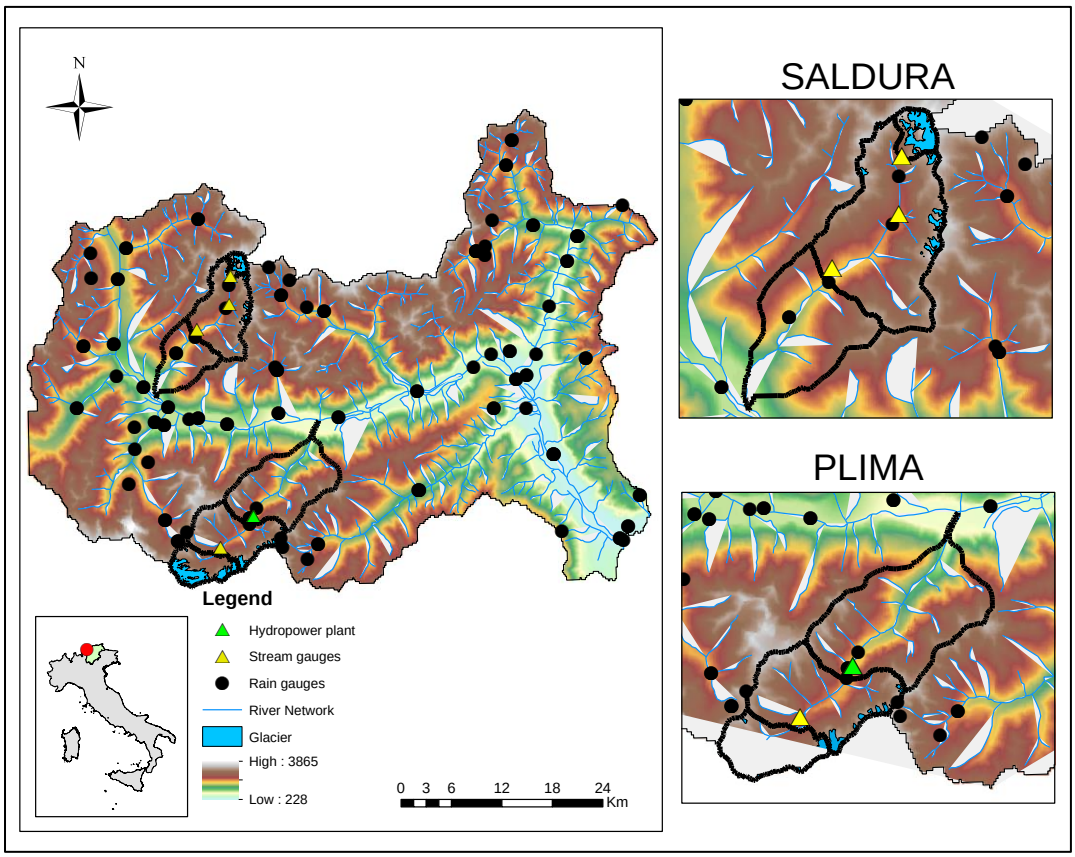

Figure 2.1 Map of Adige river basin at Ponte Adige, with the locations of the Plima and Saldura river basins and the hydro-meteorological monitoring network.

The analyses presented here are based on the availability of hourly precipitation and temperature data from 52 weather stations that are available from the regional Hydrological Office at hourly time step (Figure 2.1) for the Adige at Ponte Adige (2,719 km^2), with a density of one station per 52 km^2. Flow measurements over the Plima river basin are available from the stream gauge station, with a drainage area of 25.7 km^2, where data are available over the 2014-

2016 years and, in an indirect way, from the elaboration of the hydropower station data of Lago Gioveretto from 2004 to 2016. Saldura river flow data are available at three stream gauge stations, with drainage area ranging from 5.4 to 61.9 km^2, where data are available from 2009 to 2018.

Solar radiation data are obtained from the high resolution EXPRESS-Hydro reanalysis database, which is available at hourly temporal resolution and 0.037 deg of spatial resolution (4 km) from 1992 to 2008 (Silvestro et al., 2018). Comparison between local solar radiation data with reanalysis data have shown good results, with NSE (Nash and Sutcliffe, 1970) and R^2 values all above 0.7, which confirms the high quality of the reanalysis data.

To investigate the basin scale dependence of glaciers melt to total runoff, we considered two nested catchments within Plima and Saldura river basins. The larger catchment is further noted as Lower Basin, whereas the nested sub-catchments are denoted as Intermediate and Upper Basins. For both Plima and Saldura discharge data are available for the Intermediate and Upper basins for hydrological model calibration and validation. More details are given in Table 2.1.

	Saldura			Plima		
	Lower	Intermediate	Upper	Lower	Intermediate	Upper
Elevation range (m asl)	894 – 3,725	1,637 – 3,725	2,513 – 3,725	654 – 3,719	1,773 – 3,719	2,295 – 3,719
Surface (km^2)	99.8	61.9	5.4	160.7	77.1	25.7
Glacier coverage (%)	4.09%	6.59%	75.70%	7.72%	16.08%	48.29%

Table 2.1 The Plima and Saldura nested basins

Analysis of climate change impact is based on use of an ensemble of 13 Regional Climate Models whose boundary conditions are driven by 7 Global Circulations Models (Table 2.2) from the EU FP6 Integrated Project ENSEMBLES (van der Linden and Mitchell, 2009), as described in Gobiet et al. (2014). In total, we used 17 combinations of Global and Regional Climate Model (GCM/RCM) covering the entire 21st century, which are based on A1B emission scenario

estimating rapid economic growth, population reduction after mid-century, and more adaptation to the new efficient technology using fossil fuel and non-fossil fuel sources evenly. An empirical-statistical downscaling and error-correction method (Quantile Mapping) as described in Themeßl, et al. (2011; 2012) is applied to improve the skill of the RCMs in representing local climate at station scale. The simulations of temperature and precipitation obtained in this way are available at daily time step from 1951 to 2100. The projections are used to infer plausible changes in temperature and precipitation for two 30-year future time periods (2040-2069 and 2070-2099, the current period being 2000 – 2011).

No	Driving GCM	RCM Regional Climate Models
1	HadCM3Q16	RCA3
2	ARPEGE	ALADIN
3	ARPEGE	HIRHAM5
4	ECHAM5	HIRHAM5
5	BCM	HIRHAM5
6	HadCM3Q0	CLM
7	ECHAM5	REGCM3
8	ECHAM5	RACMO
9	HadCM3Q0	HadRM3Q0
10	HadCM3Q3	HadRM3Q3
11	HadCM3Q16	HadRM3Q16
12	ECHAM5	REMO
13	HadCM3	RECLIP
14	BCM	RCA
15	ECHAM5	RCA
16	HadCM3Q3	RCA
17	ECHAM5	CCLM

Table 2.2 List of climate projections ensemble

2.3 Methodology

Results from François et al. (2017b; 2016a) clearly show the importance of sub-daily temporal variability in weather variables for the energy complementary analysis. Reproducing sub-daily weather variability for a set of correlated variables (radiation, precipitation, temperature) under climate change conditions in a mountainous, data scarce region faces huge uncertainties. We approach this problem by using the Decision Scaling framework (Brown et al., 2012). For a climate-sensitive system, the Decision Scaling framework merges a bottom-up evaluation of the vulnerability of the system to changes in key climate drivers, with the available

climate projections. The climate projections are used ex-post to infer the likelihood of the future states of the climate drivers that could eventually lead to significant change in performance or vulnerability. Figure 2.2 provides a schematic representation of the methodology.

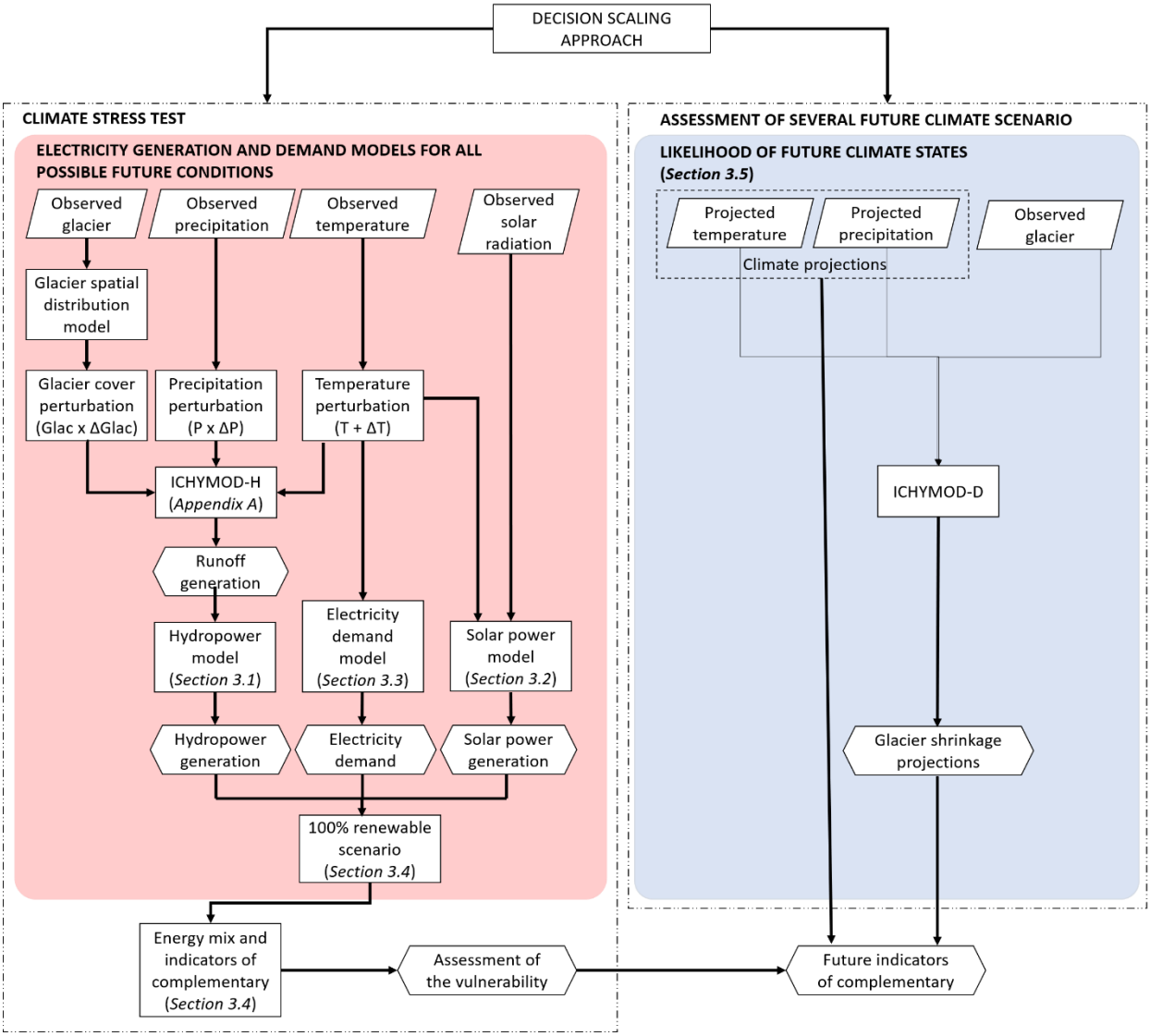

Figure 2.2 The framework of climate change and glacier shrinkage analysis using Decision Scaling approach in this article. Parallelograms are the inputs, squares are the models and calculations, and hexagons are the outputs of the models.

The first step of Decision Scaling is denoted as 'climate stress test' (left side on Figure 2.2). It assesses the sensitivity (or vulnerability) of the considered system by exploring many scenarios of future climate in climate drivers. The range of scenarios goes beyond the values listed in the

projections in order to account for the known underestimation of the future climate uncertainty by climate models (Stainforth et al., 2007). The identified drivers of the complementarity between solar PV and RoR hydropower are temperature and precipitation based on François *et al.* (2018). In addition to these two variables, we also consider the modifications of the glacier coverage on the head basins, which is the novelty of this study. We have also disregarded the impact of climate change on solar radiation.

Changes in temperature and precipitation are obtained by perturbing historical time series by mean of the change factor method (François et al., 2018). Changes in glacier coverage, representing the possible future states of the glaciers, are obtained by considering fixed glacier states. These states range from the coverage as observed in the most recent glacier regional inventory (100% coverage), to the state where the entire glacier has disappeared (0% of coverage). The glacier states are obtained by running the glacio-hydrological model called Integrated Catchment Hydrological Model (ICHYMOD-D) (described in Appendix A) at daily time resolution as fed with climate change projections.

The perturbed time series of precipitation and temperature and the glacier states represent the input data and boundary conditions for the glacio-hydrological model ICHYMOD-H (Appendix A), which is run at hourly time resolution for runoff simulation over the study basins. The resulting simulated streamflow time series are subsequently used to model hydropower generation from a hypothetic run-of-the river power plant located at the outlet of the considered basins. Note that changes in temperature also affect solar PV generation and electricity consumptions.

The complementarity between solar PV and RoR power generation is assessed at the scale for each considered basin by using three indicators. They are: i) the Pearson's correlation coefficient obtained between solar PV and RoR generation time series, ii) the standard deviation of the energy balance (i.e., generation minus demand) and iii) the percentage of demand satisfaction (hereafter denoted as penetration rate). This metric is computed by using the well-known '100 % renewable' scenario. In the context of this study, the 100% renewable scenario translates into a hypothetic configuration where power generation from solar PV and RoR hydropower equals the electricity demand on average over the considered period. This scenario

is commonly used for assessing the complementarity among several energy sources (e.g. François et al., 2018; Heide et al., 2010; Raynaud et al., 2018; von Bremen, 2010). We also assume no power transmission limitation or loss within the studied region. This configuration ensures the overall energy balance is null (e.g., the difference between total generation and total demand). However, temporal variations of both generation and consumption lead to mismatches that we further analyze as indicator of the complementarity between the two energy sources. The considered time step is hourly, which allows accounting for the daily cycle of solar PV generation and of electricity consumption.

The second step of the Decision Scaling framework (right on Figure 2.2) aims at assessing the likelihood of the various climate states explored during the sensitivity analysis. For this, we use the available ensemble of downscaled climate projections related to the 17 combinations of GCM/RCM (Table 2.2). Projected precipitation and temperature variables at daily temporal resolution are the inputs of a daily version of ICHYMOD (noted ICHYMOD-D) in order to assess the likelihood of changes in future glacier coverage for the two study periods.

2.3.1 Hourly simulation of streamflow and hydropower generation

We use the Integrated Catchment Hydrological Model (ICHYMOD-H) to simulate hourly streamflow at the outlets of the considered catchments. Details of ICHYMOD-H model are reported in Appendix A. Runoff computed from ICHYMOD-H is used for simulating the hydropower generation, which is calculated at the outlet of each catchment for a hypothetic run-of-the river power plant:

$$P_H(t) = \eta_H \, g \, h \, \rho \, q(t) \tag{2}$$

where p is power generation (kW), η_H is generator efficiency, q is the flow that passes through the turbines (m^3s^{-1}), g is the acceleration of gravity (m^3s^{-2}), ρ is water density (kgm^{-3}), and h is the head that is assumed to be constant (m). The streamflow that can be diverted is constrained by both environmental and technical constraints. A minimum flow (Q_{min}) must remain in the river to maintain ecological continuity. The design flow (Q_d), defines the maximum flow that can be diverted from the stream to the plant. Power generation from the plant must be curtailed for safety reason when streamflow in the river flow exceeds a safety threshold (Q_{max}). As discussed

by Hänggi and Weingartner (2012), common values for Q_{min}, Q_{max}, and Q_d are respectively 95th, 2nd, and 25th percentiles of the natural flows, respectively. Note finally that threshold values are estimated during the current conditions and remain unchanged under future climate conditions.

2.3.2 Solar Photovoltaic Power Generation

Solar PV power generation from an horizontal solar panel is obtained from the global horizontal irradiance (GHI) and temperature according to the model described by Perpiñan, et al. (2007), as follows:

$$P_{PV}(t) = B.GHI(t).(1 - \mu(T_a(t) - T_{C,STC}) - \mu.C.GHI(t) \quad (3)$$

where: *B* is the parameter of PV surface area and generator efficiency to convert from direct to alternative current under the standard test condition (cell temperature, $T_{c,STC}$, equals to 25°C and solar radiance, $I_{c,STC}$, equals to 1000 Wm^{-2}), *GHI* stands for Global Horizontal Irradiance, T_a is air temperature, μ and *C* are conversion efficiency parameters based on temperature and radiation.

In the study area, PV energy is mostly generated by rooftop solar systems. Accordingly, solar PV generation is estimated by averaging generation over urban areas in the Adige river basin closed at Ponte Adige.

2.3.3 Electricity Consumption

Given the lack of data concerning the electricity consumption at the scale of the study area, we use the electricity consumption model for North-Eastern Italy developed by François et al. (2016). Daily electricity consumption is estimated based on the heating and cooling degree-day method by a piecewise linear relation. Daily values of electricity consumption are then downscaled to hourly scale using a resampling approach of observed daily patterns. A comprehensive description of the model is provided by François et al. (2016).

2.3.4 Energy Mix

In the scenario of 100% renewable mix, electricity generation from RoR and solar PV are scaled to ensure equality between average generation and demand over the considered period as follows:

$$P(t) = \frac{p(t)}{\langle p(t) \rangle} \langle L(t) \rangle \quad (5)$$

where *P* is the scaled electricity generation (either from solar PV or from RoR), *p* is the electricity generation, *L* is the electricity demand, and ⟨ ⟩ is the average operator over the considered time period. Power generation from a combination of solar PV and RoR is then obtained as follows:

$$P_{mix} = s_{PV} P_{PV} + (1 - s_{PV}) P_{RoR} \quad (6)$$

where P_{mix} is power generation from the combined system, S_{PV} is sharing coefficient of solar power, P_{PV} is solar power generation, P_{RoR} is hydropower generation. Sharing coefficients for solar and hydropower energy sources are set equal to 25% and 75%, respectively, based on François et al. (2018).

2.3.5 Future climate scenarios

For the climate stress test, we consider relative changes in precipitation ranging from -40% to +40% with a 10% step, absolute changes in temperature range from +0 to +8°C with a 1°C step. For each scenario of change in precipitation and temperature, we run the ICHYMOD-H model with a set of fixed glacier coverage for the entire simulation. Future glacier coverages that are considered for the climate stress test range from 100 % of the observed coverage to 0 % of its current coverage with a 10% step. This framework leads to the analysis of 891 future possible scenarios and subsequent hydropower time series, including the 'no change' state. Note that changes in solar PV power generation and electricity demand account only the change of temperature. Given the availability of the radiation and glacier data for simulating the PV and RoR generation, the climate stress test is operated over a 9-years period (based on the 2000 – 2008 data).

The likelihood of the considered climate states is evaluated by using the available ensemble of downscaled climate projections related to the 17 combinations of GCM/RCM. Figure 2.3 illustrates the range of precipitation and temperature changes for the two future 30-year periods (2040-2069 and 2070-2099) compared to the control period (2000 – 2011), for the two considered basins. For both periods, climate projections agree toward an increase in annual temperature, with temperature changes ranging from +2°C to around +5°C, for the period 2070-

2099. Precipitation changes are more uncertain, showing changes in annual precipitation ranging from -30% to 40.0% for 2070 – 2099.

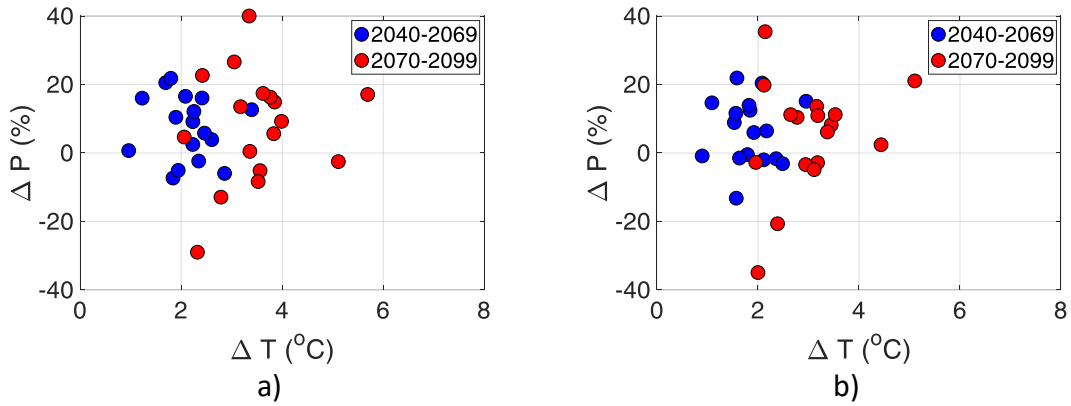

Figure 2.3 Projected temperature and precipitation changes obtained from the 17 combinations of GCM/RCMs. Blue and red colors show 2040-2069 and 2070-2099 periods, respectively. The control period is 2000 – 2011. a) Saldura; b) Plima.

2.4 Energy balance under current climate

Figure 2.4 a,b illustrates the average seasonal cycle of streamflow and solar radiation for Saldura and Plima , respectively. There is a huge difference between the runoff cycle at the scale of the Intermediate Basin and the Lower Basin for the two catchments, which is mainly due to the drier climate of Saldura with respect to Plima. Figure 2.4 c,d illustrates the seasonal variations of normalized electricity generation and demand. RoR generation follows seasonal variation of streamflow. When the river flow gets either higher than the safety thresholds Q_{max} or lower than the minimum Q_{min}, the power plant is curtailed and the generation interrupted (cf. the decrease of percentile curves in August and July respectively for Saldura and Plima). Solar PV is maximum during summer season and minimum in winter. Seasonal variation for the electricity demand is significantly lower than the ones observed for solar PV and RoR generation, although it shows slightly higher values during the winter season. The significant drops in electricity consumption during August, December and January months results from major holiday periods in the country.

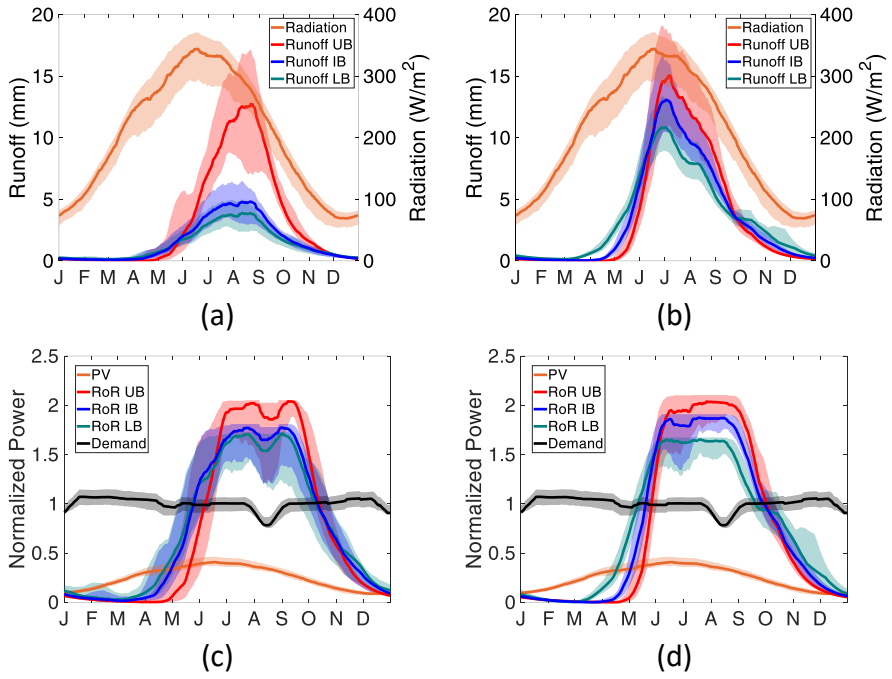

Figure 2.4 Seasonal cycles of streamflow (a and b) and normalize power generation (c and d) for Saldura (a and c) and Plima (b and d). The bold lines refer to the median while the shaded areas show the deviation between the 25th and 75th percentiles. UB, IB, and LB are acronyms for Upper Basin, Intermediate Basin, and Lower Basin. Seasonal cycles are smoothed over 10 days moving windows. The electricity demand is normalized and its average equals 1. RoR and PV cycles are normalized and then weighted according to their share into the considered energy mix (75% for RoR and 25%, cf. Section 3.5).

According to Table 2.3, which reports the complementarity statistics, the electricity demand that could be satisfied by the considered energy mix (i.e., 75% hydro and 25% solar) is higher for the Lower Saldura and Plima Basins than for the Upper Basins. Note that the satisfaction of the electricity demand decreases with the increase of elevation and decrease of basin size. This is due to an increase on streamflow variability leading to the variability of RoR generation and to a more variable energy balance the variability of the generation compared to the load, which subsequently translates into lower demand satisfaction (cf. CV values in Table 2.3). The change in streamflow variability with altitude is here due to the higher precipitation variability in high altitudes and by the larger contribution from glacier melt to total runoff, which relatively increases the amplitude of the seasonal variations.

Indicators	Saldura			Plima		
	Lower Basin	Intermediate Basin	Upper Basin	Lower Basin	Intermediate Basin	Upper Basin
Correlation between PV and RoR	0.18	0.19	0.19	0.18	0.18	0.19
Demand satisfaction (%)	66.07	61.36	57.86	65.43	63.15	58.18
CV of streamflow	1.25	1.40	1.63	1.12	1.37	1.66
CV of RoR generation	0.90	0.97	1.13	0.88	1.04	1.16
CV of solar PV	1.33					
Standard deviation of energy mix	0.81	0.91	0.99	0.80	0.86	0.97
Standard deviation of energy demand	0.20					
Standard deviation of energy balance	0.83	0.93	1.01	0.69	0.73	0.81

Table 2.3 Performance criteria of the complementary use of solar PV and RoR under the current climate conditions for Saldura and Plima basins. All indicators are calculated for the hourly time step.

2.5 Energy balance under future climate

2.5.1 Change in glacier from GCM/RCM model chains

Figure 2.5 (left column) illustrates the temporal evolution of the glacier coverage from 2006 to 2100 for Saldura (upper row) and Plima (lower row). Figure 2.5 (right column) also emphasizes the relationship between the increase in annual temperature and glacier shrinkage. Results are consistent for the two catchments; higher the temperature increase, larger the glacier shrinkage.

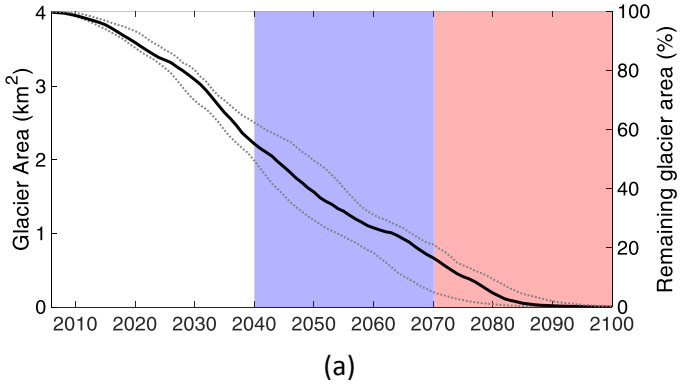

(a)

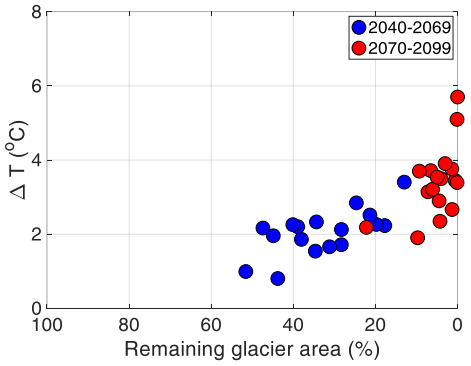

(b)

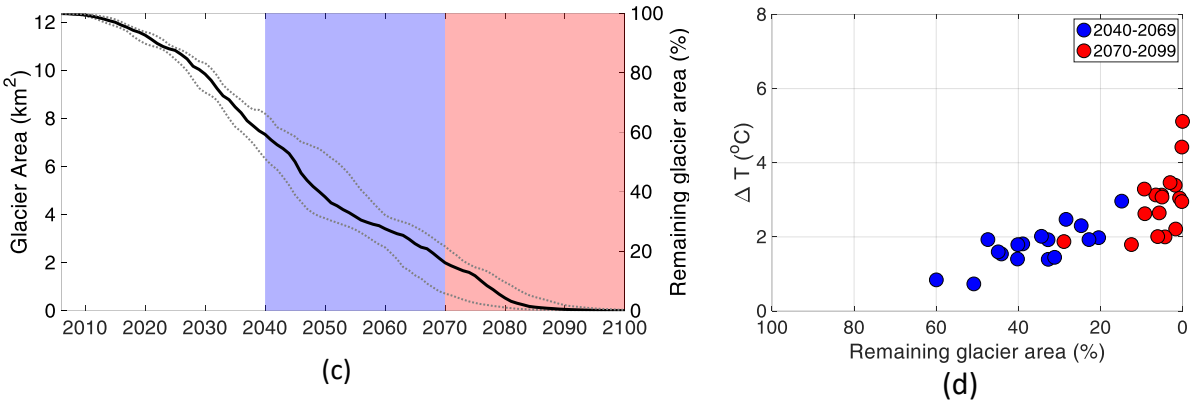

Figure 2.5 Projections of annual glacier area changes from 2006 to 2099 in Saldura (a and b) and Plima (c and c). Black lines show the median of 17 projections obtained. Gray lines represent the 25th and 75th percentile of glacier shrinkage simulation from each GCM/RCM combination. The relationship between glacier alteration and temperature change is illustrated on the right side of the figures for two future periods (2040 – 2069 and 2070 – 2099).

The simulations for glacier retreat in Saldura and Plima catchments are consistent with observations and projections published in the literature for similar climatic areas. For instance, in Northern Italy, Patro et al. (2018) showed that glaciers would shrink from 2016 to 2065 by 85-100%, including the ones located at elevations higher than 2,500 m.asl.

2.5.2 Streamflow and RoR power generation sensitivity to changes in temperature, precipitation and glacier cover

The effects of changes in temperature, precipitation and glacier coverage on streamflow at the outlet of the Upper and Lower Saldura basins are illustrated in Figure 2.6. Similar results are obtained for Plima catchments (Appendix B). The increase in temperature has two main consequences. First, it raises the fraction of liquid precipitation during the winter season, which reduces snow accumulation and subsequently enhances streamflow generation in winter and should subsequently decrease the contribution of snowmelt to the spring floods. Second, it raises the glacier melt, with an increase of runoff during the summer season. This increase is larger for the Upper Basin where ice melt is boosted by the warmer temperatures. An increase (resp. decrease) in precipitation increases (resp. decreases) snow accumulation during winter and consequently enhances (resp. reduces) streamflow during spring. The effect of precipitation change on streamflow increases with the basin size, which underlines the low contribution of

precipitation to streamflow for the head watershed. Scenarios that include both temperature and precipitation changes lead to hydrological regimes that roughly combines the changes discussed above.

The shrinkage in glacier coverage directly reduces the contribution of ice melt to total runoff, which subsequently lowers streamflow during the spring and summer seasons. This effect partly offsets the increase in streamflow due to the enhanced ice melt (cf. the difference between red and black curves for the Upper Basin and for ΔT = +5ºC, Figure 6). Because the contribution of ice melt to the total runoff is low for the Lower basin under current conditions, the reduction in glacier coverage does not influence significantly the streamflow.

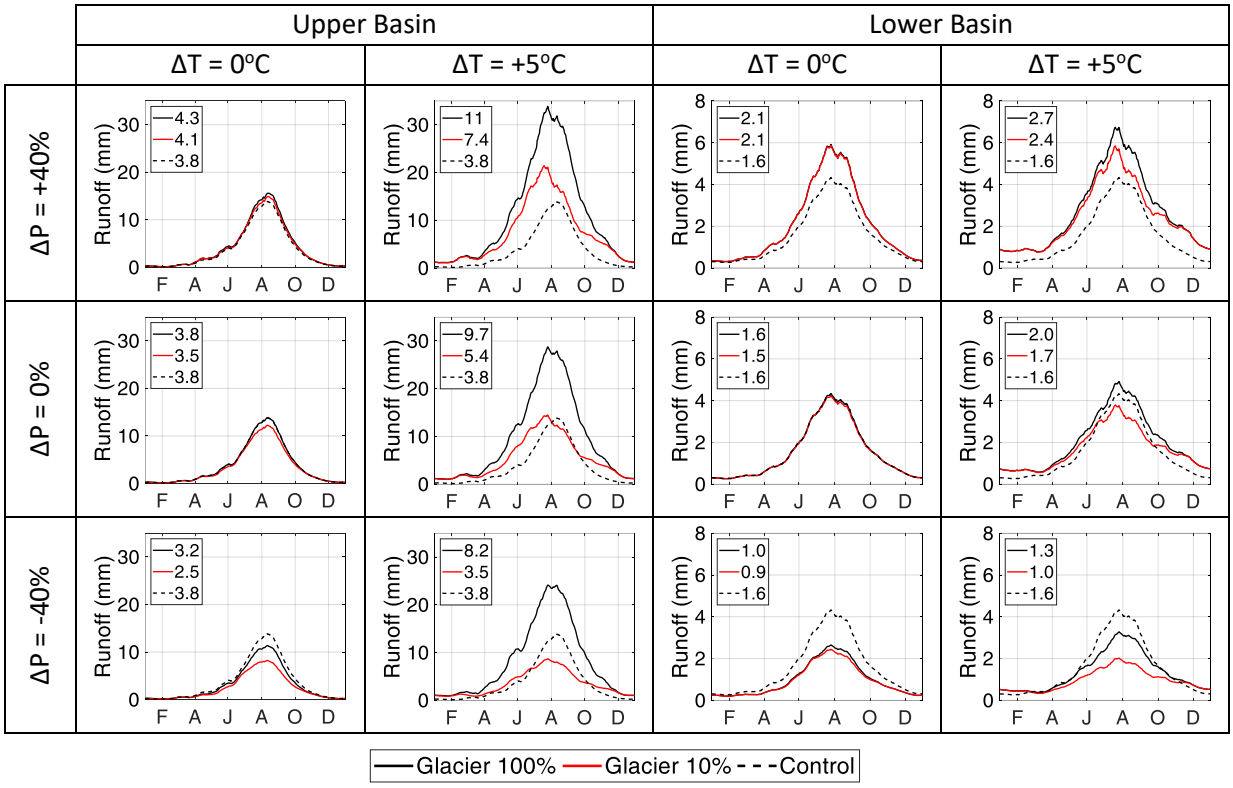

Figure 2.6 Runoff seasonal cycle of Saldura Upper Basin and Lower Basin in mm. Black dashed line is the control climate where there is no change in temperature and precipitation (ΔT=0ºC and ΔP=0%). Black and red full lines illustrate the cycle when glacier area is 100% and 10%, respectively. Values presented in the left-corner box are the mean daily values in mm in the different scenarios. Each cycle is smoothed over a 10-day window.

Figure 2.7 illustrates the effects of changes in precipitation, temperature and glacier coverage on RoR power generation for the Upper and Lower Saldura basins (results for Plima are

available in Appendix B). Similar to streamflow variable (Figure 2.6), the increase (resp. decrease) in precipitation results in higher (resp. lower) RoR power generation during the spring season, especially for the Lower Basin. The rise in temperature and the associated increase in streamflow in winter enhances RoR power generation at this season. In addition, increasing temperature boosts ice melt during spring and summer seasons, which induces a significant increase in hydropower generation at this period in the higher basin (i.e., Upper Basin). Note that such an increase may lead to streamflow conditions exceeding the power plant safety threshold (Q_{max}) and consequently get the power plant to be shut down (cf. the collapse of the generation peak obtained for $\Delta T = +5^oC$, black curve on Figure 2.7).

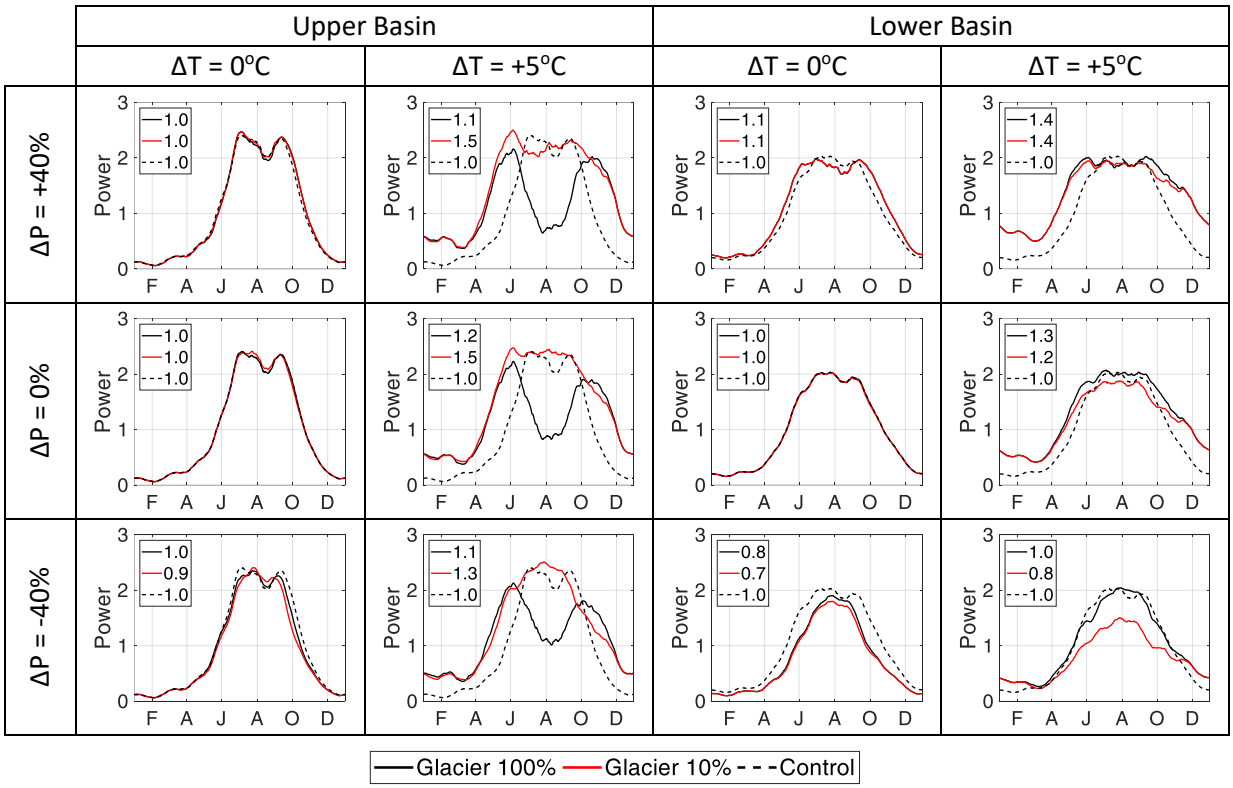

Figure 2.7 Similar as Figure 2.6 but for hydropower generation. Power time series are normalized regarding the average generation obtained for the control climate (i.e., no change in precipitation, temperature and glacier).

Figure 2.8 illustrates for each calendar day the climatology of the power plant shutdowns. To characterize these periods, we use the inactive rate metric defined as the percentage of hour

for each calendar day when hydropower generation has been curtailed due to unfavorable streamflow conditions (i.e., streamflow at the water intake that is either higher than Q_{max} or lower than Q_{min}). Under current climate conditions, the frequency and timing of generation curtailments are similar for the Upper and Lower Saldura basins; they mainly occur at the end of the winter low-flow period / early spring and during the high-flow period in spring.

For the Lower basin, a decrease in precipitation during winter season leads to an increase of the number of days when streamflow is lower than the minimum requirements (Q_{min}) and thus, to an increase the inactive rate of the power plant. For instance, the power plant could be shut down more than half of the time during February and March if precipitation decrease by 40% (Figure 2.8). Decreasing precipitation also reduces snow accumulation over the catchment, which scales down the spring flow peak and eventually decreases the curtailments at this season.

For the Upper basin where glaciers cover a larger part of the catchment, the consequences of decreasing precipitation are diametrically different. A decrease in precipitation reduces snow accumulation, including the accumulation over glacier areas that are covered by snowfall under current climate conditions. This process increases the fraction of the glacier to have a direct contact with the atmosphere that would eventually increase ice melt. Since ice has a lower albedo than snow, the combined melt from ice and snow could actually increase during given peculiar weather conditions, which may lead to a decrease of average inactivity of the power plant at the beginning of the spring season. If the precipitation increases, snowfall would cover a larger glacierized area, which would reduce the combined snow and ice-melting rate and eventually increase the frequency of curtailment of the power plant generation.

The effect of increasing temperature is similar for both Upper and Lower catchments. Higher streamflow during winter and early spring due to an increased fraction of liquid precipitation at this period leads to a decrease in number of days with non-favorable conditions, which then significantly reduces the inactive rate. During the summer season, larger streamflow following from the increase in ice melt (Figure 2.6) leads to an increase in generation curtailments (Figure 2.7). However, these curtailments are likely to be reduced with the future decrease in ice melt contribution to total runoff that follows from the glacier shrinking.

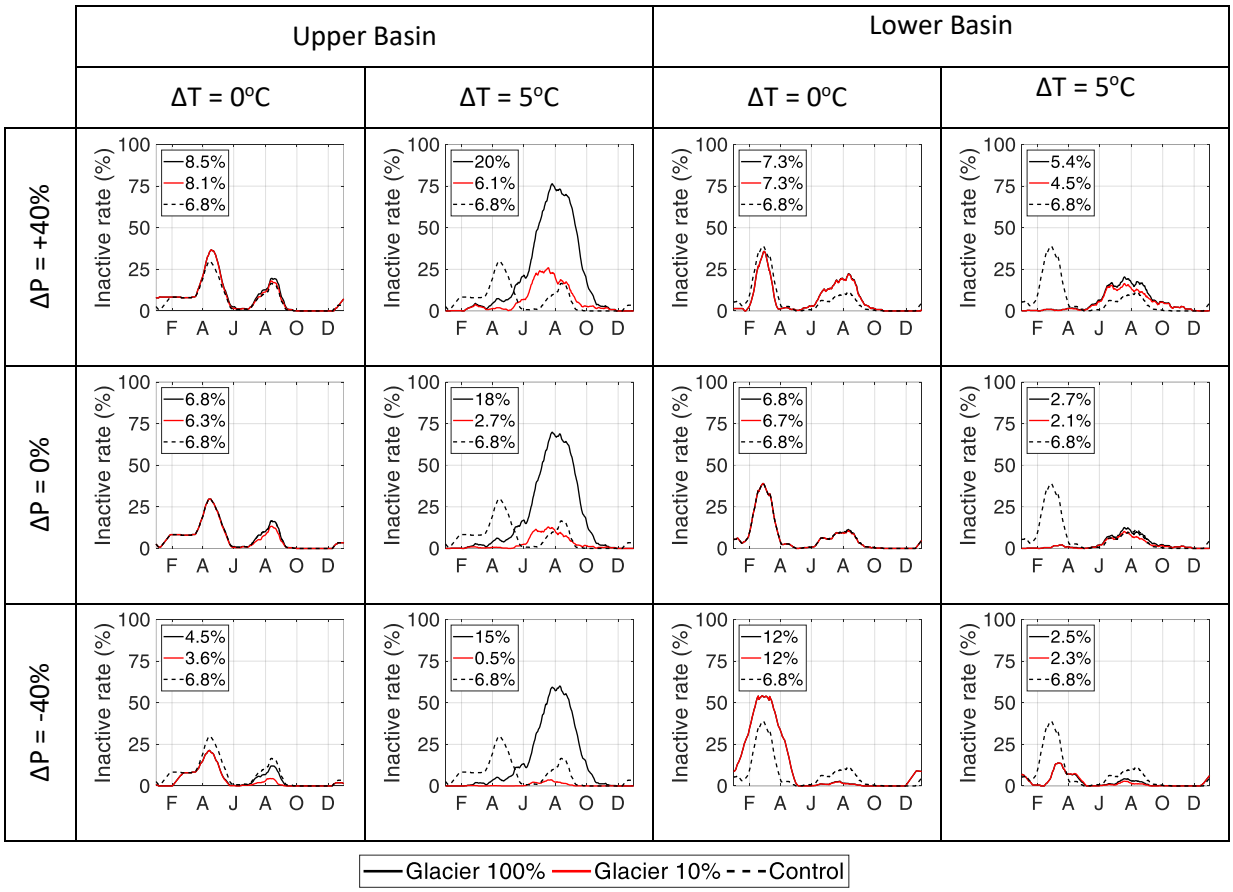

Figure 2.8 Same as Figure 2.6 but for inactivity rate (%). Each cycle is smoothed over a 10-day window.

2.5.3 Climate change impact on the combination of solar PV and RoR power generation and penetration

This section focuses on the expected changes in power generation from combining solar PV and RoR and its ability to supply the demand. The contribution from solar PV RoR into the energy mix is 25% and 75%, respectively (cf. section 2.3.5).

Here we summarize first the change in solar PV generation and electricity demand with increasing temperature. Examination of the solar PV generation model (Eq. 3) shows that the change in solar PV panel efficiency due to warming temperature is not significant. For instance, an increase in average temperature by 5°C only alters solar PV generation by less than 1%. Modifications of solar radiation is not considered in our framework (cf. Section 2.3), Increasing temperature affects the pattern of electricity demand by decreasing the need for heating during

winter months and increasing the need for cooling during summer months. For instance, according to the model described in Section 2.3.3, an increase in temperature by 5^{o}C leads to an increase in summer consumption by 3% and to a decrease in winter consumption by 2.4%. At an annual scale, such an increase in average temperature would translate into an increase in electricity consumption by 0.7%.

Figure 2.9 illustrates the modification of the correlation between RoR and PV for a range of changes in temperature, precipitation and glacier coverage. The kernel density functions on Figure 2.9 show the projected changes in temperature (i.e., 17 combinations of GCM/RCM, Table 2.2) and for two future periods. These density functions can be used to inform about the likelihood of changes in correlation caused by temperature change. For both Upper and Lower basins, precipitation changes have no significant effect on the correlation while increasing temperature tends to reduce the correlation. For instance, by increasing precipitation by 40% without any change in temperature and glacier areas, the correlation remains the same. By increasing temperature 5^{o}C without any change in precipitation and glacier areas, the correlation in Upper Basin decreases by 0.12 point. However, the results obtained for the Upper basin highlight an additional feedback mechanism between (1) the increase in streamflow during spring and summer seasons due to the enhanced ice-melting rate triggered by higher temperatures and, (2) the safety threshold that curtails generation from the RoR power plant during high-flow periods. Figure 2.9 (left) shows indeed that the diminution of the correlation between RoR and solar PV could significantly decrease, and even become negative if temperatures increase larger than by 6^{o}C. However, this decrease is significantly reduced when the glacier melt is accounted for.

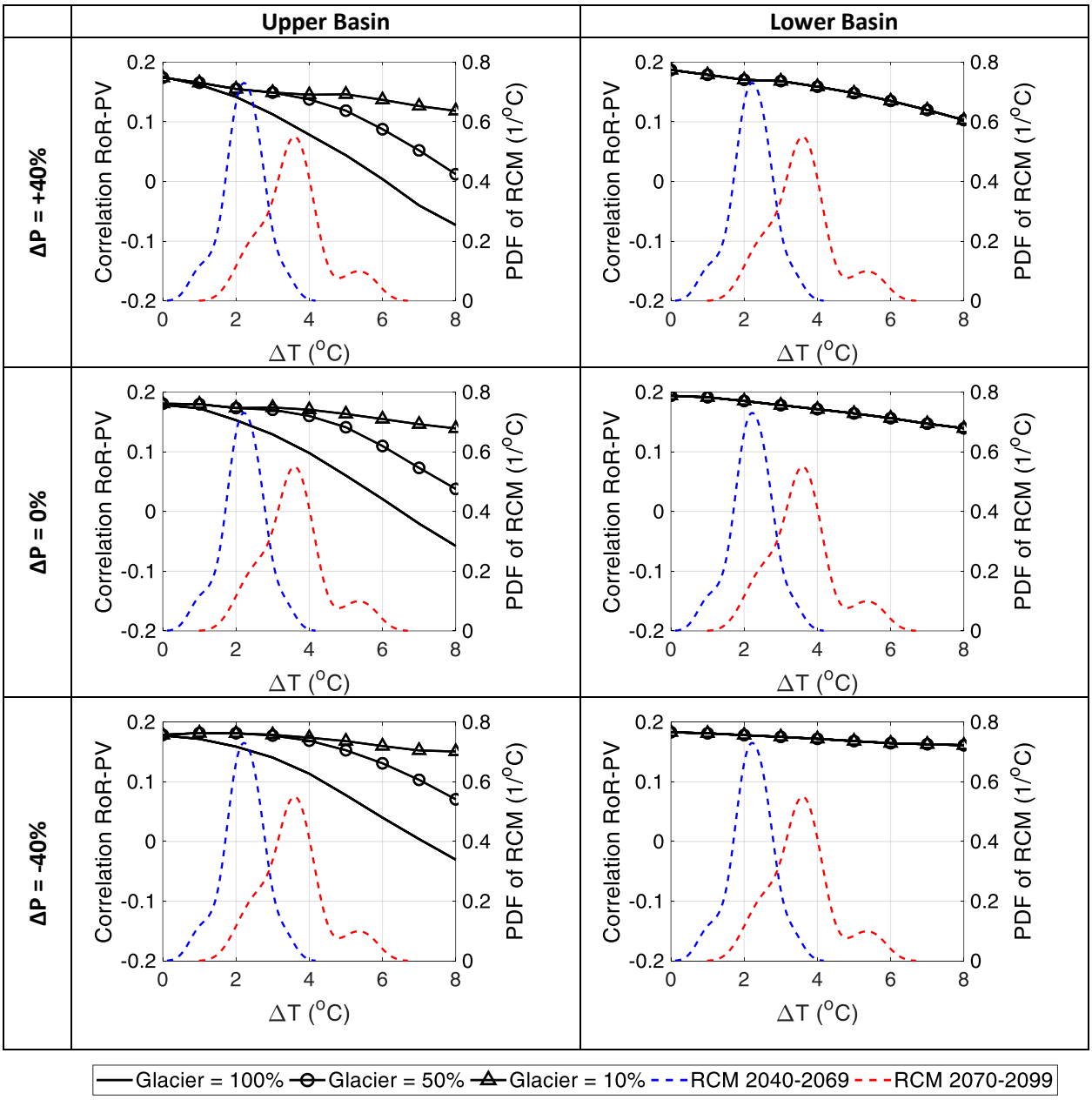

Figure 2.9 Sensitivity of the correlation between RoR and PV to changes in precipitation (row), temperature (x-axis) and glacier cover (black curves). Right and left columns show the results obtained respectively for the Upper and Lower Saldura basins. The kernel density smoothing of projected temperature changes obtained from 17 combinations of GCM/RCM are shown for the future periods 2040 – 2069 (blue) and 2070 – 2099 (red) with the values in right y-axis.

Figure 2.10 illustrates the sensitivity of the penetration rate to the changes in precipitation, temperature and glacier coverage. Temperature is the main driver of change for

the penetration rate, especially in the Upper Basin; larger the temperature increase, larger the penetration increase. For instance, the Figure shows that by increasing temperature by 5^{o}C without any change in precipitation and glacier areas, the penetration rate in Upper Basin increases by 24%. This mainly results from the effect of temperature on streamflow as discussed on Section 2.5.2. The alteration of glaciers has opposite effects on the penetration for either the Upper or the Lower basins. For the high-altitude basins, the reduction of glacier coverage and its associated contribution to streamflow during the spring and summer seasons increases the penetration, which can be partly explained by a lower frequency of power generation curtailments. It is worth mentioning that increasing precipitation is also likely to increase the penetration rate. We also note that the reduction in glacier has different impact to the penetration rate for the Lower and Upper basins. As an example, looking at the scenario that combines an increase in temperature by 5 ^{o}C and an increase in precipitation by 40%, we note that accounting for a decrease in glacier cover by 90% would lead to an estimate of the penetration rate for the Upper basin that is larger by 9% than the penetration estimated with no change in glacier. For the Lower basin, however, the penetration rate is not very sensitive to change in glacier coverage as penetration decreases by only 0.4% when comparing the two above-discussed scenarios. Note however that the effect of glacier change on the penetration change in the Lower Basin is revealed more obvious if precipitation decreases.

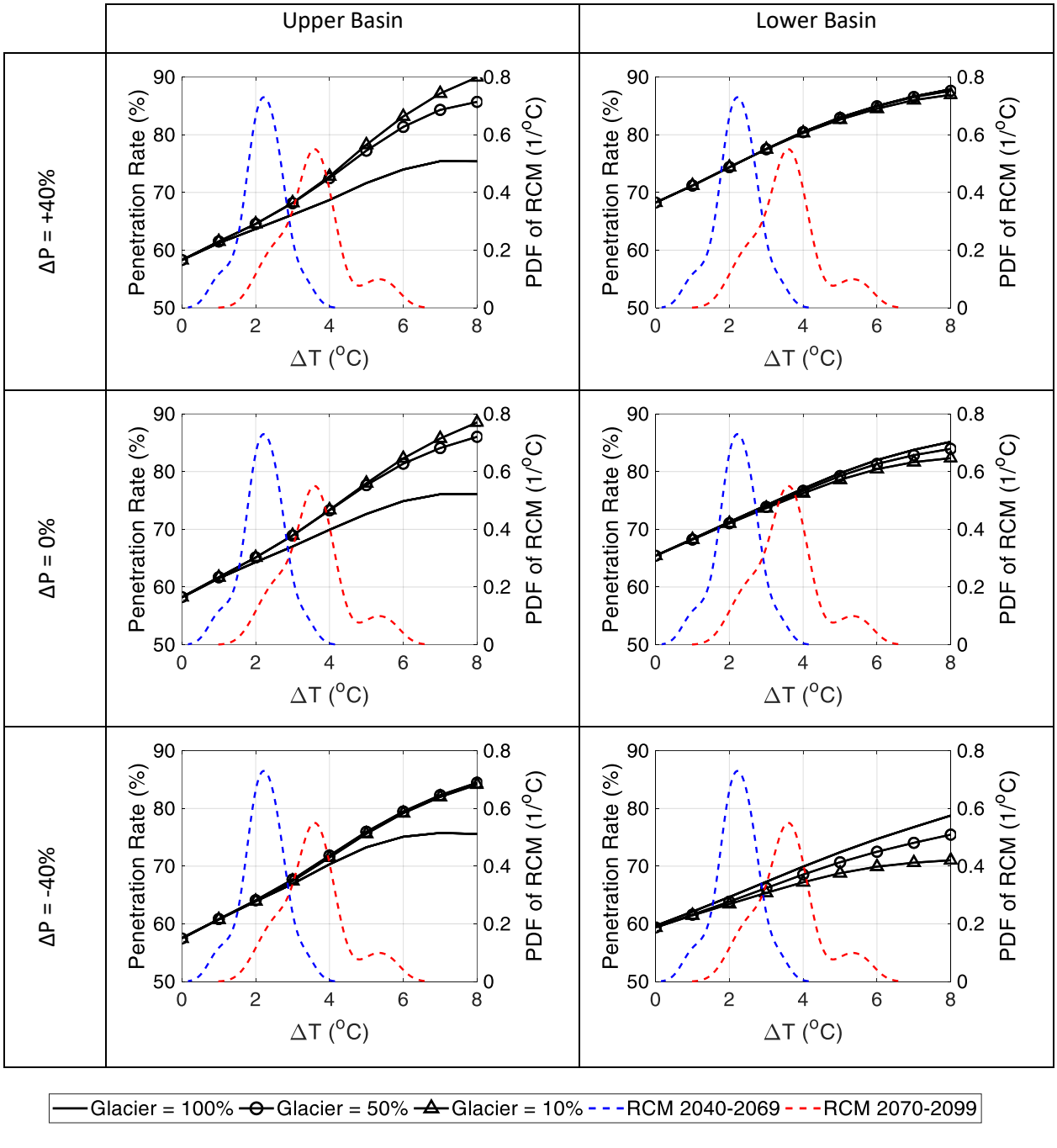

Figure 2.10 Same as Figure 2.9 but for the penetration rate.

Figure 2.11 compares the assessment of the penetration rate from PV-RoR combination for the mean changes in precipitation and temperature which are consistent with the RCM projections for 2070-2099 and for two glacier shrinkage scenarios: i) 100%, and ii) glacier extent obtained by ICHYMOD-D for the year 2070 by using the corresponding RCM projections. This

permits to appreciate the impact of accounting for glacier shrinkage in the assessment of penetration rate. Each box plot shows the distribution of the penetration rate resulting from the 17 RCM projections. Results are reported for the two study basins and for the three nested basins in each of them, and show that the penetration rate increases with increasing the basin size and decreasing the glacier cover percentage and basin's mean elevation. This is true for both glacier scenarios (100% and altered glacier). Accounting for glacier shrinkage is important for the Saldura Upper Basin, where the difference between the medians corresponding to the two glacier scenarios are statistically significant (at 5% significance). For all other cases, the differences between the two medians are not statistically significant. This is not surprising, since Saldura Upper Basin is the basin characterized by the largest glacier coverage in the 100% scenario. The difference in the spread of the penetration rate is also important for this basin. This indicates that decreasing the glacier extent, which regulates the streamflow during spring and summer seasons, inflates the uncertainty in penetration rate. With glacier decreasing, streamflow becomes more dependent to the changes in precipitation that can lead the changes in inactive rate of hydropower and hydropower production itself. This effect is less apparent for the Plima basin, given the relative lower extent of the glacier area.

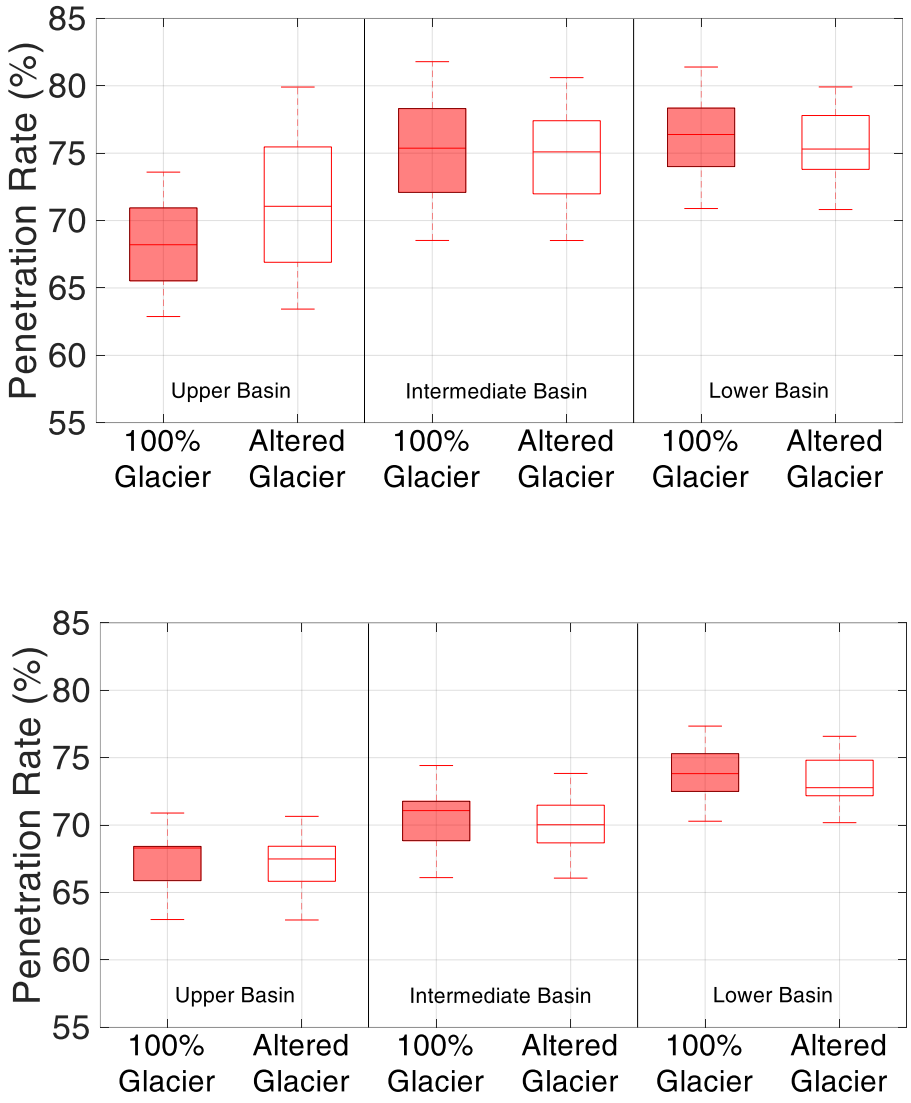

Figure 2.11 Influence of the alteration of glacier on the penetration rate in Saldura (top) and Plima (bottom). The box plots represent the range of future values that are inferred from 17 climate projections and for the period 2070-2099. Red filled box plots show results when glacier coverage changes are disregarded and thus there is no change in glacier coverage from 2006 to 2099, while the red empty box plots show the range of values when alteration of glaciers is accounted for.

2.6 Conclusion

This study considered two high elevation Alpine catchments, with significant glacierized areas. Changes in glacier cover appeared to have significant impact on streamflow pattern for high elevation catchments. The results show that consideration of warming in temperatures and neglecting the effects from glacier shrinkage is likely to lead to an incorrect representation of

streamflow pattern, with especially a significant overestimate of streamflow during spring and summer seasons. This overestimation is expected to be large for high altitude glaciered catchments with glacier covering typically more than 50 % of their surface.

Due to temperature rise affecting higher rate of ice melt that enhances the spring and summer streamflow, average of RoR generation increases at these periods. Disregarding glacier shrinkage could lead to an underestimation of the RoR power generation and to a significantly different seasonal cycle of the production in high elevation catchments. For RoR hydropower power plant with typical ecological flow requirements and other constraints associated with plant safety especially in the tails of the distribution, change in streamflow distribution caused by the changes in glacier, can lead to an increase in power plant shutdown frequency.

This study also focuses on the potential change in complementarity between solar PV and RoR hydropower generation in mountainous areas. On the basis of future projections for the study area (François et al., 2016a), the energy mix considered in the study is composed of 75% of RoR hydropower and 25 % of solar power generation. Three indicators of the complementarity between solar PV and RoR hydropower have been considered: the Pearson's correlation coefficient between solar PV and RoR, the standard deviation of the energy balance, and the penetration rate. Results show that change in glacier coverage leads to significant different estimates of the energy penetration. However, the effect of glacier change on the complementarity estimate decreases quickly with increasing catchment size (and then decreasing influence of ice melt to total runoff). We thus recommend including the effect of glacier change in any climate risk assessment for hydropower investments in high elevation region where glaciers currently have a significant influence on the hydrology regime, especially in summer.

Results from this study are subject to several uncertainty sources and assumptions that future works should address in order to strengthen the above conclusion. First, only two Alpine catchments have been considered. Additional case studies should be considered, including case studies from other mountainous areas where combined solar PV and RoR hydropower systems are either running or planned (e.g. the Himalayas as in Kedia and Kedia (2009)). Change in solar

radiation should also be accounted for. Although comparatively small, such changes in solar radiation could either decrease or increase the complementarity between solar PV and RoR hydropower at the seasonal scale. Although comparatively small, changes in solar radiation could either decrease or increase the complementarity between solar PV and RoR hydropower at the seasonal scale. Solar radiation on 2070 – 2099 in central and southern Europe is projected to be 5 – 10% brighter during summer, but its brightness in winter is estimated to be 5 – 15% lesser than the value on 1971 – 2000 (Burnett et al., 2014; Ruosteenoja and Räisänen, 2013). Several shared of PV and RoR in 100% renewable energy scenarios can also be considered in the future studies since it allows exploring the changes in optimal mixture when there is less glacierized areas.

Chapter 3

Complementarity between Combined Heat and Power systems, solar PV and hydropower at a district level: application to the North Eastern Alps[2]

[2]This chapter is based on a paper that has been prepared as: **Puspitarini, H.D.**, François, B. Zaramella, M., Baratieri, M., Brown, C., Borga, M. 2019. Complementary between Combined Heat and Power systems, solar PV, and hydropower at a district level: Application to the North Eastern Alps. Manuscript in preparation

3.1 Introduction

Heating and hot water are essential needs in many urban areas around the world. Private heaters and boilers fueled by energy sources generated in centralized locations (e.g., electricity, fuel oil or natural gas) are commonly used to satisfy these basic needs. District heating, on the other hand, are systems within which heat and/or hot water are first generated in a centralized location, and then distributed to residential and commercial buildings through networks of pipelines, reducing by this mean the need for in-situ generation through private heaters and boilers. Such systems become more popular, especially with the growing installed capacity of Combined Heat and Power (CHP) plants. CHP plants have the advantage of combining the generation of heat and electricity within a single process, which leads to higher overall efficiency. As an example of higher efficiency, Gvozdenac et al. (2017) highlighted CHP overall efficiencies ranging from 70 to 90% while efficiency of conventional electricity production means range from 30 – 40% (Rashid et al., 2016). Denmark and Finland are world leaders in this technology, which current supplies 75% of their heat demand (Virasjoki et al., 2018) .

Power generation from CHP plants within district heating is often considered as incidental since CHP are most of the time operated for supplying heat and hot water first (Çakir et al, 2012; Wang et al., 2015), although associated electricity generation can represent a significant share of the district supply. Using the above example of Denmark, CHP power generation has represented 50% of the national electricity production (Virasjoki et al., 2018). At the scale of the European Union, CHP plants have for instance supplied around 15% of the electricity demand, a share that is expected to increase to 22 – 25% by 2030 (CODE2, 2015).

Although already significant, the installed capacity of CHP plants is expected to increase worldwide during the next decades. The recent UNFCCC (United Nation Framework Convention on Climate Change) Paris Agreement on 2015 (COP21) has indeed gathered 190 countries around the common goal to reduce greenhouse gas (GHG) emissions at a global scale. One major objective of the agreement is to limit the global temperature rise below 2^{o}C above pre-industrial levels (United Nations, 2015). Such a goal requires a structural transformation of the energy sector, mainly relying on the use of fossil fuel, into a more environmentally friendly energy sector, for instance based on renewable energy sources. As an illustration of the carbon footprint,

supplying electricity demand for residential and commercial buildings around the world via coal power plants contributes to 30% global CO_2 emission (IEA, 2018b). In order to reach the Paris Agreement goal, the International Energy Agency suggests that at least 80% of the electricity generation must be supplied by low carbon energy sources (IEA, 2016). Such a transformation for the current energy sector is a real challenge for planners and operators because disruptive changes are required while demand for electricity is surging due to economic and demographic growth at global scale (Lin and Ouyang, 2014).

The usage of renewable energies, and more specifically of Variable Renewable Energies such as wind, solar, and hydro-power (hereafter denoted as VRE) is widely considered for the replacement of conventional electricity production means (IPCC, 2014b; Moriarty and Honnery, 2016). A well-known challenge regarding the use of VRE sources for replacing conventional production means, however, relies on the variability and intermittency of VRE electricity generation, which would tend to significantly increase the dependence of the electricity generation and demand on weather and climate across a large range of temporal and spatial scales (Engeland et al. 2017, Staffell and Pfenninger 2018). Despite substantial research showing the benefit of combining various VREs from local to continental scales (e.g., Heide et al., 2010; von Bremen, 2010; François et al., 2016a; François et al., 2016b; Jurasz and Ciapała, 2017; Ming et al., 2018; Raynaud et al., 2018), the need for storage or backup generation is acknowledged for balancing electricity generation from high shares of VRE with the demand.

Several studies investigated the potential of CHP plants to serve as back-up electricity generation for the VRE sources. For example, Söder et al. (2018) reviewed the power production within the Nordic electricity market. They highlight that in 2015 Denmark supplied 70% of its electricity demand by using a combination of wind power and CHP generation, the remaining being covered by buying from the Nordic electricity market, mainly from Norway and Sweden. Romero Rodríguez et al. (2016) shown in various climate areas in Spain that a combination of electricity generation from solar photovoltaic (PV) panels and CHP is a tangible solution for reducing the emission of GHG.

In this study, we analyze the integration of CHP in combination with other VRE sources at the basin level. The size of the selected basins is small enough to be confounded with a district equipped with a heating system. Using a 100% renewable energy scenario, we investigate how the replacement of variable renewable energy sources by CHP generation modifies the overall electricity balance within the districts. Results obtained from assessing the electricity balance over several basins located along a climate transect from high to low elevation give insights for a large range of climate conditions about the benefit of using CHP in addition to other VRE sources within a district. Different penetration levels for CHP heat generation are considered within the districts, together with the use of storage capacity to balance generation with demand for electricity. To demonstrate the case, we consider case studies located in Northeastern Italy where hydropower and solar PV are the two main energy sources that are currently used for supplying the electricity demand.

The paper is organized as follows: Section 2 presents the analysis framework, including modeling of the CHP heat and electricity generation, the heat and electricity demand models, and the considered renewable sources and associated electricity generation. Section 3 describes the application for the Northeastern Italian Alps. It includes the description of the study area and the database used for this application. Section 4 presents the results while Section 5 concludes and gives insights for further research.

3.2 Analysis framework

The developed analysis framework aims at assessing the benefit of combining electricity generation from CHP plants operating within a district heating system, with electricity generation from other renewable energy sources. The benefit of combining generation from CHP plants with other renewable energy sources is evaluated using two indicators of interest for the grid operators. They are i) the electricity demand satisfaction within the district and ii) the standard deviation of the energy balance, defined as the difference between supply and demand, which provides insights about the required balancing system costs for handling the remaining balance variability. This section describes the analysis framework that is considered for modeling electricity and heat generation from CHP, electricity and heat demand, electricity

generation from the renewable energy sources that are accounted for within the considered case studies (i.e., solar photovoltaic and run-of-the river power generation) and the energy balance.

3.2.1 District Heat System and CHP heat generation

For a given urban or sub-urban area, we assume that CHP plants are primarily operated to supply heat demand through the district heating system. In locations where district heating system is not the only source for heat supply, CHP are often operated to satisfy a given share of the demand (Equation 1):

$$H_{CHP} = H_s H_D, \quad (1)$$

where H_{CHP} is the heat energy generated from the CHP plants within the district, H_D is the heat demand, H_s is the share of heat demand that is on average covered by H_{CHP}. Note that H_s can be higher than 1 if the district heating systems is oversized. Conversely, $H_s = 0$ corresponds to an urban or sub-urban area that is not equipped with a district heating system. Due to its lack of flexibility, heat generation from CHP plants is commonly kept constant for a given period and adjusted at a chosen frequency (e.g., monthly). Despite the variations of heat demand due to air temperature fluctuations at small temporal scales (e.g., hourly and daily), the heat demand can still be satisfied thanks to the thermic inertia of the district system (Gu et al., 2017; Romanchenko et al., 2018). This means that even though CHP heat generation at a given time is lower than the demand, supply can still be ensured by using the remaining heat from a previous day for instance.

Time series of regional heat demand are often available at the country or regional level and at an annual time scale only. However, the heat demand can be downscaled to district scale and to finer temporal resolution using the Heating Degree Day method (Lundström and Wallin, 2016). The heating degree day (HDD) for a given day 'j' is defined as the sum of the positive deviations between the outdoor temperature and a temperature of confort:

$$HDD(j) = \sum_{j,h=1}^{j,h=24} (T_b - T_a(j,h))^+, \quad (2)$$

where $T_a(j,h)$ is the outdoor air temperature for the day j at the hour h; T_b is the temperature threshold from which the heat demand starts increasing. Note that T_b is often set to 12°C (e.g.,

Christenson, et al., 2005; Lindelöf 2017). The '+' symbol indicates that negative values within the brackets are set to 0. Following Ashfaq et al. (2017), the heat demand for the district and for a given day j can then be estimated from equation 3:

$$H_D(j) = w.p.HDD(j), \quad (3)$$

where p is the number of inhabitants living within the district and w is a heat factor (Wh.^{o}C^{-1}.inhabitant^{-1}). The heat factor w represents the marginal increment in heat demand per inhabitant and per degree Celsius that can be estimated from the observed total annual heat demand (Ashfaq et al., 2017):

$$\omega = \frac{\sum_y H_D(\mathrm{y})}{p \cdot \sum_y \sum_{j=1}^{365} HDD(j)}, \quad (4)$$

where y is a dummy variables for the specific years when annual heat demand is available.

3.2.2 Electricity balance

The electricity balance is solved within the district considering the 100% renewable scenario, which corresponds to the scenario for which total electricity generation from various renewable energy sources within the district covers on average the electricity demand (Equation 5).

$$\sum_j \sum_h \sum_i E_i(j,h) = \sum_j \sum_h E_D(j,h) \quad (5)$$

where $E_i(j,h)$ is the electricity generation (*Wh*) from the source 'i ' for the day 'j' during the hour 'h' and E_D is the electricity demand within the district (*Wh*).

3.2.3 CHP Electricity Generation

The relationship between electricity generation and heat generation from a CHP plant differs from one technology to another (cf. Raj et al. (2011) for a review of CHP technology). In this study, we consider the biomass-based CHP technology because it is the most common in the study area (cf. Patuzzi et al. (2016) and Section 3). For this specific CHP technology, the ratio between the heat energy and the electric energy generation is kept constant and only adjusted

at a seasonal basis depending on the heat demand in the district and the operator management strategy (Equation 6):

$$E_{CHP}(j,h) = A(j) \times H_{CHP}(j,h), \quad (6)$$

where H_{CHP} and E_{CHP} are respectively the heat and electric energy generated from the CHP plant, and A is the power-to-heat ratio (Frangopoulos, 2012). This ratio is a decision variable for the plant operator who can decide to boost either heat or electricity generation during some period. It usually varies at seasonal scale. Because CHP plants are usually operated to supply heat demand first, the value of the power-to-heat is lower than 1.

3.2.4 Solar Photovoltaic Generation

Hourly solar photovoltaic (PV) generation is estimated from hourly air temperature T_a and hourly global horizontal irradiance (GHI) using the model defined by Equation 7 and adapted from Perpiñan, et al. (2007):

$$E_{PV}(\mathrm{j,h}) = B\ GHI(j,h)(1 - \mu(T_a(j,h) - T_{C,STC}) - \mu\ C\ GHI(j,h), \quad (7)$$

where μ and C are the solar panel temperature and radiation efficiencies, B is a constant parameter equal to the product between the invertor efficiency under standard test conditions (i.e., solar cell temperature $T_{C,STC}$ equal to 25°C and solar irradiance equal to 1,000 Wm^{-2}) and the surface covered by the solar panels (m^{-2}).

3.2.5 Run-of-the river hydropower generation

Hydropower generation from run-of-river power plants depends on the water availability in the river network (Equation 8).

$$E_H(j,h) = \eta_H\ g\ h\ \rho\ Q(j,h), \quad (8)$$

where $E_H(j,h)$ is electricity generation (kWh) during the day j at the hour h, η_H is generator efficiency, Q is river flow that pass through the turbines ($m^3\ s^{-1}$), g is the acceleration of gravity ($m^3\ s^{-2}$), ρ is water density (kg m^{-3}), and h is the head (m). The volume of water that can be diverted from the riverbed to the power plant is limited by both environmental and technical constraints. The first constraint is a minimum water discharge that must remain in the riverbed to preserve the ecological continuity. The maximum water flow that can be diverted to the power

plant depends on the existing infrastructure (e.g., the penstock and turbine capacity). This flow is often defined as *design flow*. The third constraint relates to the safety of the power infrastructure. When the river flow exceeds a given threshold, the safety of the power plant is threatened if it keeps running. To avoid any damages, the generation must stop. Common values for these constraints are 95^{th}, 2^{nd}, and 25^{th} percentiles of the historical flows (Hänggi and Weingartner, 2012; François et al., 2017).

Time series of river flows Q is required for assessing RoR power generation (Equation 8). In this study, we use simulated rather than observed river flows in order to avoid the issue of missing data and gaps in time series. Using simulated streamflow has also the advantage to use a database that is consistent for all the considered basins (both in terms of data quality and availability), which facilitates the comparison among the considered case studies. Note also that using hydrological simulations has been demonstrated to preserve well the complementarity between RoR power generation and solar PV generation in the studied region (François, et al., 2017). We use the Integrated Catchment Hydrological Model (ICHYMOD) to simulate hourly streamflow at the outlet of the considered catchments (Norbiato et al., 2009). ICHYMOD is a semi-distributed rainfall-runoff that includes simulation of the potential evapotranspiration via the Hargreaves formula (Hargreaves and Samani, 1985) and simulation of snow and ice accumulation and melt processes based on the version of TOPMODEL presented by Zaramella *et al.* (2018). The simulation of surface and subsurface flows is carried out by means of the Probability Distribution Model (PDM) from Moore (2007). More detailed information about ICHYMOD is available Appendix A.

3.2.6 Electricity demand modeling

The demand for electricity varies seasonally, with higher demand during cold and hot days associated with usage of heating and cooling systems, respectively. It also varies significantly within a day, with low values commonly occurring at night and high values during daylight hours around noon and late afternoon. Daily demand for electricity is often modeled using the Temperature Dependence Pattern (TDP, Hekkenberg et al., 2009b) that uses a piecewise linear regression of the daily temperature to estimate electricity demand (Equation 9):

$$E_D(j) = \begin{cases} a_{i,j,T_{Heat}} \times [T_{Heat} - T_a(j)] + b_{i,j} & if\ T_a(j) < T_{Heat} \\ b_{i,j} & if\ T_{Heat} < T_a(j) < T_{Cool} \\ a_{i,j,T_{Cool}} \times [T_a(j) - T_{Cool}] + b_{i,j} & if\ T_a(j) > T_{Cool} \end{cases} \quad (9)$$

where $E_D(j)$ is simulated electricity demand for the day j (*Wh*), *T* is air temperature, *i* and *j* are dummy variables refer to the day of the week (weekday, Saturday, Sunday, and holiday periods such as the summer and winter holiday seasons and some relevant religious celebration such as Easter). Simulated daily electricity demand $E_D(j)$ is then downscaled to hourly temporal scale $E_D(j,h)$ by means of a resampling approach described in François, *et al.* (2016a).

3.2.7 Electricity mix of CHP, solar PV and RoR power generation

For a given share of heat supply H_s, the share of the electricity demand that is supplied by generation from CHP plants operating within the district is given by:

$$S_{CHP} = \frac{\sum_{j,h} E_{CHP}(j,h)}{\sum_{j,h} E_D(j,h)} = \frac{\sum_{j,h} A(j) \times H_{CHP}(j,h)}{\sum_{j,h} E_D(j,h)}. \quad (10)$$

Note that the share of the CHP electricity generation results from the share of heat demand H_s covered by the CHP plants within the district (Equation 1). Given the case studies that are further described in section 3, we here consider that solar PV and RoR power plants are operated within the district in addition to CHP power plants, even though the described methodology could be extended to other electricity sources such as wind or tidal energy sources, for example.

Given the 100% renewable scenario (Equation 5 and Equation 11 below), the share of electricity demand covered by solar PV (S_{PV}) and RoR Hydropower (S_{RoR}) power generation can then be defined by:

$$S_{PV} + S_{RoR} + S_{CHP} = 1. \quad (11)$$

The electricity generation from solar PV and RoR within a district is then given by:

$$E_{PV,district}(\mathrm{j,h}) = S_{PV} \frac{\sum_{j,h} E_{PV}(j,h)}{\sum_{j,h} E_D(j,h)} \quad (12)$$

$$E_{RoR,district}(\mathrm{j,h}) = S_{RoR} \frac{\sum_{j,h} E_{RoR}(j,h)}{\sum_{j,h} E_D(j,h)} \quad (13)$$

Note finally that $(1 - S_{CHP})E_D$ is the the residual demand to be supplied by solar PV and RoR. Defining the variable α as the share of the residual demand that is supplied on average by solar PV generation, the share S_{PV} and S_{RoR} can be rewritten such as:

$$S_{PV} = \alpha(1 - S_{CHP}) \quad (14)$$

$$S_{RoR} = (1 - \alpha)(1 - S_{CHP}) \quad (15)$$

The variable α, which ranges from 0 to 1, is further used to discuss the relative contribution from either solar PV or RoR hydropower for a fixed S_{CHP}.

3.2.8 VRE storage

In addition to backup generation capacity, storage is mainly used to balance temporal mismatches between electricity generation and demand. We here considered consider that electricity generation from solar PV can be stored, for instance using batteries (Chaudhary and Rizwan, 2018), which is a scenario very likely for the considered region:

$$S(t+1) = \begin{cases} \min\left[S_{max}, S(t) + \left(\eta_{in} \cdot \Delta(t)\right)\right], & if\ \Delta(t) > 0 \\ \max\left[S_{min}, S(t) + \left(\eta_{out} \cdot \Delta(t)\right)\right], & if\ \Delta(t) < 0 \end{cases}, \quad (16)$$

where S is the storage, S_{max} and S_{min} are the maximum and minimum capacities of the storage, η_{in} and η_{out} are the efficiencies of storage and power generation. For the sake of simplicity, we here assume a perfect storage with generation and storage efficiencies η_{out} and η_{in} both equal to unity. S_{min} is set to 0. A range of maximum storage capacity S_{max} is considered. It includes storage capacities that correspond to 3, 6, 12, 24, 48, and 72 hours of hourly average demand. Electricity is stored when solar PV generation is larger than the demand and, inversely, stored electricity is released when generation for all available sources during the current time step is lower than the demand.

3.3 Application

3.3.1 Study Area

The study area is located in the Upper Adige River basin (Figure 3.1). In this region, the share of heat demand covered by generation from CHP plants within the various district-heating systems is significant. For instance, in 2014, CHP power plants supplied the district heating systems more than 1,050 GWh, which nearly corresponded to 25% of the regional heat demand

(http://www.eurac.edu/). Electric or gas heating are commonly used in the area to supply the remaining heat demand.

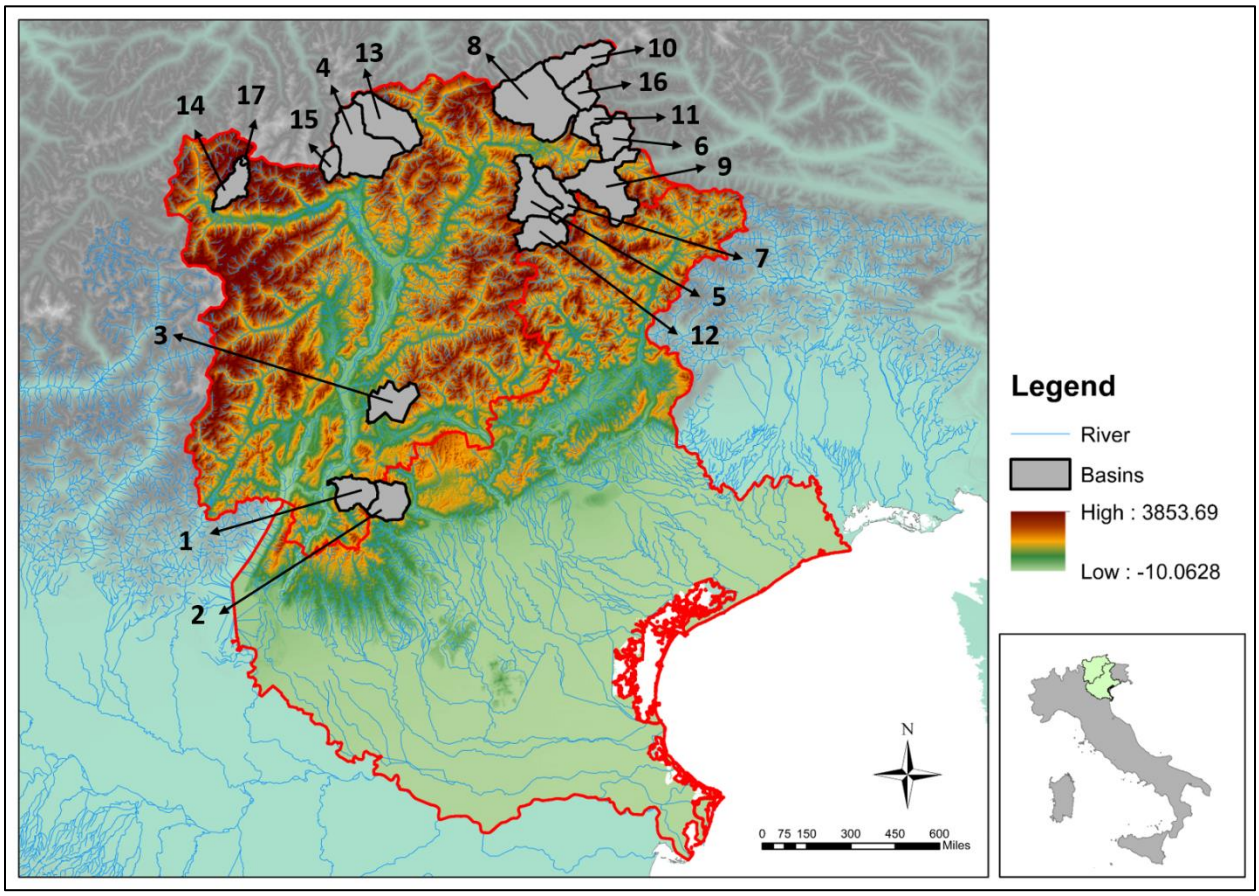

Figure 3.1 Map of the study area. Considered basins are highlighted in grey colors. The various basins are ranked (e.g., from 1 to 17) according to their ratio between solid precipitation and total precipitation (S/P ratios are given in Table 1).

The regional electricity demand is supplied by a combination of several production means and resources. Taking advantage of the elevation ranges and the above-average precipitation within the mountainous area, electricity generation from numerous hydropower plants (either dammed or run-of-the river power plants) supplies most of the regional electricity demand. Part of the electricity supply comes also from privately owned solar photovoltaic rooftop systems. Note that power capacity of rooftop PV systems is on the rise due to increasing environmental concerns from both policy makers and public (cf. for example the C3-Alps project; http://www.c3alps.eu). Electricity generation from CHP plants used for district heating also

contributes to supply. As an example, Prina et al. (2018) explain that CHP generation fueled by forest biomass in one of provinces in our study area, South Tyrol, covers 50% of its heat demand and contributes roughly 10% in its renewables mix to supply electricity demand in 2014. Hydropower generation, producing almost 200% of electricity demand, is the main electricity source in South Tyrol and 3690 GWh out of 5663.8 GWh of its generation is exported to other regions. CHP is used to be a back-up source to supply the electricity demand of this province. According to the grid operator (Gestore Servizi Energetici, GSE 2018), the electricity production of CHP, hydropower, and solar power in Northeastern Italy in 2016 are 686.3 GWh, 9165 GWh, and 2319 GWh. Based on the above description, Northeastern Italy is an interesting study area that uses the high shares of VREs, and CHP plants for producing electricity and heat.

Within the study area, we specifically focus on a set of 17 basins (Figure 3.1). We deliberately chose small basins with surface areas ranging from several km to slightly less than 400 km^2 (Table 3.1). Focusing on small basins allows considering each basin as a potential urban or sub-urban district within which the balance between heat/electricity supply and the demand is solved using the analysis framework presented in Section 3.2. The location of the considered basins also allows exploring the sensitivity of the energy balance to a range of climate conditions. Basins are indeed located at elevations ranging from slightly more than 1,000 meters to more than 3,000 meters (Table 3.1). The changing climate conditions with the elevation impacts hydrology regimes, with larger influence of snow accumulation and melt processes on streamflow in high elevation and larger influence of rainfall events at lower elevations (e.g., from convective systems during fall season). This dependence between elevation and hydrology regimes is illustrated in Table 3.1 via the ratio between snow and total precipitation (S/P ratio). High S/P ratio values (i.e., above 0.6) show a snowmelt dominated hydrologic regime while low S/P ratio values indicates a rainfall-dominated regime (i.e., below 0.4). Hydrology regimes at locations with intermediate S/P ratio values (i.e., in-between 0.4 and 0.6) are influenced by both snow accumulation and melt dynamic and by rainfall events.

No	Basin Name	Area (km^2)	Mean elevation (m.asl)	S/P ratio
1	Leno	113.0	1139.5	0.16
2	Posina Stancari	116.0	1268.0	0.20
3	Fersina	138.0	1373.5	0.21
4	Passirio at Saltusio	292.2	1850.5	0.35
5	Gadera at Mantana	166.8	1882.5	0.36
6	Casies at Colle	117.0	1969.0	0.37
7	San Vigilio at Longega	103.7	1990.5	0.37
8	Aurino at San Giorgio	380.2	2077.5	0.48
9	Rienza at Monguelfo	264.5	2087.5	0.48
10	Aurino at Cadipietra	155.8	2156.0	0.52
11	Anterselva at Bagni	82.7	2161.5	0.59
12	Rio Gadera	124.9	2170.0	0.63
13	Ridanna at Vipiteno	204.6	2171.0	0.64
14	Mazia at Adige	99.8	2309.5	0.72
15	Plan at Plan	49.8	2447.0	0.73
16	Riva at Seghe	78.9	2460.0	0.72
17	Mazia Glacierized	5.39	3116.0	0.86

Table 3.1 Main characteristics of the considered basins. S/P ratio is the ration between solid precipitation and total precipitation. A high S/P ratio is observed for hydrologic regime dominated by snowmelt while a low S/P ratio usually indicates hydrology regimes more dominated by precipitation events variability.

3.3.2 Database

We use a large panel of databases that are either open source datasets available online or directly provided by local and regional environmental agencies. We below describe these various databases and give references and locations when available. Given the temporal availability of the needed database, the analysis extends over a period of nine years starting in 2000 and ending at the end of 2008. The considered time step is hourly so that the daily cycles of electricity demand and solar PV electricity generation are accounted for.

The hydrology model ICHYMOD requires observed temperature and precipitation over the considered basins. Temperature and precipitation gage data were provided by the regional environmental agency. However, high quality observations over long periods are lacking at several locations, especially in the high altitude catchments where good quality observations are critical to correctly model snowpack accumulation and melt processes. When needed, we

adjusted temperature and precipitation observations at lower altitudes to higher elevation using specific seasonal correction factors. More details about this adjustment are available Chapter 2. For modeling the demand for heat and hot water (Equation 3), we use the total annual demand H_D for the year 2014 provided by EURAC (c.f. http://www.eurac.edu and Prina et al. (2018). Hourly air temperature T_a used for assessing the heating degree-day HDD (Equation 2), solar PV generation (Equation 7) and the electricity demand (Equation 9) are ground observations mentioned above. We also assume that each basin (i.e., district) have a constant population p of 10,000 inhabitants. The hourly electricity consumption data used to calibrate the model are obtained from the European Network of Transmission System Operators of Electricity (ENTSOE, https://www.entsoe.eu/home/). Note that we used the model parameters calibrated by François et al., (2016a) for the study area. Hourly Global Horizontal Irradiation (GHI) data used for simulation of solar PV generation (Equation 7) are reanalysis data available from the EXPRESS-Hydro database (Silvestro et al., 2018). According to most common CHP plant specification in Trentino Alto-Adige and Veneto regions, CHP are operated so that the power-to-heat ratio A varies at a seasonal basis (Equation 6). During cold months (November through February), CHP electricity generation is low ($A = 0.15$) to prioritize heat generation. During summer months (May to August), CHP electricity generation is increased ($A = 0.45$) since heat demand is usually low at this season. For the rest of the year, the power-to-heat ratio takes an intermediate value ($A = 0.30$).

3.4 Results

3.4.1 Outlook of the energy and electricity balance within the districts

Figure 3.2 illustrates the heat and electricity demand and generation in Mazia at Adige and Posina at Stancari districts under the 100% heat penetration scenario (i.e., $H_s = 1$). These two districts illustrate very distinct climate conditions within the study area. Mazia at Adige is located at high elevation where winters are cold. Snowfall being the main source of precipitation at this elevation, hydrology is mainly influenced by snowpack accumulation and melt dynamics. On the other side of the spectrum, Posina at Stancari is located at lower elevation, temperatures are milder, and the influence of rainfall on hydrology regime dominates over snowfall as streamflow regime is more influenced by the occurrence of storms during spring and fall seasons.

Due to its lower altitude, and thus higher average temperature, both heat and electricity demand within Posina district are lower than for Mazia's. In both districts, heat demand has much larger seasonal variations than electricity demand. Because of the considered 100% heat penetration scenario (i.e., $H_S = 1$), heat generation varies at a monthly basis with monthly generation equal to the average monthly demand (Figure 3.2, left). CHP electricity generation (Figure 3.2, right) follows from the combination between the CHP heat generation pattern and the power-to-heat ratio (cf. Section 3.2). As a result, CHP electricity generation is maximum during mild months as a tradeoff between mild air temperature and relatively high power-to-heat ratio.

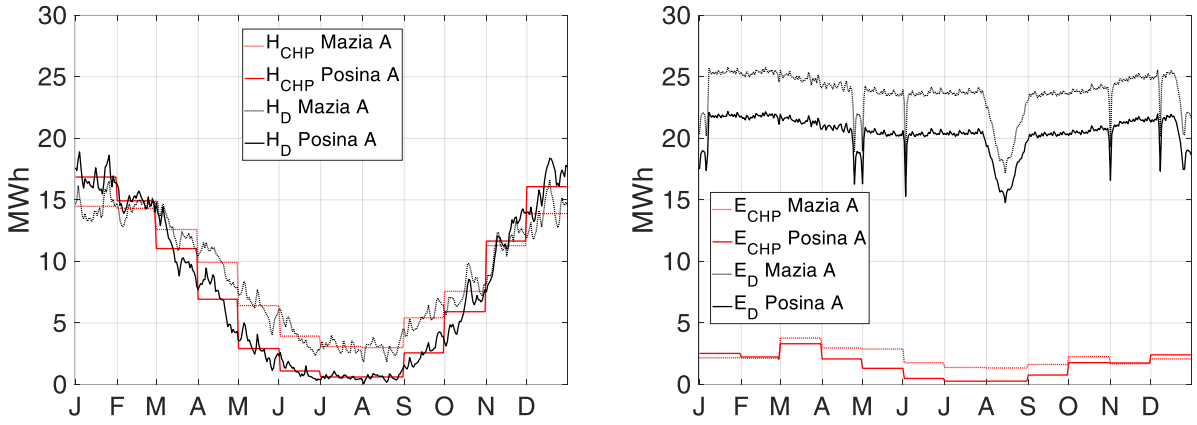

Figure 3.2 Left: Seasonal heat demand and CHP heat generation in Posina at Stancari district (written as Posina, catchment #2 on Figure 1) and Mazia at Adige district (written as Mazia A, catchment #14 on Figure 1). Right: Seasonal electricity demand and CHP electricity generation in Posina and Mazia A. Note: the average cycle are obtained over the period 2000 – 2008. Heat demand values are smoothed by 10-days moving window. Significant decreases in electricity demand follow from major holiday period in Italy.

Figure 3.3 illustrates the daily and seasonal profiles of electricity generation and demand for the two-above districts. We note that solar PV generation is rather consistent across the two districts, which suggests a rather low impact of the elevation range on solar PV variability at both daily and seasonal scales. On the other hand, RoR hydropower generation profiles differ significantly from low to high elevations, which obviously results from differences in snowpack dynamic that plays a more important role at high elevation (e.g., François et al., 2016a). For Mazia at Adige, hydropower generation peaks during summer months (i.e., from mid-May to mid-September) when snow and ice melt rates are maximum. Besides this period, generation is

low due to the winter drought period. Further South, at lower elevation where Posina at Stancari is located, RoR hydropower generation presents a completely different seasonal pattern as generation is low from mid-June through September and high during Spring and Fall seasons when intense precipitation and rainfall-over snow events are common and lead to moderate to high flows. CHP electricity generation patterns are rather similar at low and high elevation, although the seasonality is more pronounced at low elevation mainly due to warm temperatures in summer season that almost reduce heat demand to null values while demand can still be significant in high elevation at this season (Figure 3.2). At a seasonal scale, we retrieve the well-known result that generation variability is larger than electricity demand variability. Combining these different energy sources in the right proportion could thus help reducing the total generation variability and better match electricity demand.

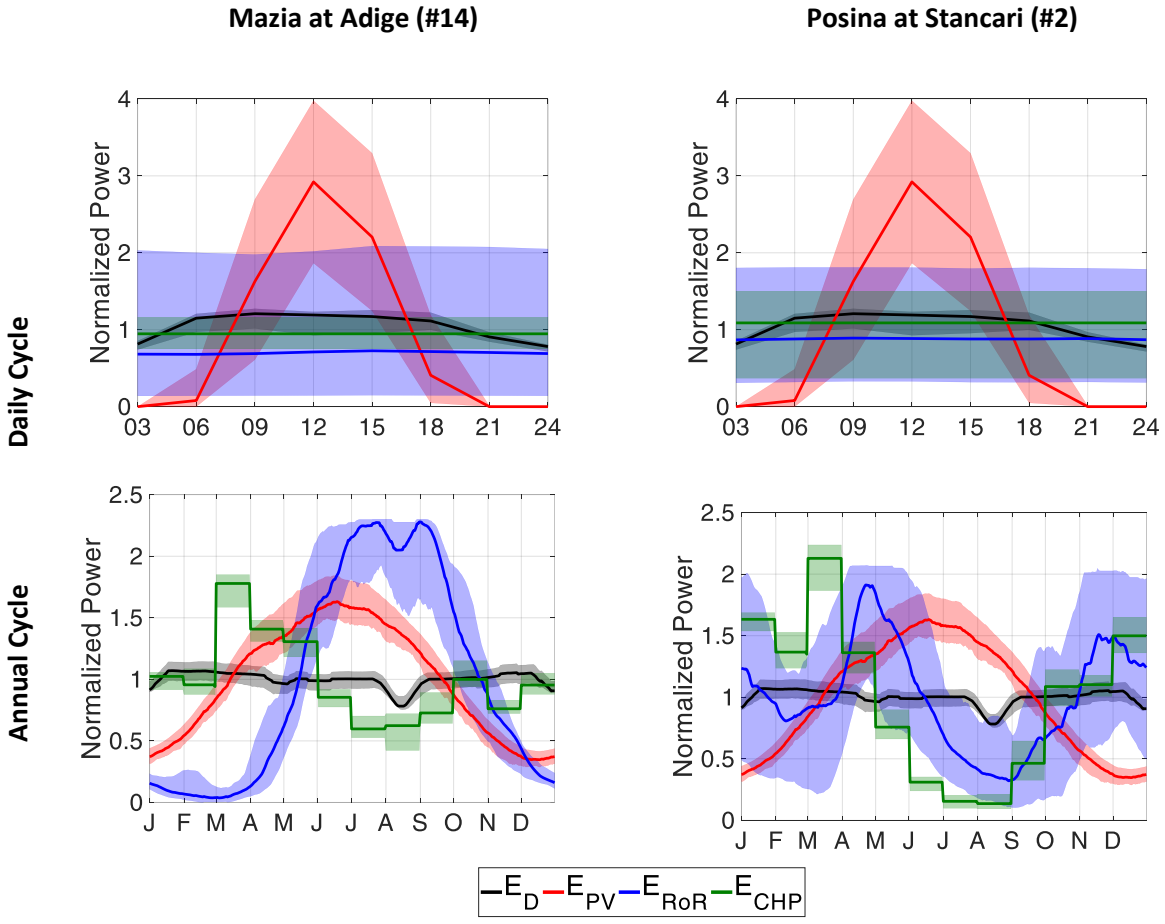

Figure 3.3 Daily (first row) and annual (second row) average cycles of solar PV (red), RoR hydropower (blue) and CHP (green) electricity generation for Mazia at Adige district (left column) and Posina at Stancari district (right column). Demand is illustrated in black color. Average cycles are obtained for the

period 2000-2008. The shaded areas illustrate the variability by showing the deviation between the 25th and 75th percentiles. Annual cycles are smoothed over a 10-day period. All cycles have been normalized (average=1) to highlight the various patterns of demand and electricity generation at both temporal scales.

3.4.2 Effect of CHP integration on the electricity balance

The development of CHP within district heating systems is likely to affect the electricity demand satisfaction and the variability of the electricity balance. As detailed in Section 3.2, we assume that within the considered districts solar PV and RoR hydropower are, in addition to the incidental electricity generation from CHP plants, the two other sources for electricity. Considering the 100% renewable scenario defined by equations 5, 11 and 14, an increase in CHP electricity generation (i.e., an increase in S_{CHP}) that follows from an increase in CHP heat penetration (i.e., an increase in H_s), replaces electricity generation from solar PV and RoR hydropower (i.e, decreases either S_{PV}, S_{RoR} or both). This section describes the effect of replacing solar PV and/or RoR power to CHP power generation while CHP heat penetration increases.

We note on Figure 3.4 that for Mazia at Adige and Posina at Stancari districts, without CHP plants (S_{CHP}), neither solar PV generation (α=1) nor RoR hydropower generation (α=0) alone maximizes the demand satisfaction or minimizes the electricity balance variability. Instead, combining solar PV and RoR power generation appears to be beneficial for the system. This result is consistent with previous study that analyze the complementarity between PV and RoR hydro in Europe (e.g., (François, *et al.*, 2016b). We also note that when solar PV and RoR power generation is combined with the incidental electricity generation from CHP plants, demand satisfaction improves and the variability of the temporal mismatch between demand and total generation reduces. This mainly follows from the fact solar PV and RoR power plants have to be curtailed during peak generation around noon for solar PV and during the high flows seasons for RoR plants (cf. Figure 3.3). On the other hand, CHP electricity generation has low penetration, and so even for high CHP heat penetration levels (cf. Figure 3.2 right and S_{CHP} coefficients in Table 3.2 that are almost always lower than 10%). As such, CHP generation can fully be absorbed by the demand (i.e., no curtailment/loss of generation). Replacing solar PV and RoR power capacity,

which generates losses due to their significant variability, by CHP electricity generation that does not lead to losses even for high heat penetration, is thus an efficient way to maximize demand satisfaction for the same amount of generated electricity. For a given share between solar PV and RoR (i.e., for a given α coefficient), the increase in demand satisfaction (or decrease in electricity balance variability) appears to be a linear function of the CHP heat penetration (i.e., H_S coefficient). This is shown on Figure 3.4 by the constant distance between two consecutive curves in color (for a given α). This result implies that, from the electricity balance perspective, there is no drawback in integrating CHP power up to a heat penetration of 100% (i.e,. $H_S = 1$).

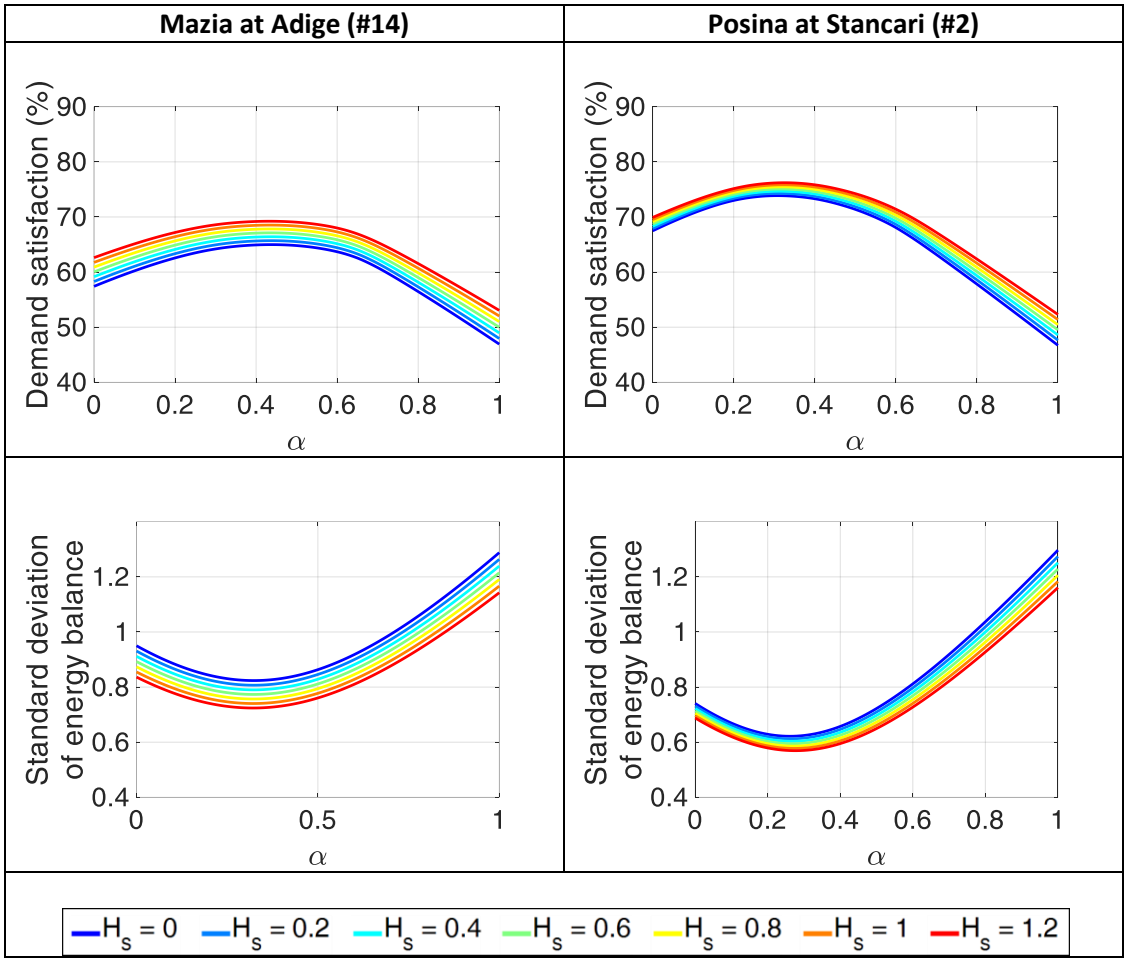

Figure 3.4 Demand satisfaction (first row) and standard deviation of the electricity balance (second row) as function of the share of solar PV generation (α) that covers the residual load (1-S_{CHP})E_D. Note that the share of RoR hydropower generation is (1- α). Results for Mazia at Adige and for Posina at Stancari are illustrated in the left and right columns respectively. The various curves in color show changes in

demand satisfaction and electricity balance variability as a function of the penetration level of CHP heat generation.

Basin	H_s scenario	S_{CHP}	S_{PV}	S_{RoR}	Demand Satisfaction (%)	Losses due to temporal mismatches (%)	Stdev electricity balance (scaled value)
Mazia at Adige (S/P=0.72)	0	0.00	0.44	0.56	64.98	35.02	0.82
	0.2	0.02	0.43	0.55	65.70	34.3	0.81
	0.4	0.04	0.42	0.54	66.41	33.59	0.79
	0.6	0.06	0.42	0.53	67.12	32.88	0.77
	0.8	0.07	0.40	0.53	67.82	32.18	0.76
	1	0.09	0.39	0.52	68.53	31.47	0.74
	1.2	0.11	0.38	0.51	69.22	30.78	0.72
Aurino at San Giorgio (S/P=0.48)	0	0.00	0.26	0.74	71.55	28.45	0.70
	0.2	0.02	0.26	0.73	72.15	27.85	0.69
	0.4	0.04	0.25	0.71	72.75	27.25	0.67
	0.6	0.05	0.25	0.70	73.34	26.66	0.66
	0.8	0.07	0.24	0.69	73.92	26.08	0.65
	1	0.09	0.24	0.67	74.50	25.5	0.63
	1.2	0.11	0.23	0.66	75.07	24.93	0.62
Posina at Stancari (S/P=0.20)	0	0.00	0.31	0.69	73.87	26.13	0.62
	0.2	0.02	0.31	0.68	74.27	25.73	0.61
	0.4	0.03	0.30	0.67	74.67	25.33	0.60
	0.6	0.05	0.31	0.65	75.07	24.93	0.59
	0.8	0.06	0.30	0.64	75.46	24.54	0.59
	1	0.08	0.30	0.63	75.84	24.16	0.58
	1.2	0.09	0.30	0.61	76.21	23.79	0.57

Table 3.2 Effect of CHP integration on demand satisfaction, variability of the electricity balance and contribution from solar PV and RoR hydropower electricity sources. Results are shown for three districts with different climate conditions; Mazia at Adige (S/P=0.72), Aurino at San Giorgio (S/P=0.48) and Posina at Stancari (S/P=0.20)

Figure 3.5 illustrates the change in demand satisfaction and electricity balance variability along the climate transect shown on Figure 3.1. We note that districts located in snow-dominated catchments benefit more from the integration of CHP plants than districts located in rain-fed catchments. This is both true in term of demand satisfaction (Figure 3.5, top) and electricity balance variability (Figure 3.5, bottom). This difference does not come from the balance at the hourly scale for which the generation patterns for each energy source are almost identical over both rain-fed and snowmelt dominated catchments (Figure 3.3, top). This result actually follows from the difference in complementarity at the seasonal scale between solar PV and RoR power generation in both climate areas. In snowmelt dominated areas, because solar PV and RoR power

are both maximum during summer months (Figure 3.3), the contribution from each energy source to the optimal mix is nearly even. RoR power has actually a slightly higher share than solar PV has (i.e, 56% and 44% respectively, Table 3.2) because its generation does not collapse to null values during the night and can thus supply demand during dark hours. This means that even for the optimal combination, a significant fraction of the generated power is lost (i.e., about 35%, Table 3.2). We note on Table 3.2 that when CHP plants are used within the district to supply heat demand, electricity from CHP replaces both solar PV and RoR power generation in proportion nearly equal. On the other hand, for districts located in rain-fed catchments, the initial complementarity between solar PV and RoR power is better. This can be observed looking at the seasonal patterns on Figure 3.3 or by comparing the demand satisfaction values in Table 3.2 for the scenario $H_S = 0$. In this case, the initial proportion of solar PV is significantly lower than the one observed for snowmelt dominated areas (i.e., 31%, Table 3.2), likely to prevent losses at both daily and seasonal scale. As a result, the integration of electricity from CHP plants mainly replaces RoR power generation, which, with a higher initial share (69%, Table 3.2), is more likely to have losses.

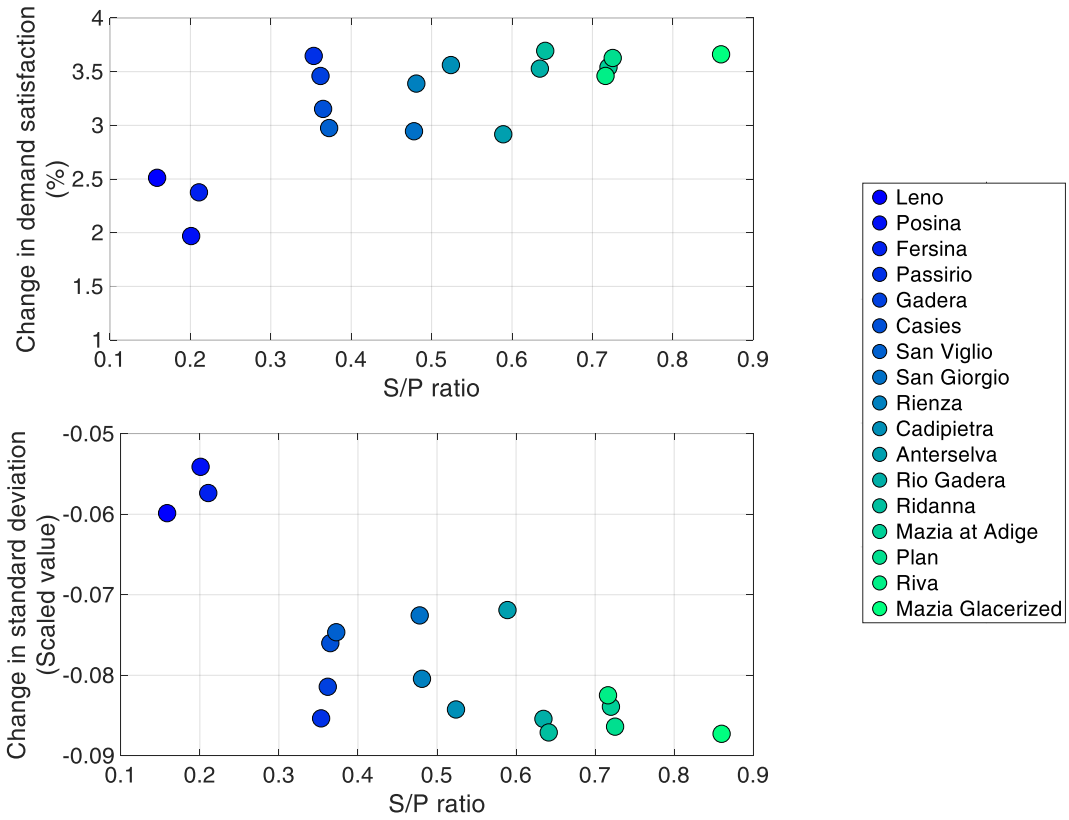

Figure 3.5: Change in electricity demand satisfaction (top) and electricity balance variability (bottom) when moving from an urban/sub-urban area with no district heating system ($\mathrm{H_S} = 0$) to an area equipped with a district heating system covering 100% of the heat demand (i.e., $\mathrm{H_S} = 1$). The considered districts are ordered according to their ratio between snowfall and total precipitation (S/P). The change in demand satisfaction are obtained by comparing the demand satisfaction (or the standard deviation of the electricity balance) for the best energy mix with or without CHP plants within the district (i.e., either $\mathrm{H_S} = 0$ or $\mathrm{H_S} = 1$).

3.4.3 Effect of solar PV storage in addition to CHP integration

Figure 3.6 illustrates the increase in demand satisfaction for Mazia at Adige and Posina at Stancari heating districts ($H_S = 1$) when a storage capacity for solar PV is considered (i.e., one day of average load storage capacity). By construction, the storage capacity for solar PV generation has no effect if the district only uses RoR power generation in addition to electricity from CHP plants (i.e., when α=0). Even for low shares of solar PV, the influence is not significant. This is explained by the fact that at low penetration level (i.e., low α values), solar PV generation is likely to remain below the load, which means no loss. However, if solar PV is the main source

of electricity with CHP (e.g., value for α lager than 0.6), the increase in demand satisfaction is sharp for the first hours of storage capacity. The marginal increase in demand satisfaction for additional storage capacity above 12 to 24 hours is then not significant, which highlights the fact that in-between 12-24 hours of average load storage is enough to prevent the districts from losing a significant amount of solar PV generation. This results clearly follows from the strong daily pattern for solar PV that dominates its seasonal pattern.

For both catchments, as soon as solar PV share is large enough so that PV storage matters, the optimal share of solar PV tends to increase. However, the response of the two considered districts is different. For Mazia at Adige (Figure 3.6, left), as soon as PV storage capacity is larger than 6 hours, the share of PV that maximizes the demand satisfaction becomes α=1, which means that RoR is no more required in the mix. For Posina at Stancari (Figure 3.6, right), the optimal share of PV is close to 0.6, which means that even when a significant storage capacity is given for solar PV generation, the complementarity among RoR, Solar PV and CHP generation is such that RoR is somehow as valuable as storage.

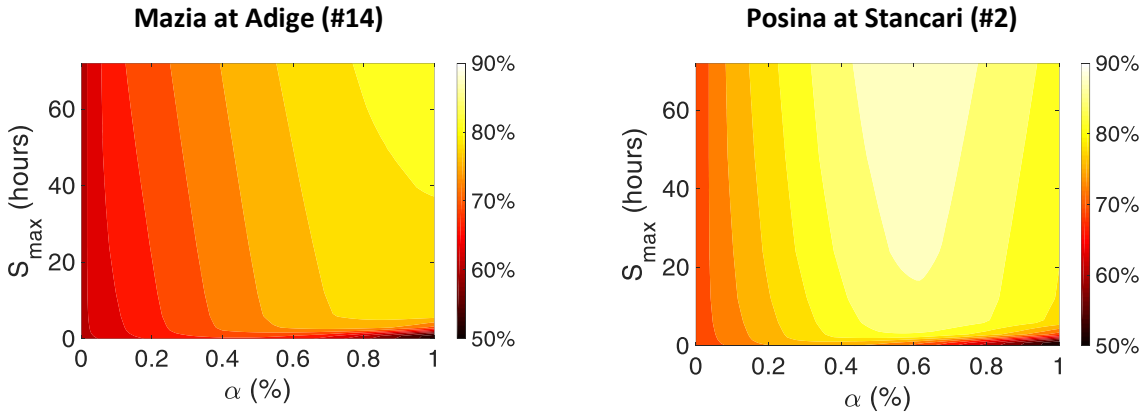

Figure 3.6 Influence of storage capacity available for solar PV (y-axis) on the electricity demand satisfaction (color map) as a function of the share between solar PV and RoR power generation within the mix (x-axis). Results are shown for Mazia at Adige (top) and Posina at Stancari (bottom) and are obtained for a CHP heat penetration level $H_s = 1$, which correspond to CHP electricity share $S_{CHP} = 0.09$ and $S_{CHP} = 0.08$, respectively

The influence of PV storage capacity on the optimal demand satisfaction (i.e., the one obtained by using the optimal share of each electricity source) is illustrated on Figure 3.7 with and without a district heating system. As discussed previously, solar PV share increases significantly with PV storage capacity for snowmelt dominated Mazia catchment (i.e., up to 91%), while it barely gets larger than 56% for the rain-fed Posina catchment. When CHP plants are integrated within the districts, PV storage above 6 hours of average load capacity leads to the complete abandon of RoR power generation in the energy mix, while nearly 40% of RoR remain for rain-fed catchments, once again highlighting the better complementarity between solar PV and RoR plants in this climate area.

When comparing the demand satisfaction with and without CHP for different solar PV capacity (Figure 3.7, third row), we note that whatever the storage capacity, CHP integration always increases the demand satisfaction. The larger increase associated with the integration of CHP within the district located in snowmelt dominated catchments (cf. Section 3.4.2) tends to be become similar to the one obtained for rain-fed catchments as soon as PV storage gets larger than 1 day of average load storage.

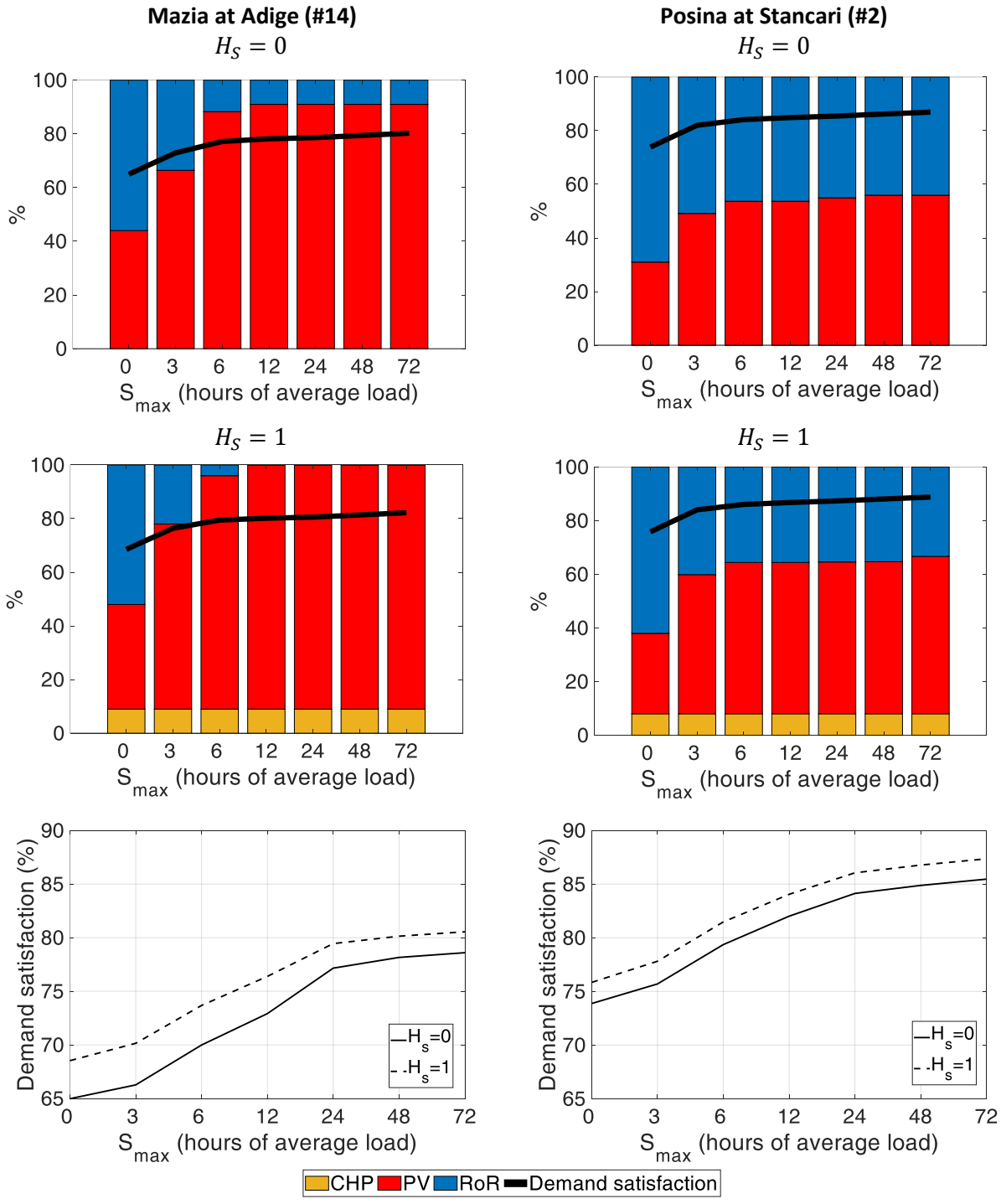

Figure 3.7 Influence of PV storage capacity (x-axis) on demand satisfaction (black line, %) and on the optimal mix combination between solar PV and RoR (top) and solar PV, RoR and CHP (middle). The color bars show the share (%) of each electricity source. The third rows compare the demand satisfaction with and without CHP plants within the districts. Results are shown for Mazia at Adige (left columns) and Posina at Stancari (right column).

3.5 Conclusion

District heating systems become more common worldwide with the development of CHP technology. Although driven by the heat generation, CHP electricity generation can provide a low fluctuating base generation that could reduce the need in variable renewable capacity. This study investigates this scenario by combining at the district level CHP electricity generation with both solar PV and RoR hydropower generation. The results show that integration of CHP electricity reduces the variability and the electricity balance and increases the demand satisfaction, and this for all the considered locations along a climate transect in the Northeastern Italian Alps.

The introduction of CHP plants within a district may modify the optimal contribution from solar PV and RoR power generation. These modifications appear to be more significant for location where hydrology and associated RoR power generation are dominated by the intermittency of rainfall events of storms. In these locations, the electricity from CHP tends to replace more generation from RoR generation for which the seasonal patterns are less complementary to match the electricity demand (cf. Figure 3.3).

It is also interesting to highlight that for districts with installed solar PV storage capacity, for instance a storage capacity that correspond to 12 hours of average demand), using CHP plants may appear to be a better solution for increasing further the demand satisfaction than building more storage. For instance on Figure 3.7 (bottom), when comparing the demand satisfaction for Posina at Stancari with or without CHP, one note that a system with CHP and 12 hours of solar PV storage provides a similar demand satisfaction than a system without CHP but with double solar PV storage capacity (i.e., 24 hours). As such, decision makers willing to invest in both a district heating system based on CHP cogeneration and in new renewable power capacity, accounting for the avoided cost for electricity storage could be wise.

Several future research works should follow this preliminary analysis. For instance, our results are based on a single CHP technology (i.e., biomass) while other technologies with different constraints in their operations could provide different results. While the currently operations of the considered CHP plants (i.e., power-to-heat ratio) have been chosen regarding the heat demand, they could be optimized to increase even more the electricity demand

satisfaction, while solar PV and RoR power losses could be in turn used to generate heat via centralized heater systems. Applying the developed analysis framework could also allow considering other renewable energy sources such as wind. Finally, the assessment of the robustness of the above conclusion within a climate change context would be interesting, especially since heat demand is likely to decrease in the future warmer climate. As a result, CHP plants operators could increase electricity generation at the expense of heat generation. Such a change in the operations of the CHP plants would modify the temporal patterns of CHP electricity generation, and thus its complementarity with other energy sources. This question remains explore thus far.

Chapter 4

Statistical analysis of energy supply droughts from renewable energy sources across an Alpine transect[3]

[3]This chapter is based on a paper that has been prepared as: **Puspitarini, H.D.**, François, B., Borga, M. 2019. Statistical analysis of energy supply droughts from renewable energy sources across an Alpine transect. Manuscript in preparation

4.1 Introduction

A power system, comprising a fleet of electricity generators and a transmission system that links those generators to electricity users, is planned and operated to avoid shortfalls between electricity demand and supply, and it is deemed adequate if shortfall risk is managed at a sufficiently low level. Planners typically schedule new generating capacity investments to deal with the effects of projected socioeconomic change (e.g., population growth) and capacity retirements, although there is a growing body of science literature highlighting the mechanisms by which climate change may affect power shortfall risk. On the demand side, warming temperatures are likely to affect power loads for building heating and cooling (Auffhammer et al., 2017; Dirks et al., 2015; Shen, 2017; Wang and Chen, 2014). On the supply side, the integration of Variable Renewable Energies such as wind, solar, and hydro-power (hereafter denoted as VRE) allows for the replacement of conventional electricity production means and thus reduce GHG emission (Moriarty and Honnery, 2012) . However, the inherent intermittency of the VREs and their much larger variability with respect to the electric load (François et al., 2016b) may trigger the occurrence of supply deficiency and imbalance of production and demand. Engeland et al. (2017) recently review the intermittent and variable features of VRE across a large range of temporal and spatial scale. They especially highlighted that complementary among VREs in time and space can reduce the variability of power supply and help matching the electricity demand curve that is much less variable in time. Several previous studies investigate the complementarity among demand and several VREs. Heide et al. (2010) consider the co-variability of wind and solar power in Europe; François et al. (2016a) analyze the solar power and hydropower complementary in Northern Italy; Bagatini et al. (2017) investigate solar-, wind-, and hydropower complementarity in Brazil and François et al. (2016b) assessed the complementary between those three VREs in 12 regions of Europe.

One limitation of these studies is that the production-demand mismatch is typically represented by means global statistics, for instance by using the standard deviation of the energy balance or the penetration rate. A more comprehensive form of analysis is needed if results are used for informing practical power system policy and planning. First, shortfall risk may be misrepresented if the assessment fails to incorporate the dynamics of the whole interconnected

power system (Miara et al., 2017) . For example, climatic variability may impair the generating capability of a particular resource type, and the associated impact may be absorbed if it occurs during a non-peak demand season. Climate impacts must therefore be placed in a broader systems context by studying the response of regional power supply networks. A second complexity—rarely assessed—is the potential for compound events caused by multiple interacting weather-related impacts. For example, a trend of warmer, drier summers with increased occurrence of heatwave and drought conditions may cause higher peak loads and reduced water availability simultaneously. Studied separately, these impacts may be insufficient to register concern. But taken in the combination, these events may cause severe power shortfalls (Turner et al., 2019) .

Raynaud et al. (2018) introduce the concept of "energy drought" with two distinct definitions: i) Energy Production Droughts as uninterrupted periods with a power production less than a low production threshold, and 2) Energy Supply Droughts as uninterrupted periods with mismatch between production and demand. Energy Production Droughts are a signature of weather and hydrometeorological variability. Conversely, Energy Supply Droughts depend on both demand and production, and are therefore controlled by a number of socio-economic and technical factors, including those pertaining to the energy mix and the power system considered. Raynaud et al. (2018) were able to show strong variations in Energy Drought patterns among twelve regions located in Europe and North Africa (each region having a surface area of about 40000 km^2) by using a daily temporal resolution.

The objective of this work is to characterize the main statistical properties of energy supply droughts and to identify suitable probability distribution for the prediction of energy droughts associated to specific return periods, by using a fine temporal resolution (hourly data are considered). More specifically, this study analyzes the statistical distribution of the duration, severity and energy supply drought peak. The study presents the analysis of the effect of a 100% renewable energy mix composed by solar and run-of-the-river (RoR) in Northern Italy where these two energy sources are the main renewable energy sources. The analysis is carried out along an Alpine transect characterized by a climate gradient from the Alpine crest (snow melt dominated area) to the Veneto plain (rainfall dominated area). On the transect, solar power is

generated in the flat plain, and run-of-the-river hydropower over two medium size mountainous basins, Aurino at Cadipietra and Posina at Stancari, representing snow- and rain-dominated areas, respectively. We characterize the drought properties for all possible mixes of these two sources of energy, analyzing in this way the climatic control on the statistical distribution of energy drought duration, severity and peak.

The meteorological and hydrological datasets are presented in section 4.2, whereas the different weather-to-energy conversion models and the energy drought properties are described in Section 4.3. The statistical analysis is illustrated in Section 4.4, whereas section 4.5 concludes our study.

4.2 Study area and data availability

The statistical analysis is carried out along a climate transect going from the Alpine crest to the Veneto plain, with a focus on relatively small, rural communities (Figure 4.1). This transect provides a range of climatic, environmental and ecological variability. It includes runoff regimes that gradually move from snow-melt dominated to rainfall dominated, with a ratio of solid to liquid precipitation decreasing from 0.6 in the northern part to almost 0 in the Veneto plain.

Two catchments in the transect (Figure *4.1*4.1), that have different hydroclimatic regimes, have been chosen as the study area. These are Aurino at Cadipietra (149.8 km^2) and Posina at Stancari (116 km^2). The altitude range of Aurino at Cadipietra is 1,049 to 3,263 m asl and Posina at Stancari is 390 to 2,146 m asl.

Aurino at Cadipietra has a snow-dominated regime with a mean annual precipitation around 1,500 mm and a fraction of precipitation as snow around 60%. The mean annual streamflow is 6.2 m3/s with a flow peak in summer due to snow and ice-melt contribution. As a rain-dominated catchment, Posina at Stancari is characterized by a fraction of precipitation as snow around 20%. The mean annual precipitation and streamflow for this basin is 1,325 mm and 3.7 m^3/s. Streamflow in Posina at Stancari is concentrated on spring and autumn, due to large precipitation contribution during these seasons.

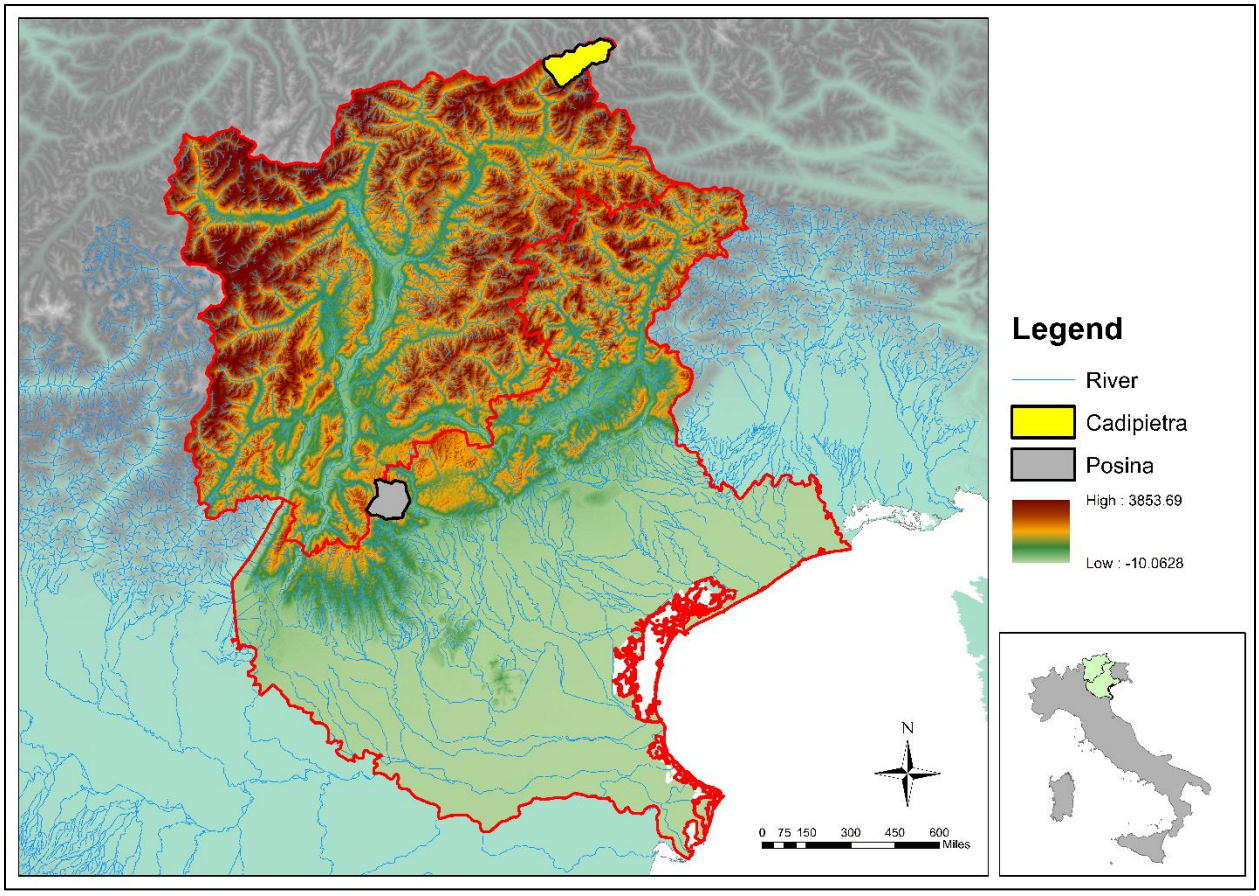

Figure 4.1 Location of Aurino at Cadipietra and Posina at Stancari catchments in Northeastern Italy

The period selected for the statistical characterization of the supply energy drought ranges from 1992 to 2011. Over this period, discharge data are available from the streamgauges located at the outlet of the two study for simulating Run-of-River generation at hourly temporal resolution. Solar radiation and temperature data are available from 17 stations managed by the Regional Environmental Protection Agency of Veneto (ARPAV) over the period 1992 – 2011 to simulate solar PV generation and electricity demand.

4.3 Energy drought and models of energy production and demand

4.3.1 Energy drought property

Energy drought (ED) events are defined based on the energy Supply Deficit (SD) at time t as follows:

$$SD(t) = \max[D(t) - P_{mix}(t), 0] \quad (1)$$

where *D(t)* is demand at time t and $P_{mix}(t)$ represents the total power generation from the different energy sources.

An energy drought event is a period with an uninterrupted positive Supply Deficit. **Error! Reference source not found.** provides a definition sketch of energy drought events and of the relevant properties. Each energy drought event is characterized by six main properties: energy drought duration (Dd), energy drought severity (Sd), energy drought intensity peak (Id_{peak}), energy drought intensity mean (Id_{mean}), drought interarrival time (Ld), and number of events per year (Ev). Dd is defined as the number of consecutive intervals (hours) where SD remains positive. Sd is defined as a cumulative SD value during a drought period, $Sd = \sum_{i=1}^{Dd} SD(t)$. Ld is defined as the period elapsing from the initiation of a drought to the beginning of the next drought. Id_{peak} is the maximum SD value within a drought period and Id_{mean} is the ratio of severity and duration (Sd/Dd). Ev is total number of drought events per year.

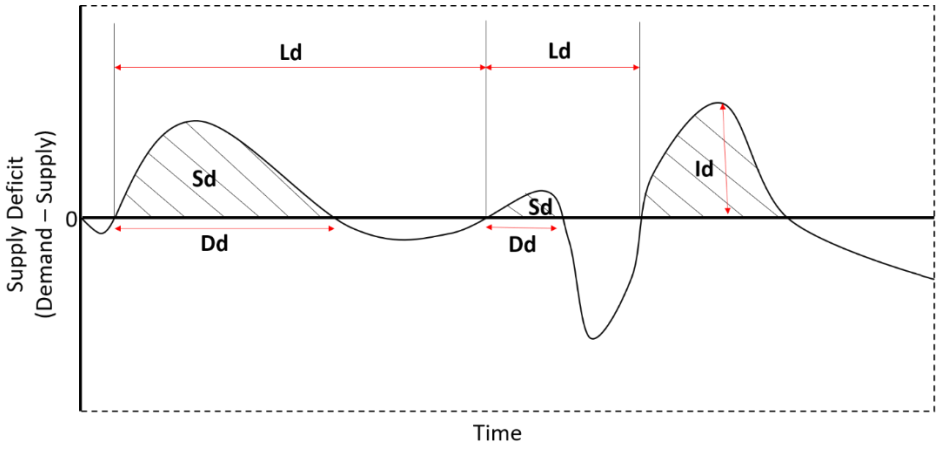

Figure 4.2 Definition sketch of energy drought events and of the relevant properties. Dd is energy drought duration, Sd is energy drought severity, Id is energy drought intensity, and Ld is the interarrival time.

We then classify the drought events based on their energy drought severity. For the energy drought severity, we consider two thresholds with severity equal to 48 hours and 72 hours of the average demand), respectively. The two thresholds are identified with s = 48 and s = 72, respectively. As a consequence, three energy drought classes are considered in the study; i) All droughts includes all drought events without any threshold application (s = 0), ii) Medium droughts contains drought events which exceed the first threshold (s = 48), and iii) Large droughts, which includes the events exceeding the second threshold (s = 72).

4.3.2 Run-of-river generation

Electricity generation from run-of-the river power plant at time t ($P_{RoR}(t)$) is computed as follows:

$$P_{RoR_{(Snow\ or\ Rain)}}(t) = \eta_H\ g\ h\ \rho\ q(t) \quad (2)$$

where P_{RoR} is power generation (kW) in rain- or snow-dominated area, η_H is generator efficiency, q is runoff flowing through the turbines of power plants (m^3s^{-1}), g is the acceleration of gravity (m^3s^{-2}), ρ is water density (kgm^{-3}), and h is the head (m). For the sake of environmental and power plant safety, we apply two flow boundaries, Q_{min} and Q_{max}. Q_{min} is the minimum flow that has to remain in river network for preserving the ecosystem and Q_{max} is the maximum flow that can pass the turbine for power plant safety. Another threshold called design flow threshold (Q_d) is also applied in this model to limit the maximum flow that can be extracted from the river to the plant. The values of Q_{min}, Q_{max}, and Q_d are 95th, 2nd, and 25th percentiles of the flows following Hänggi and Weingartner (2012).

4.3.3 Solar photovoltaic generation

PV generation at time t ($P_{PV}(t)$)is simulated based on the model from Perpiñan, et al. (2007):

$$P_{PV}(t) = B.Rad(t)(1 - \mu(T_a(t) - T_{C,STC}) - \mu.C.Rad(t)) \quad (3)$$

where *B* is a parameter for converting from direct to alternative current under the standard test condition (cell temperature, $T_{c,STC}$, equals to 25°C and solar radiance, $I_{c,STC}$, equals to 1000 Wm^{-2}), *Rad* is observed solar radiation, T_a is air temperature, μ and *C* are the conversion reduction factors based on temperature and radiation.

4.3.4 Electricity demand

We use the electricity consumption model for Italy developed by François et al. (2016a) because observed electricity consumption in our study area is not available. This model allows the accountability of temperature increase to the of electricity consumption. This model simulates the Temperature Dependence Pattern of daily electricity consumption identified from the observed data that is provided by European Network of Transmission System Operators of electricity (https://www.entsoe.eu/home/). A resampling approach is then used to downscale daily consumption to hourly data. The reader is invited to read the study by François et al. (2016a) for a comprehensive description of this model.

4.3.5 Energy mix

To simulate the varying effect of snow- and rain-dominated runoff regime on RoR generation along the climatic transect, we used the runoff data for the Aurino and for the Posina as representative for a snow-dominated and a rain-dominated regime, respectively. A mixed run-of-the-river power generation from these two hydro-climatic regions P_{RoR} is given by:

$$P_{RoR}(t) = S_H P_{RoR_{Snow}}(t) + (1 - S_H) P_{RoR_{Rain}}(t) \quad (4)$$

where $P_{RoR_{Snow}}$ and $P_{RoR_{Rain}}$ are the hydropower generated by RoR plants located on snowmelt and rainfall dominated regions, respectively, and S_H is the sharing coefficient between the two hydro-climatic regions ($0 < S_H < 1$). When $S_H = 1$, the hydropower generation comes only from the Alpine area and when $S_H = 0$, the hydropower generation comes from the downstream area only.

Power generation time series obtained for each production mean (RoR and PV) are scaled to obtain a regional 100% scenario. To do this, PV and RoR power time series are divided by their

average and multiplied by the load average. The average production of the mix is thus equal to the average of the simulated electricity consumption of the study area during the whole period 1992-2011.

Power generation from a combination of solar PV and RoR power generation is then obtained using a sharing coefficient as follows:

$$P_{mix}(t) = s_{PV}P_{PV}(t) + (1 - s_{PV}).(S_H P_{H_{Snow}}(t) + (1 - S_H)P_{H_{Rain}}(t)) \quad (5)$$

where P_{mix} is the power generation from the combined system, S_{PV} is the sharing coefficient of solar power ($0 < S_{PV} < 1$), and P_{PV} is solar power generation. When $S_{PV} = 1$, the power generation comes only from solar PV and when $S_{PV} = 0$, the power generation comes only from RoR.

Our sensitivity study explores 121 scenarios of energy mix defined by different sharing coefficients S_{PV} and S_H ranging from 0 to 1 using regular steps of 0.1 (Figure 4.3).

We use mean, coefficient of variation (ratio of standard deviation over mean values, CV), and autocorrelation function (ACF) to explore the effects of different PV and RoR combination on the drought properties for the events in the three severity classes. Based on this analysis, we selected annual maxima for the identification of suitable probability distribution models for the various energy drought properties. Given the limited samples, we use the L-moment method from Hosking and Wallis (1997) to identify the probability models based on the four different sampling spaces defined in Figure 4.3.

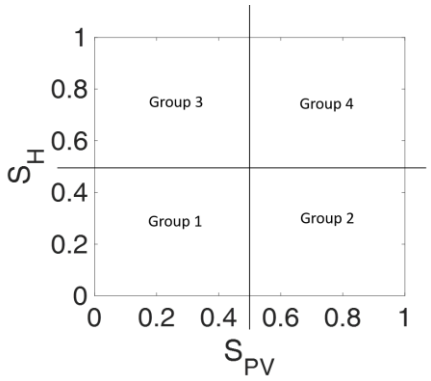

Figure 4.3 Sampling regions used to identify suitable probability distributions for the energy drought properties.

4.4 Statistical characterization of energy droughts

Figure 4.4 illustrates the daily and annual pattern of electricity demand and generation from the various sources considered here. Figure 4.4a illustrates the large variability of solar PV generation, compared to RoR generation and demand, at the daily scale. Examination of the annual cycle (Figure 4.4b), shows that the shortage of PV production is located during the winter season, due to short daytime length. RoR from snow-dominated area shows a production shortfall during winter because of snow and ice accumulation. RoR production from snow-dominated area (RoR_{snow}) starts increasing during spring and summer because of the snow and ice melt. Typically, RoR form rain-dominated area exhibits a shortfall at the beginning of spring and in middle of summer because precipitation is lower during those months. The shortage and different peak timing between PV and RoR generation shown in Figure 4.4b triggers the imbalance between demand and generations.

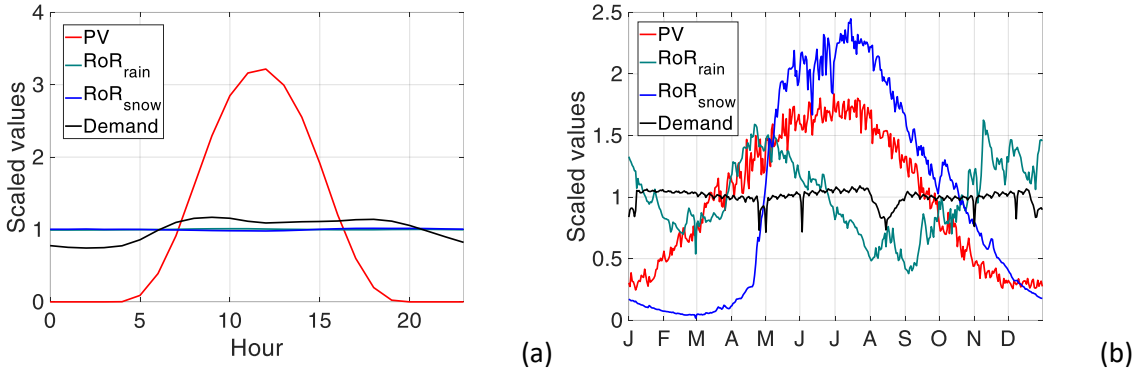

Figure 4.4 Daily (a) and annual cycle (b) of electricity demand (black) and generation from PV (red), RoR from Aurino at Cadipietra (blue), and RoR in Posina at Stancari (green).

The analysis of the statistical properties of the energy droughts is presented in the following for the three different classes. The corresponding results are reported in Figure 4.5a for all energy droughts, in Figure 4.5b for medium energy droughts (s = 48) and in Figure 4.5c for large energy droughts (s = 72). Each figure reports the mean, CV, and ACF for the six drought properties (drought duration, severity, peak intensity, mean intensity, interarrival time, and number of events per year).

Figure 4.5a shows that for supply system that depends only on PV (S_{PV} = 1, S_H = 0), mean drought duration is even less 18 hours. The duration increases by decreasing S_{PV} and in particular it increases for supply systems with S_{PV} equals 0 and S_H equals 1 or 0. The daily pattern of irradiance, with no irradiance at night, is clearly related to the large number of low duration (less than one day) energy droughts for PV-ruled systems. A system, which integrates high share of either $P_{RoR_{Snow}}$ or $P_{RoR_{Rain}}$, have the lowest number of event per year, with a duration which is 40% longer than that for PV-ruled systems. Systems which depend on snow-dominated runoff regimes are characterized by very long mean values of duration, due to the seasonal pattern of deficit revealed by Figure 4.4b. Figure 4.5a shows also that the pattern of drought duration is strongly correlated with severity, and that the pattern of drought peak strongly resembles with drought mean intensity. The pattern of the number of events per year is just the inverse of that of duration, with the number of hourly drought events increasing from 60 times per year for low values of S_{PV} = 0 to 366 times per year for S_{PV} = 1. The energy drought peak increases by roughly 100% moving from S_{PV} = 0 to S_{PV} = 1, while the share parameter S_H exerts limited impact..

The high correlation between duration and severity mean is also emerging in the pattern of CV of both properties. In a similar way, CV of peak and the mean intensity have similar patterns which are different from those reported for duration and severity. Globally, this shows that with increasing the share parameter of S_{PV}, i) the mean values of duration and severity decreases, together their variability ii) the mean values of peak and of the mean intensity increases, whereas their variability decreases, iii) the number of events per year increases.

Moreover, ACF values of duration and severity lessen rapidly from 1 to 2-hours of time lag, when we apply low share of PV. When we use high share of RoR, ACF drops below 0.5 at around 6 hours for all properties. These results show that both duration and severity have the lowest decorrelation time, particularly for Spv=0,5.

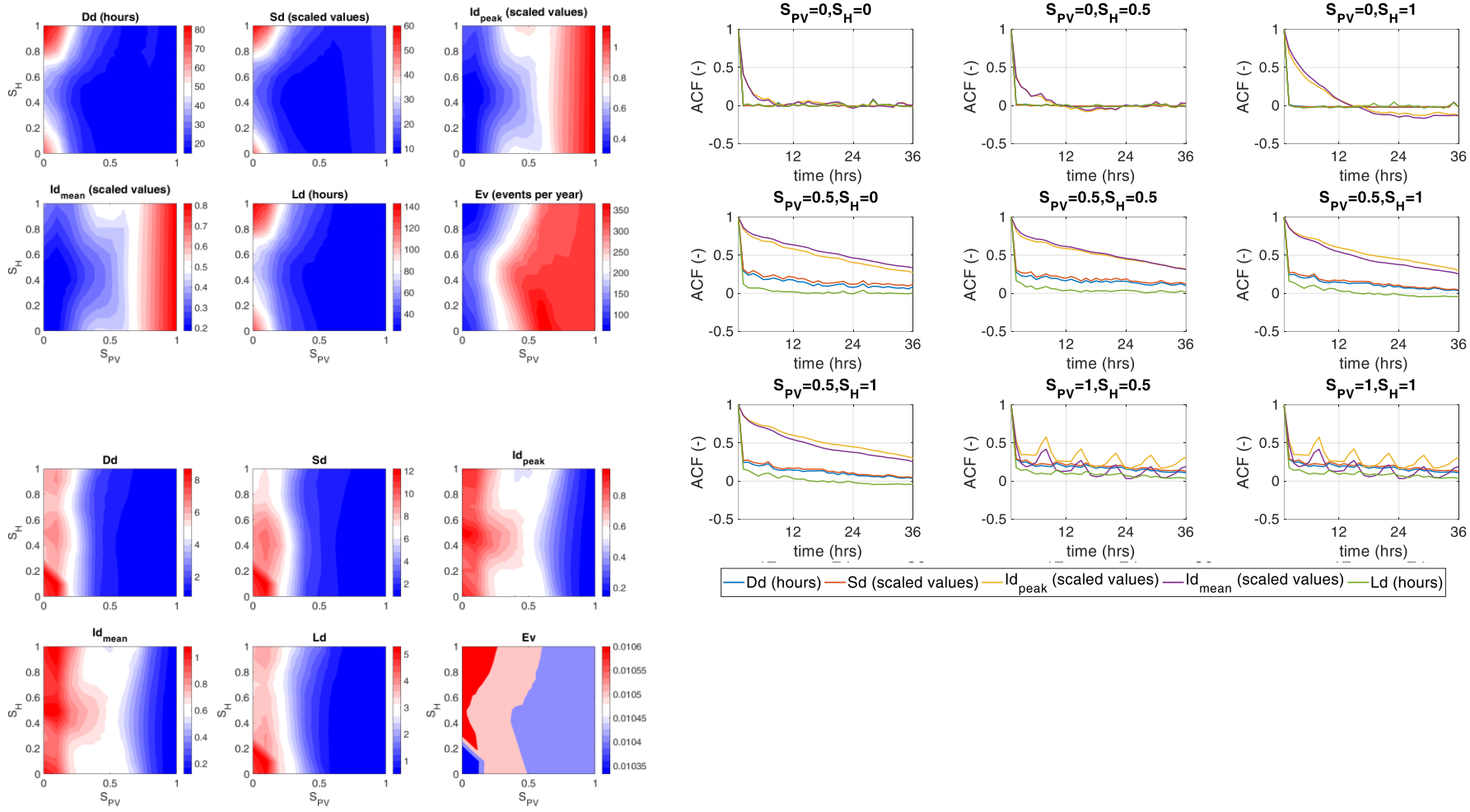

Figure 4.5a Mean (upper left), CV (lower left), and autocorrelation function (ACF) (upper right) for 6 drought properties for all drought (s = 0). Lag time in the ACF plots (x-axis) is in hours and ACF values in y-axis is in logarithmic scale.

When considering medium and large droughts (Figure 5b,c), the values of all the properties increases, with the obvious exception of the number of events per year. The lowest mean values of durations for medium and large drought are 100 and 200 hours, respectively.

The pattern of duration, severity, and interarrival time are almost similar with those reported for the 'all drought' class (Figure 5a). However, the pattern of peak intensity shows some important changes. For medium droughts, low peak intensity appears for PV less than 0.3. For large droughts, low peak intensity also happens for low share of PV. Another noticeable pattern change is the changes in number of events per year. In the 'all drought' class, the highest number of events per year correspond to high share of PV. for the 'medium drought' class, there are two combinations that have high number of events per year (more than 7 times per year): S_{PV} at least 0.3 and S_H at least 0.5, and low S_{PV} – low S_H. For the 'large drought' class, combinations that have high number of events per year are more concentrated in high S_{PV} – high S_H, and in low S_{PV} – low S_H. These shifted combinations of high number of events per year from s = 0 to s = 72 is caused by the shortage production of RoR from both hydrological regimes. It is also worth to be noted that the beneficial effect of mixing together RoR from snow and rain-dominated runoff regimes becomes less evident with increasing the magnitude of the events.

Autocorrelation values from both medium and large droughts show low values (less than 0.5) for all drought properties. Thus, by applying the severity threshold, we are able to analyze not only the rare events but also the independent events.

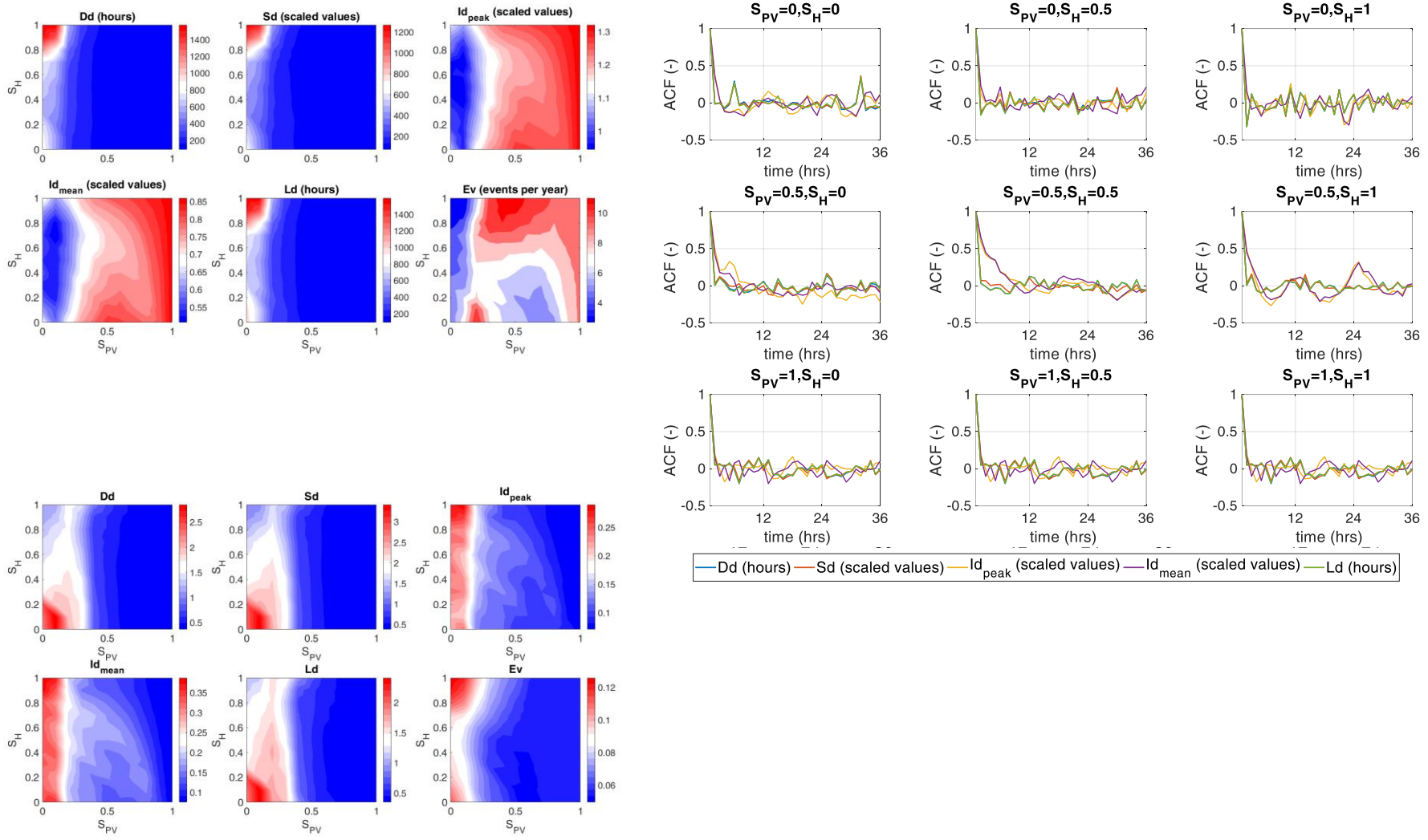

Figure 4.5b Same as Figure 5a, but for medium droughts (s = 48)

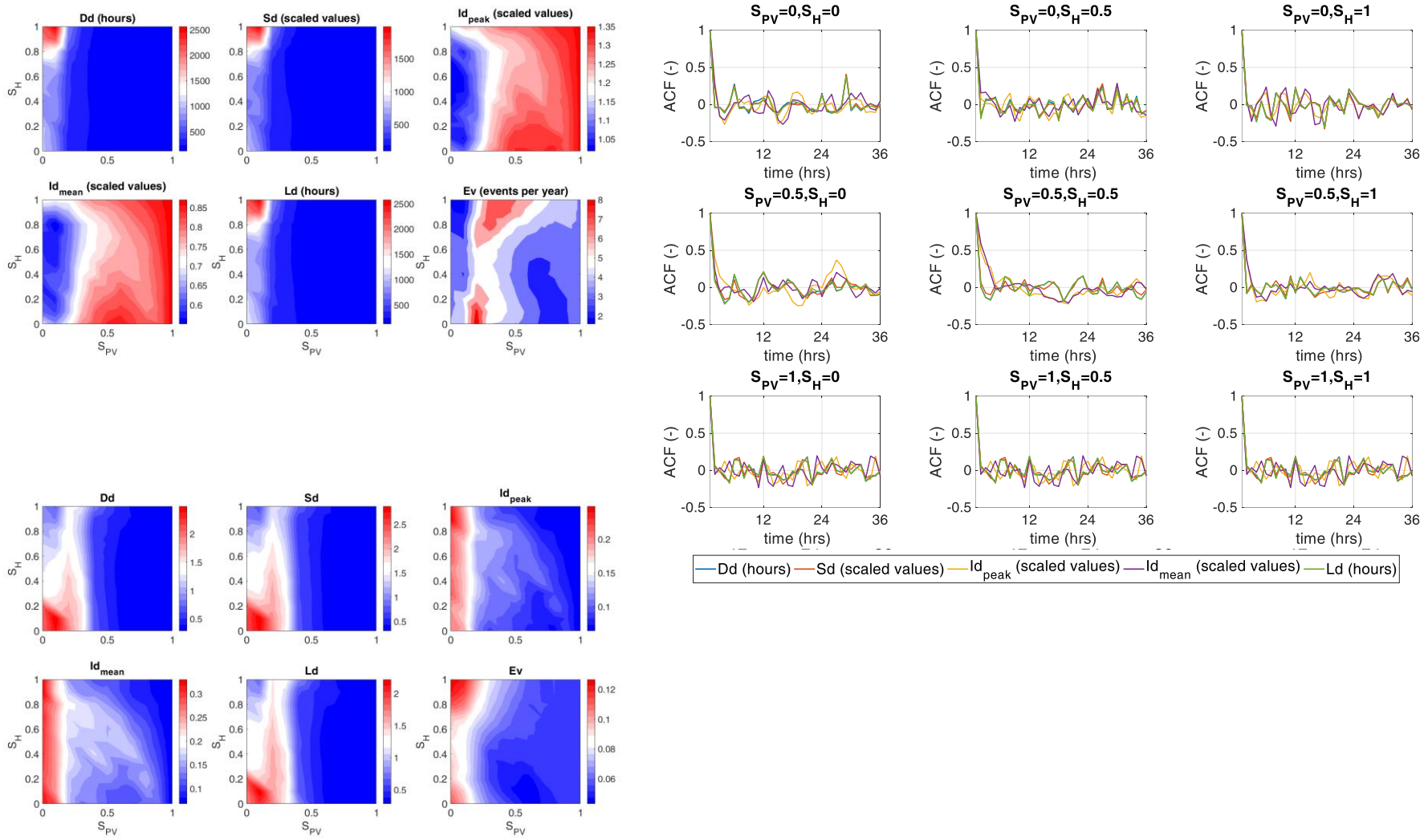

Figure 4.5c Same as Figure 5a, but for large droughts (s = 72)

Error! Reference source not found.5 show that the pattern of duration and severity are similar, as well as that of peak and mean intensity. To analyze the relation between drought characteristics, we then calculated the correlation between three drought properties for the case of large droughts (Figure 4.6). Figure 4.6a show that duration and severity exhibit very high correlation. This is expected, because severity is the deficiency accumulation during the drought, thus most of long drought duration correspond to large severity. Correlation between duration and peak (Figure 4.6b) is generally less than 0.6, therefore less that the correlation between duration and severity. We also check the relation between peak, duration, and severity using the correlation analysis of peak and mean intensity since mean intensity is the ratio of severity over duration. Results show that high correlation is in low S_{PV} and high S_H. The shortage of RoR during winter triggers big severity and long duration, but low peak of drought.

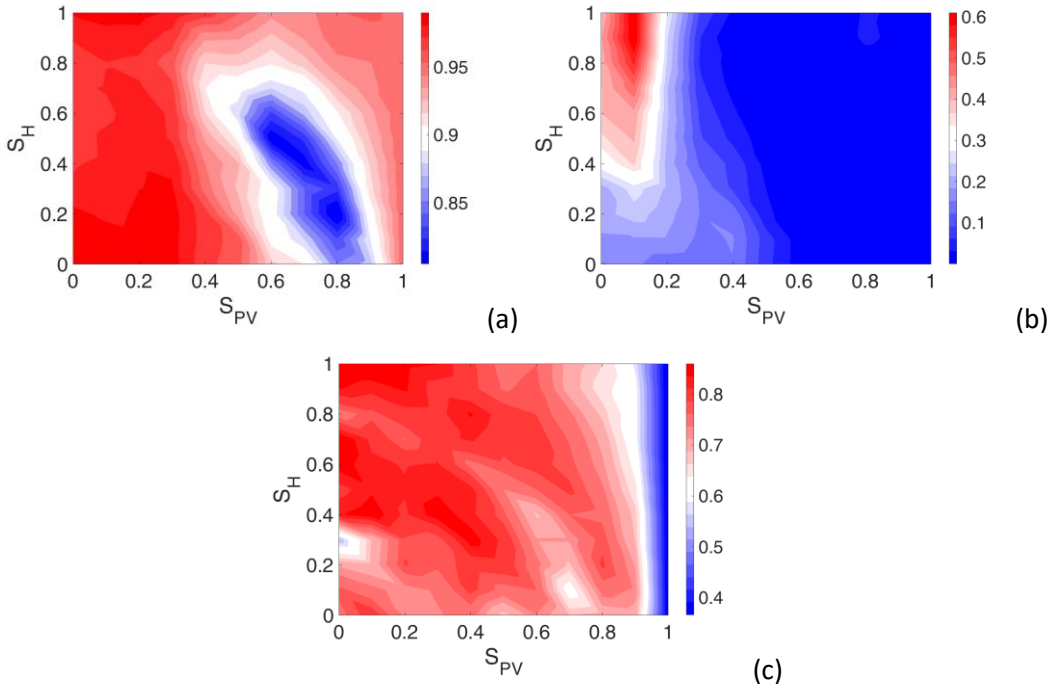

Figure 4.6 R-square values between duration and severity using s = 48 (a), between duration and peak intensity (b), and between peak intensity and mean intensity (c)

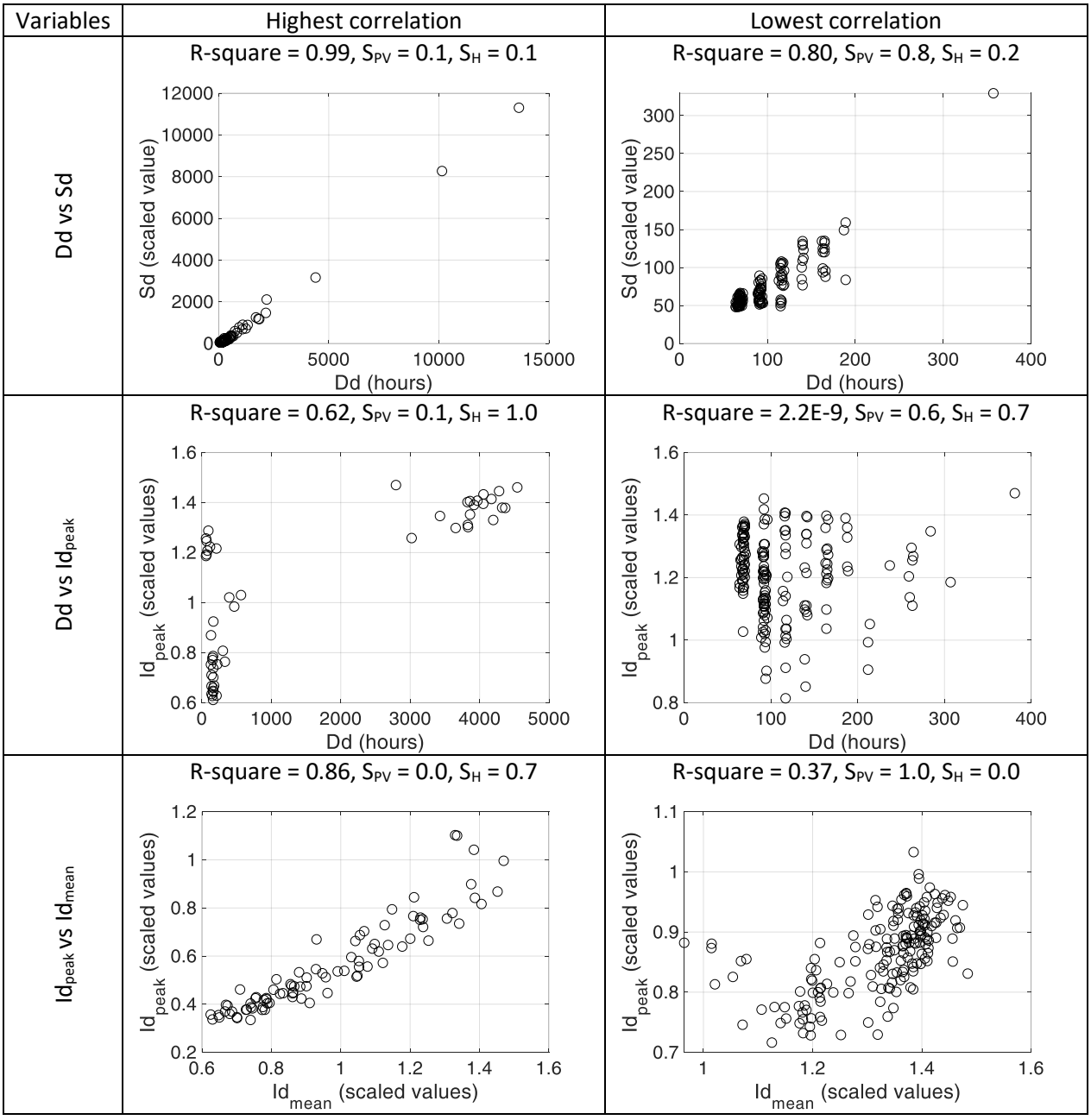

Figure 4.7 Scatter plots for best and worst correlation from Figure 4.6 between; duration and severity, duration and peak intensity, peak intensity and mean intensity

Further than mean and CV, we analyze also the pattern of skewness of the three main drought properties: duration, severity and peak. The relevant patterns are reported in **Error! Reference source not found.** The patterns are similar, but the ranges of the skewness values show different variability between duration and intensity, on one side, and between severity and intensity, on the other side. Duration and severity plot show that both properties are right-skewed or has positive skewness (**Error! Reference source not found.**a and **Error! Reference source not found.**b) meaning that duration and severity data are concentrated in their low values. The highest skewness for duration and severity is in low S_{PV}-low S_H combination, i.e. for RoR in rain-dominated runoff regime. This corresponds to cases of hydrological droughts that were observed during the study period. Peak intensity is mostly skewed to the left or has negative skewness (**Error! Reference source not found.**c). Although most of peak intensity data from low S_{PV} have positive skewness, the value is not as high as the skewness of duration and severity.

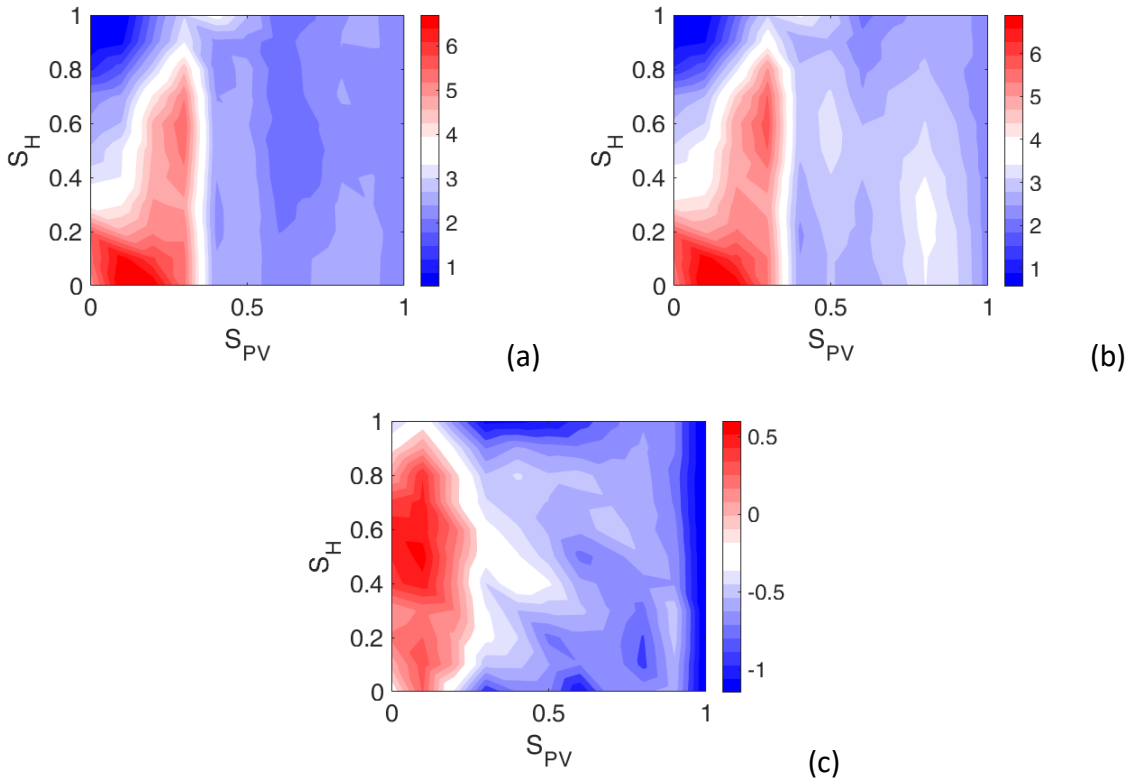

Figure 4.8 Skewness of duration (a), severity (b), and peak intensity (c) from medium severity threshold (s = 48)

4.5 Assessment of frequency distributions

We used the method of L-Moment (see Hosking and Wallis, 1997) to identify suitable frequency distributions for the analysis of the three main drought properties. Moreover, we applied the method by considering the four different sampling regions reported in Figure 4.3. A common method for pooling summary statistics from different sites is the index variable procedure. The main assumption of an index variable procedure is that the sites in a homogeneous region have an identical frequency distribution apart from a site-specific scaling factor, the index variable. The index variable is usually the mean of the site specific data (Hosking and Wallis, 1997) . Regional analysis involves the following steps: i) identification of the region, i.e., the sites that belong to the region, and testing whether the proposed region is homogeneous, ii) choice of the distribution to fit the regional data, and iii) estimation of parameters and quantiles.

For testing the quality of the region identification, we used a heterogeneity measure called the *H*-statistic, which is used to compare the between site variation in sample *L*-moments for a group of sites with what would be expected for a homogeneous region. To determine what would be expected, repeated Monte Carlo simulations of a homogeneous region with sites having record lengths equal to those of the observed data are performed. A large positive value of the *H*-statistic indicates that the observed L-moments ratios are more dispersed than is consistent with the hypothesis of homogeneity. Generally, a region is said to be heterogeneous if $2<H\leq4$; it is described as strongly heterogeneous if $H>4$.

For the identification of suitable frequency distributions, we compared the relation of L-Kurtosis versus L-Skewness for various commonly used distributions with the corresponding relations obtained from the at-site and regional data. Furthermore, we use the Z-statistic introduced by Hosking and Wallis (1997). This statistic was developed for three-parameter distributions and measures how well the theoretical L-kurtosis of the fitted distribution matches the regional average L-kurtosis of the observed data. The fit of the distribution is considered satisfactory if $|Z|\leq1.64$, corresponding to an acceptance of the hypothesized distribution at a confidence level of approximately 90% (Hosking and Wallis, 1997).

The application of the methodology to the data series included in the four regions displayed in Figure 4.3 is summarized in Figure 4.9a,b,c, for duration, severity and peak intensity, respectively. The statistical assessment revealed that the four regions are homogeneous. However, the three drought properties may be fitted with different probability models. According to the plot of L-moment ratio diagram in Figure 4.9a and Figure 4.9b, the best probability distribution for drought duration and severity are the Generalized Logistic Distribution and Pearson Type III (indicated as GLO and PE3 in Figure 4.9). Specifically, duration in group 2 and 4 follow GLO, while other groups follow PE3. Severity group 2, 3, and 4 may follow GLO, while group 1 follow PE3. This result agrees with the explanation from Ahmad et al. (1988) who state that Generalized Logistic Distribution is suitable for data that have heavy tail, such as flood and drought, represented by high positive skewness in the duration and severity data (Figure 4.8).

Meanwhile, all groups of peak intensity follow Generalized Extreme Value distribution (indicated as GEV in Figure 4.9). As stated by Martins and Stedinger (2000) and Holmes and Moriarty (1999), Generalized Extreme Value distribution is suitable for analyzing extreme values or high peak values. Thus, drought properties corresponding to large droughts should be modelled with different probability distributions.

Quantiles for return time equal to 10 and 20 years are reported for event duration and peak intensity in Figure 4.10. As expected, the figures corresponding to the two return times are strikingly similar, showing (for the duration) a decrease with an increase of S_{PV}, and (for small values of S_{PV}) an increase for values of S_H corresponding to 1 and to 0. The first of these last peaks is due to the observed increase in mean duration, whereas the last is due to the increase of CV of the duration. The opposite behavior emerges for the peaks, with a general increase with increasing S_{PV}.

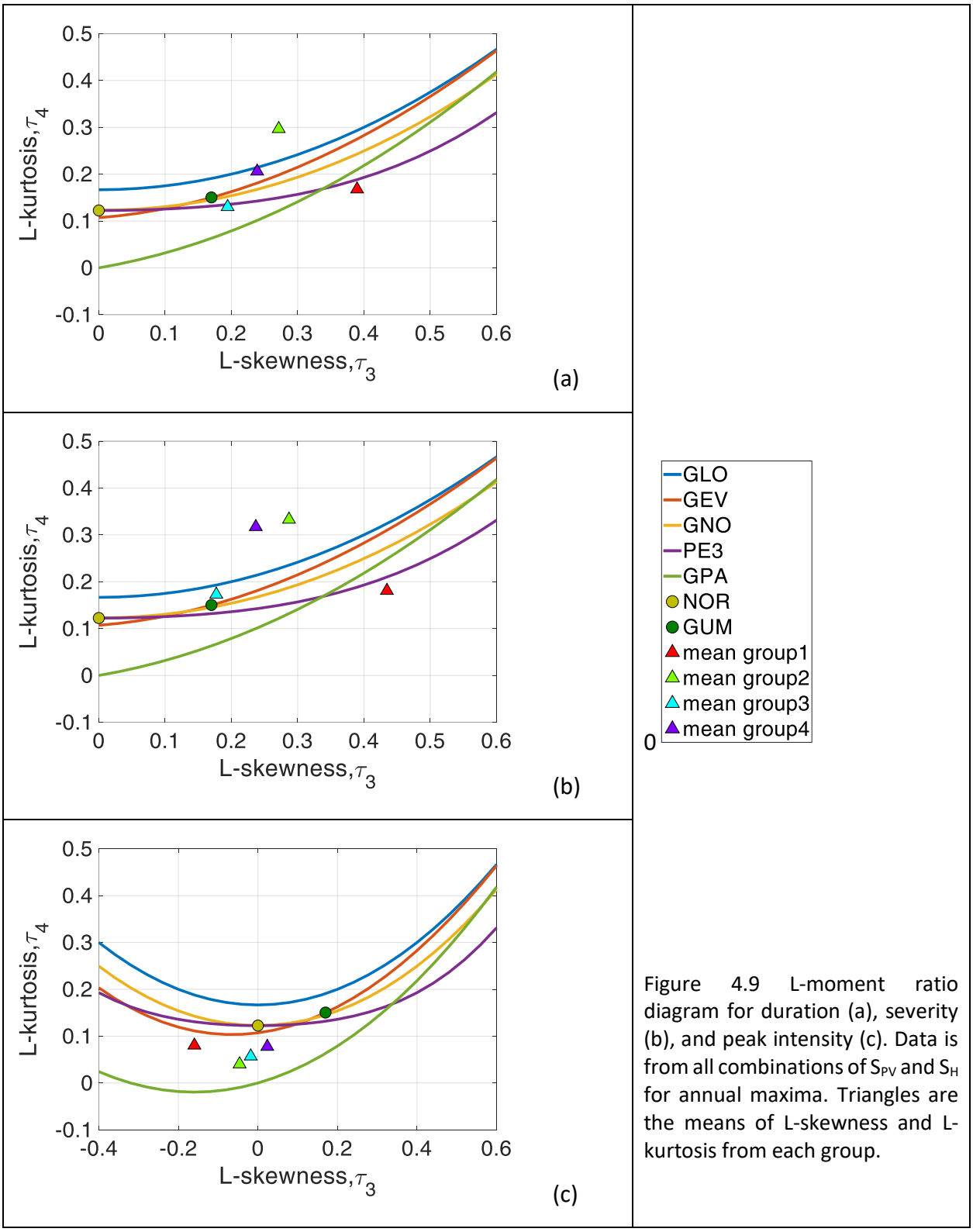

Figure 4.9 L-moment ratio diagram for duration (a), severity (b), and peak intensity (c). Data is from all combinations of S_{PV} and S_H for annual maxima. Triangles are the means of L-skewness and L-kurtosis from each group.

Return period	Duration (hours)	Peak intensity (scaled values)
10-year	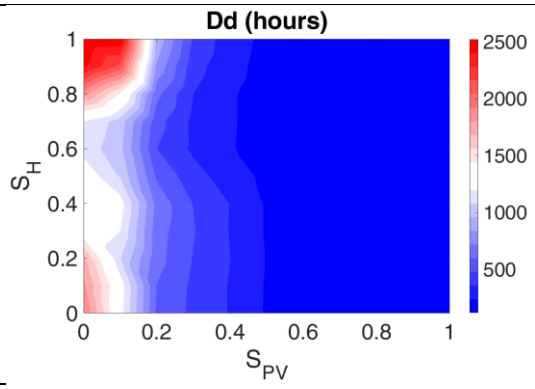	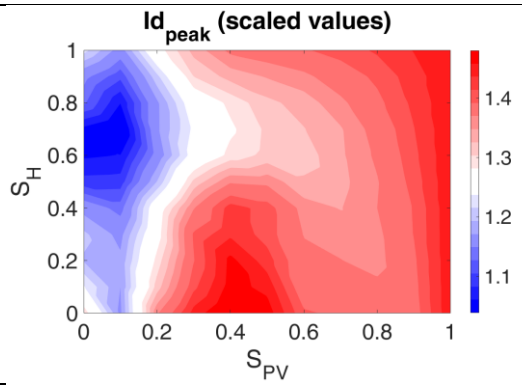
20-years	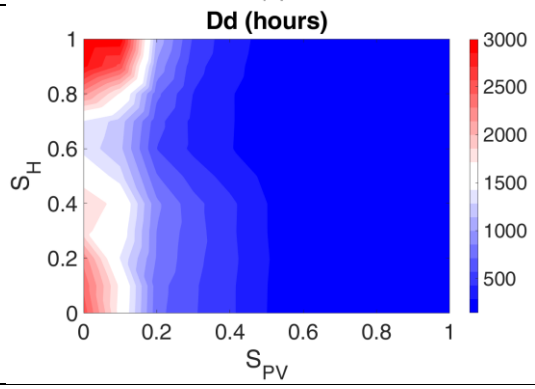	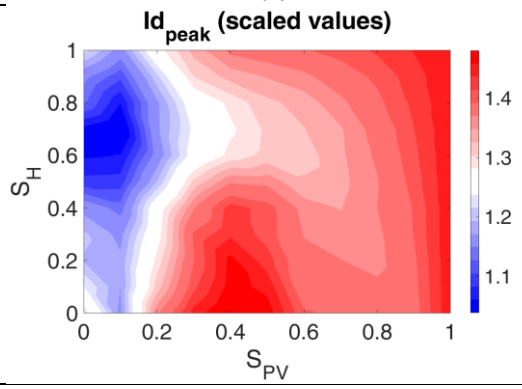

Figure 4.10 Return period of duration and peak intensity calculated by the quantile of chosen distribution from Figure 4.9

4.6 Conclusion

In this study we consider the statistical analysis of energy droughts from a 100% renewable energy supply in a geographical transect in Northern Italy, which includes solar PV and RoR as energy sources. Solar energy comes from the populated areas of the plain and is more evenly distributed through the year around the seasonal modulation. Hydropower is from run-of-the-river production on small rivers (less than 1000 km2) under two different hydrologic regimes (snow-dominated and rain-dominated). There are six principal observations from our work. In Alpine snow dominated catchments the spring snowmelt flood yields most of the power, while in plain to Piedmont catchments peaks of production are obtained in spring and autumn due to rainfall. For each hydrological regime, we assumed that the sum of the power generated at two locations is a good indicator for what could be the regional generation in terms of temporal organization. We analyzed six main energy drought properties: duration, severity, peak, mean intensity, interarrival time and number of events per year.

There are four main conclusions from the study. First, the main statistical properties (mean and CV) of energy drought duration and severity are very similar, as well as those of energy drought peak and mean intensity. This shows that the shape of the energy drought events is typically quite heterogeneous, whereas there is a good correlation between drought duration and mean intensity.

Second, the hydro-climatic characteristics of the transect and the temporal pattern of the radiation distribution strongly impact on the statistical characteristics of the energy droughts. Our result show that with increasing the share parameter $S_{PV\,i}$) the mean values of duration and severity decreases ii) the mean values of peak and of the mean intensity increases, iii) the number of events per year increases. On the other side, with increasing the share parameter $S_{PV,}$ the variability of the three main properties (duration, severity and peak) decreases. This is due mainly to the daily and seasonal systematic variability featured by solar radiation. The variation of the share parameter S_H imparts less important variations. Nevertheless, it is interesting to observe that the drought duration and severity is high for both S_H equals 0 or 1, whereas it is relatively

low for intermediate values, thereby showing the benefit of integrating these two energy sources.

Third, the pattern of the statistical properties remains considerable similar with moving from small to medium and to large energy drought events. Only the impact of the share parameter S_H become progressively less important, even though the duration and severity of snowmelt-controlled RoR always remain very high.

The last, Generalized Pareto distribution is a suitable distribution for the estimation of energy drought duration and severity quantiles, as expected based on hydrological drought assessment. If quantiles are desired for energy drought peak, however, the Generalized Pareto distribution shouldn't be considered. In this case, depending on the share values, the Generalized Normal and the Generalized Extreme values represent suitable distributions. Based on these findings, the assessment of duration-severity distributions appears to be straightforward, whereas more complex is the case of duration-peak or severity-peak distributions.

Chapter 5

Conclusion

Over the last years, Variable Renewable Energy sources (VREs) have become a cost competitive and environment-friendly alternative to supply power to isolated and large-scale power grids around the globe. Nevertheless, because of their intermittent (or variable, or stochastic, or non-dispatchable) characteristic, they cannot provide the grid with various additional and mandatory services for delivering a certain volume of energy. Combining several VREs according to the complementary principle is one main strategy to deal with the variability of VRE production in order to minimize energy shortfall. This thesis aims to identify the climatic control on the structure of the complementarity between different VREs, analyzing the balance between energy demand and energy generation along a geographical transect across the Italian Alps.

In mountainous areas, climate change is acknowledged to have significant impacts on the meteorological drivers (temperature, precipitation) and land cover (glacier) that would subsequently drive the change in local hydrology, leading to alteration of local hydropower generation capacity and temporal patterns. The first study in this Thesis investigates the impact of glacier shrinkage on the complementarity between solar energy and run of the river hydropower. Changes in glacier cover appeared to have significant impact on streamflow pattern for the high elevation catchments. The results show that consideration of warming in temperatures and neglecting the effects from glacier shrinkage is likely to lead to an incorrect representation of streamflow pattern, with a significant overestimation of streamflow during spring and summer seasons. This change of RoR production consequently affects the changes in demand satisfaction (or penetration rate) and complementarity between RoR and PV. The impact of glacier shrinkage on the energy mix from RoR and PV is stronger in the high elevation region and decrease with the increase of catchment size. Thus, disregarding the impact of glacier shrinkage, especially in the areas where glaciers strongly impact on local hydrology, causes the underestimation of future complementarity between solar energy and hydropower.

Given the characteristics of the transect, where biomasses represent a consolidated source of energy, a second study analyzes the benefit of combining electricity generation from biomasses through CHP plants, with electricity generation from RoR and PV production, in order to increase demand satisfaction. A particular focus is placed on the climatic control on the increase of penetration rate. We show that the increase of demand satisfaction in snow-dominated area is higher than in rain-dominated area, implying that areas that have lower complementarity between PV and RoR takes more benefits from the additional supply sources, such as CHP fueled by biomass. In the areas where runoff regime is dominated by rainfall, although CHP also increase the demand satisfaction, the reduction of electrical losses due to temporal mismatch is lower than in snow-dominated areas. In addition, the introduction of CHP tends to modify the optimal share of PV and RoR, specifically by replacing the contribution of RoR in the supply system.

The third study is focused on providing a more comprehensive analysis form of shortfall risk, which may be helpful if results are to inform practical power system policy and planning. The study focuses on the assessment of the statistical properties of energy droughts along the geographical transect. The hydro-climatic characteristics of the transect and the temporal pattern of the radiation distribution strongly impact on the statistical characteristics of the energy droughts. Our result show that with increasing the PV percentage in the PV-RoR energy mix, i) the mean values of duration and severity decreases ii) the mean values of peak and of the mean intensity increases, iii) the number of events per year increases. This is mainly due to the daily and seasonal systematic variability featured by solar radiation. Moreover, it is shown that the Generalized Logistic distribution is a suitable distribution for the estimation of energy drought duration and severity quantiles.

This work provides also a platform to identify suitable research objectives. We have found that even a modest climate change has a profound impact on the performance of an integrated 100% renewable energies power system in the Alps, generally by increasing the penetration rate and reducing shortfall. Climate change may therefore be viewed as both a risk and an opportunity for power system performance, depending on the estimation of damage and ability to adjust operations in relation to shortfall duration and magnitude. Yet to focus on probability of failure

alone may be too narrow criterion for power system planning; it is equally important to incorporate the potential damage caused by compound events, due to multiple interacting climate impacts. Moreover, future research should incorporate the effects of runoff disturbance due to hydropower operations on the aquatic environment and its ecosystem services, future changes in solar irradiance for estimating PV generation, and the use of electricity for heating, cooling, and mobility sectors.

Annex A

The ICHYMOD hydrological model and the snow-glacio routine TOPMELT

In the ICHYMOD model the hydrological processes within a catchment are modelled by four different routines, a snow–glacier routine, a soil moisture routine, a response routine, and, finally, a streamflow routing routine. The soil-moisture and propagation model has been already reported in the literature (Borga et al., 2006; Norbiato et al., 2009, 2008) and only a cursory description is reported here. The snow glacial routine (termed TOPMELT) is described with mode detail below.

The snow glacial routine - TOPMELT

The snow-glacier routine incorporates a new snowpack model (termed TOPMELT, Zaramella et al., 2018) which integrates an enhanced temperature index model into a semi-distributed basin scale hydrological model by exploiting a statistical representation of the distribution of clear sky potential solar radiation. In TOPMELT, the basin area is subdivided into elevation bands to account for air temperature variability with elevation. Then, each elevation band is subdivided into a number Nb of radiation classes. This is carried out by dividing each elevation band into a number Nc of equally distributed radiation classes. Therefore, the model spatial domain is represented by the Nb elevation bands and by the Nc radiation classes for each elevation band. Each one of the Nb*Nc model cells is characterised by a fraction of glacier area.

Snow accumulation is estimated by precipitation and temperature in each elevation band. Temperature in each band, itself, is calculated by the vertical temperature lapse rate. Solid and liquid precipitation is simulated by the use of temperature lapse rate and temperature threshold accordingly.

The model includes a routine, which accounts for the variability of clear sky radiation distributions with time, ensuring a consistent temporal simulation of the snow mass balance. The model allows to provide the representation of spatially continuous water equivalent maps (as well as any other model cell state variable) at a given time. This is carried by exploiting a routine which links each model cell to the corresponding topographic elements, accounting for variation

of the radiation index maps. Then, the water equivalent maps may be easily converted to snow cover maps by using suitable threshold values.

The spatial subdivisions in elevation bands and radiation cells controls the balance between computational efficiency and model accuracy in the snowpack model. Thus, the model resembles a classical temperature-index model when only one radiation class for each elevation band is used, whereas it approximates a fully distributed model with increasing the number of the radiation classes (and correspondingly decreasing the area corresponding to each class).

For the generic model cell represented by the *i-th* elevation band and the *j-th* radiation class, snow melt rate $F_{i,j}(t)$ [mm h^{-1}] at time *t,* is computed taking into account air temperature, clear sky radiation and albedo. During day hours, the snowmelt is given by:

$$F_{i,j}(t) = CMF \cdot RI_{i,j}(t) \cdot (1 - alb_i(t)) \cdot MAX[0, (T_i(t) - T_b)] \quad 1)$$

where: $T_i(t)$ is the elevation band temperature[°C]; $RI_{i,j}(t)$ [J $m^{-2}h^{-1}$] is the cell radiation power; CMF [mm°$C^{-1}J^{-1}m^2$] is the combined melt factor, accounting for both thermal and radiative effects; $alb_i(t)$ [-] is the albedo of snow, T_b [°C] is a threshold base temperature.
When the snow water equivalent $WE_{i,j}$ is less than a threshold (termed *WETH*), ice melt starts. This is computed similarly to snow (Eq. 1), but where the snow albedo is replaced by a constant glacial albedo, $albg$ [-], as follows:

$$F_{i,j}(t) = CMF \cdot RI_{i,j} \cdot (1 - albg) \cdot \mathrm{MAX}[0, T_i(t) - T_b] \quad 2)$$

The detailed description of the snowpack and ice model is reported in Zaramella et al. (2019). The representation of the transition from snow to firn, as well as the redistribution by wind and avalanches is based on the simplified approach described by Seibert et al. (2018).

TOPMELT incorporates a coupled glacio-hydrological model which allows the glacier extent to be linked directly to the simulated glacier mass balance. The coupling is based on the so-called Δh parameterization, which describes the glacier thickness change at a certain elevation in response to an overall change in ice mass (Huss et al., 2010). This approach requires limited glacier input data, is mass-conserving and well suited for hydrological modelling studies. In particular, TOPMELT incorporates the conceptual implementation of the Δh parameterization

described by Seibert et al. (2018) , which also allows the representation of glacier advance phases.

Potential evapotranspiration and soil moisture routine

Potential evapotranspiration is estimated by using the Hargreaves and Samani method (Hargreaves and Samani, 1982). The soil moisture routine uses a probability distribution model (PDM) to describe the spatial variation of water storage capacity across a basin. Saturation excess runoff generated at any point in the basin is integrated over the basin to give the total direct runoff entering the fast response pathways to the basin outlet. Drainage from the soil enters slow response pathways. Storage representations of the fast and slow response pathways yield a fast and slow response at the basin outlet which, when summed, gives the total basin flow. The PDM model configuration used here employs a Pareto distribution of storage capacity, c. The instantaneous rate of fast runoff generation from the basin is obtained by multiplying the rainfall rate by the proportion of the basin which is saturated.

Losses due to evaporation are calculated as a function of potential evaporation and the status of the soil moisture store. The dependence of evaporation loss on soil moisture content is introduced by assuming a simple function between the ratio of actual to potential evaporation, E/EP, and soil moisture deficit.

Runoff propagation routine

Drainage to the slow flow path is represented by a function of basin moisture storage. The slow or base flow component of the total runoff is assumed to be routed through an exponential store. Direct runoff from the proportion of the basin where storage capacity has been exceeded is routed by means of a geomorphology-based distributed unit hydrograph. With this procedure, a geomorphologic filter based on a threshold drainage area is used to distinguish hillslopes and channel network starting from the space-filling representation of the drainage system directly obtainable from DEMs (Da Ros and Borga, 1997a). The routing time of each site in the basin is evaluated assigning different typical velocity values in each pixel pertaining to the basin and classified as hillslope or channel. The two velocities used to describe the flow routing

process in each of the two components of the drainage system are assumed here constant; they maintain a physical meaning as the average velocities on hillslopes and in channel network. Total runoff is computed as the sum of slow and fast runoff.

ICHYMOD is available in two different versions, based on the time step used in the simulations (either hourly or daily). The hourly version of ICHYMOD, termed ICHYMOD-H has been calibrated and validated over the period 2000-2008 and 2008-2011, respectively, and NSE has been considered as goodness-to-fit criteria for the model performance analysis. Table A.1 shows NSE values for each catchment and for calibration and validation periods. Both Saldura and Plima show high NSE values during the calibration and validation periods.

Period	Saldura	Plima
Calibration (2000 – 2008)	0.75	0.79
Validation (2008 – 2011)	0.69	0.71

Table A.1 The result of ICHYMOD-H performance using NSE in the period of calibration and validation

Annex B

Results of Plima catchment

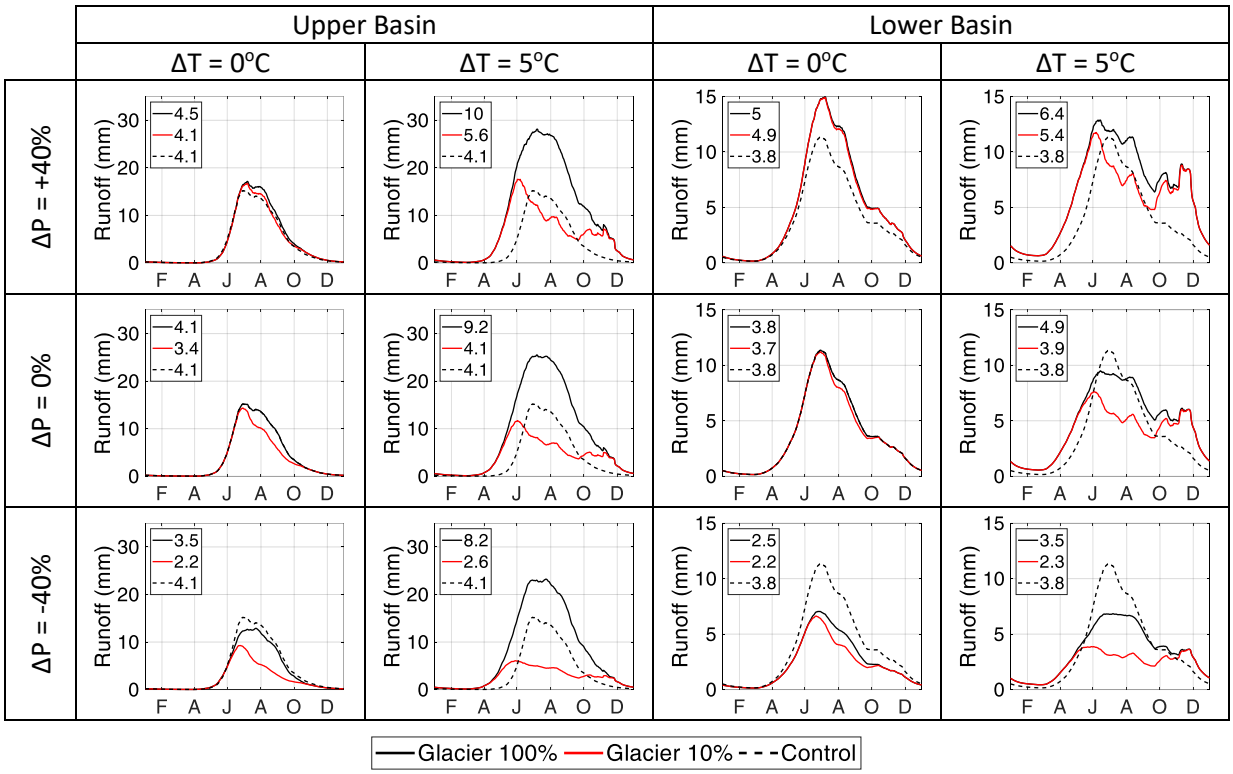

Figure B.1 Runoff seasonal cycle of Plima Upper Basin and Lower Basin in mm. Black dashed line is the control climate where there is no change in temperature and precipitation (ΔT=0°C and ΔP=0%). Black and red full line illustrate the cycle when glacier area is 100% and 10%, respectively. Values presented in the left-corner box are the mean daily values in mm in the different scenarios. Each cycle is smoothed over a 10-day window.

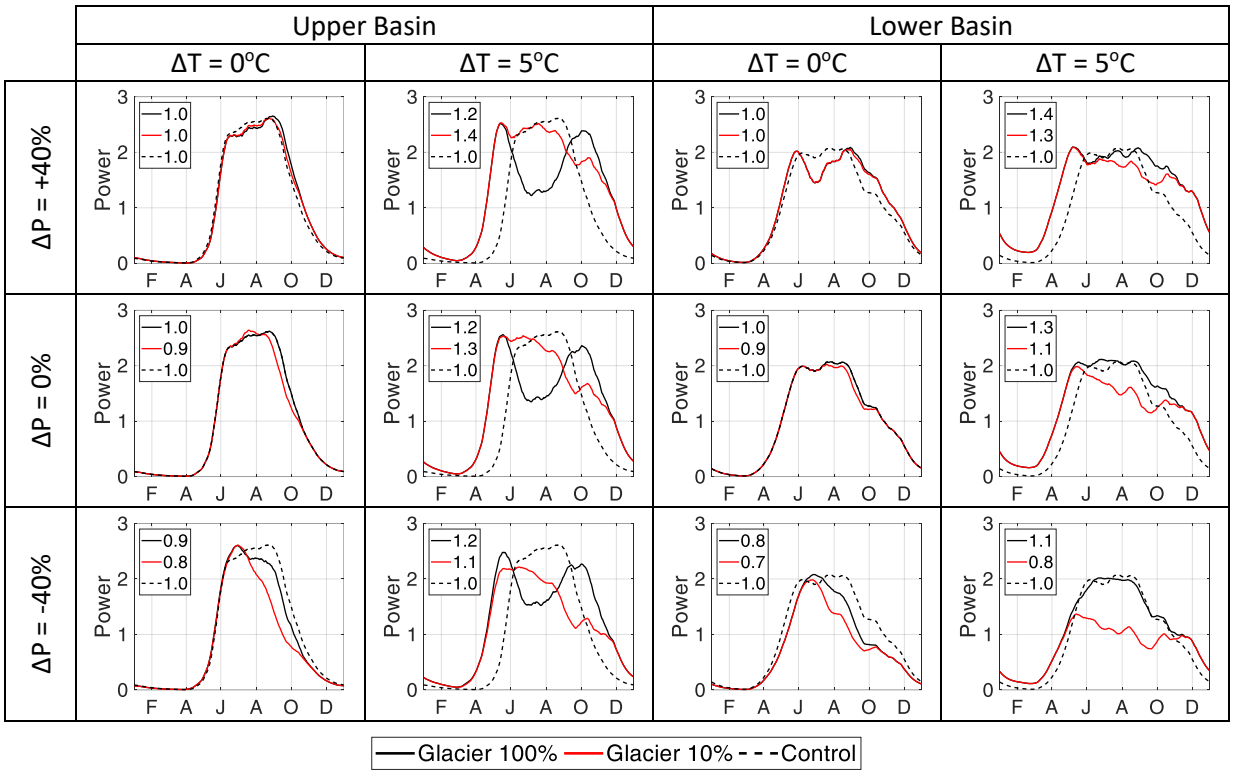

Figure B.2 Similar as Figure C.1, but for hydropower generation in Plima. Power time series are normalized regarding the average generation obtained for the control climate (i.e., no change in precipitation, temperature and glacier).

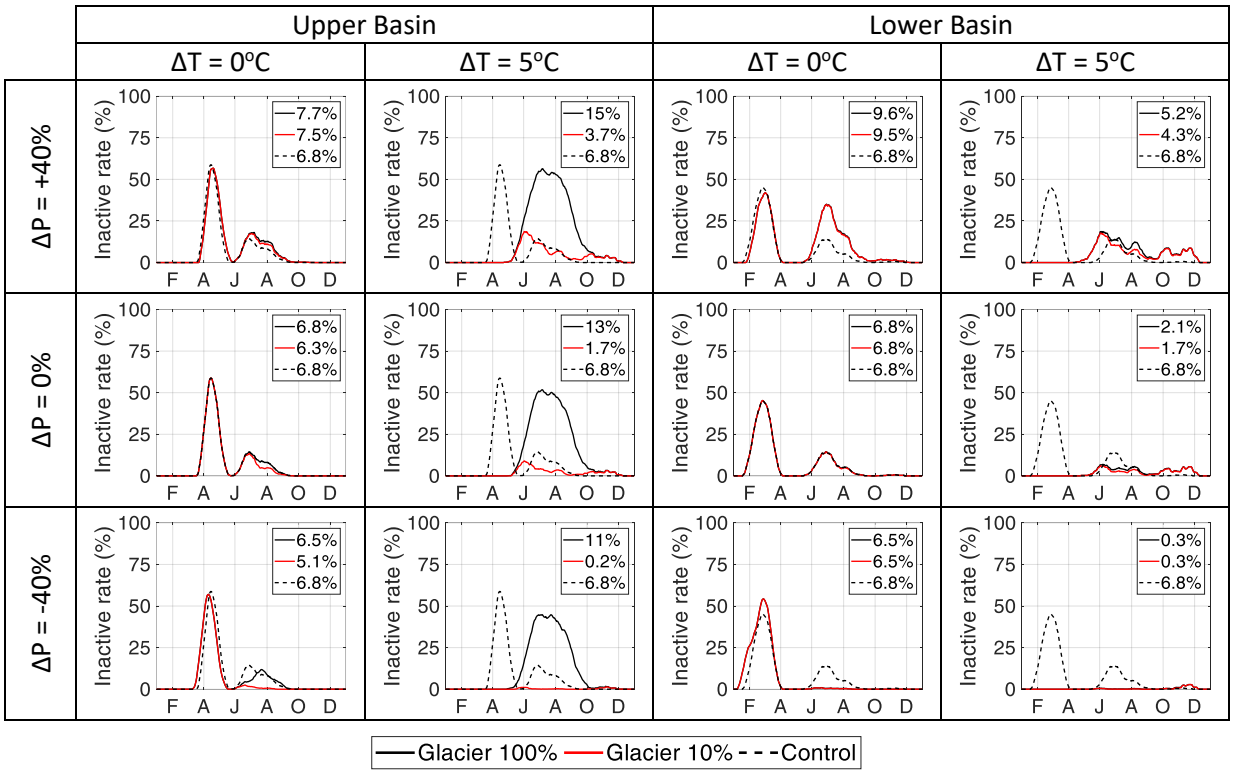

Figure B.2 Similar as Figure C.1, but for inactive rate in Plima. Each cycle is smoothed over a 10-day window.

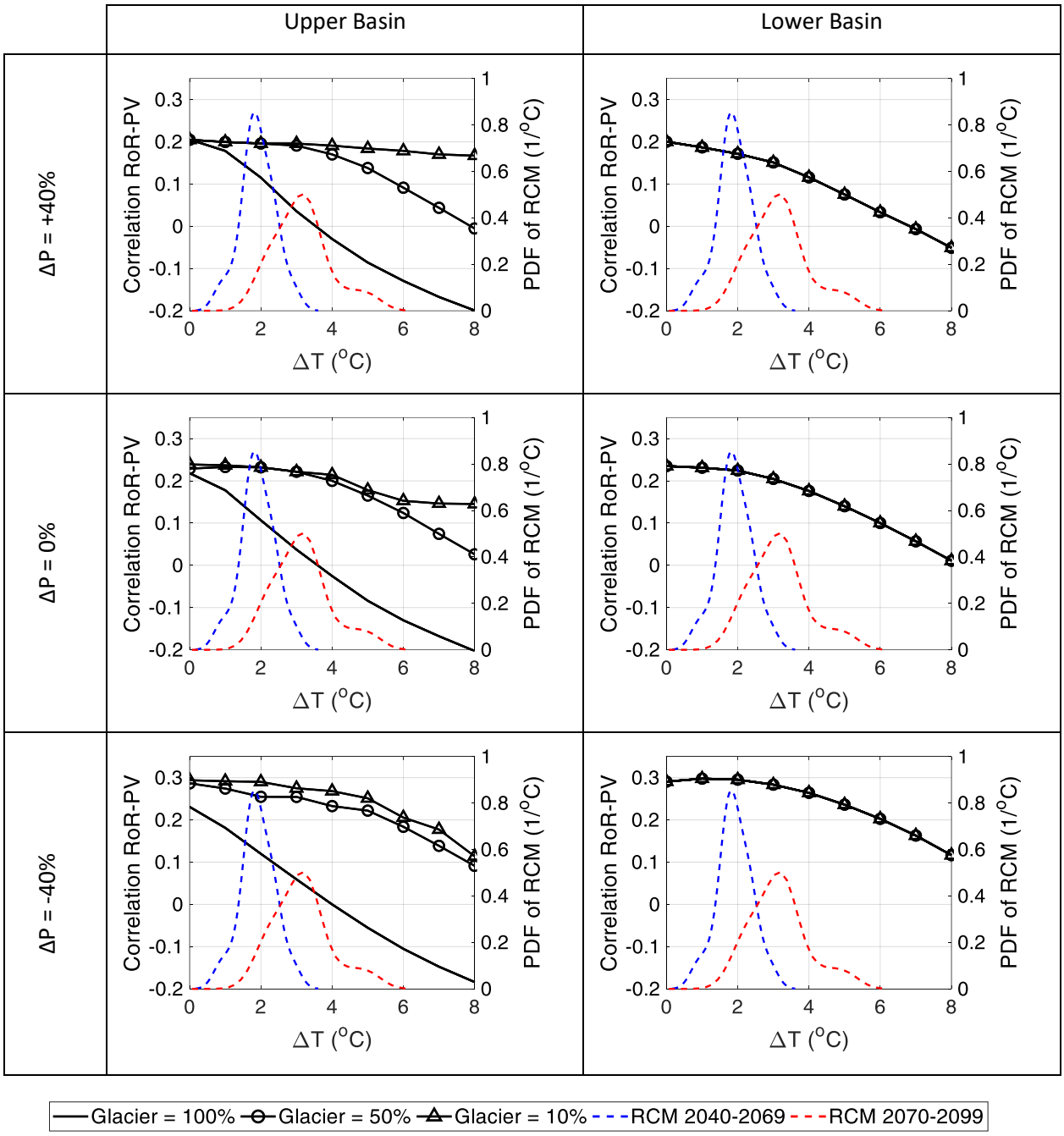

Figure B.3 Sensitivity of the correlation between RoR and PV to changes in precipitation (row), temperature (x-axis) and glacier cover (black curves). Right and left columns show the results obtained respectively for the Upper and Lower Plima basins. The kernel density smoothing of projected temperature changes obtained from 17 combinations of GCM/RCM are shown for the future periods 2040 – 2069 (blue) and 2070 – 2099 (red) with the values in right y-axis.

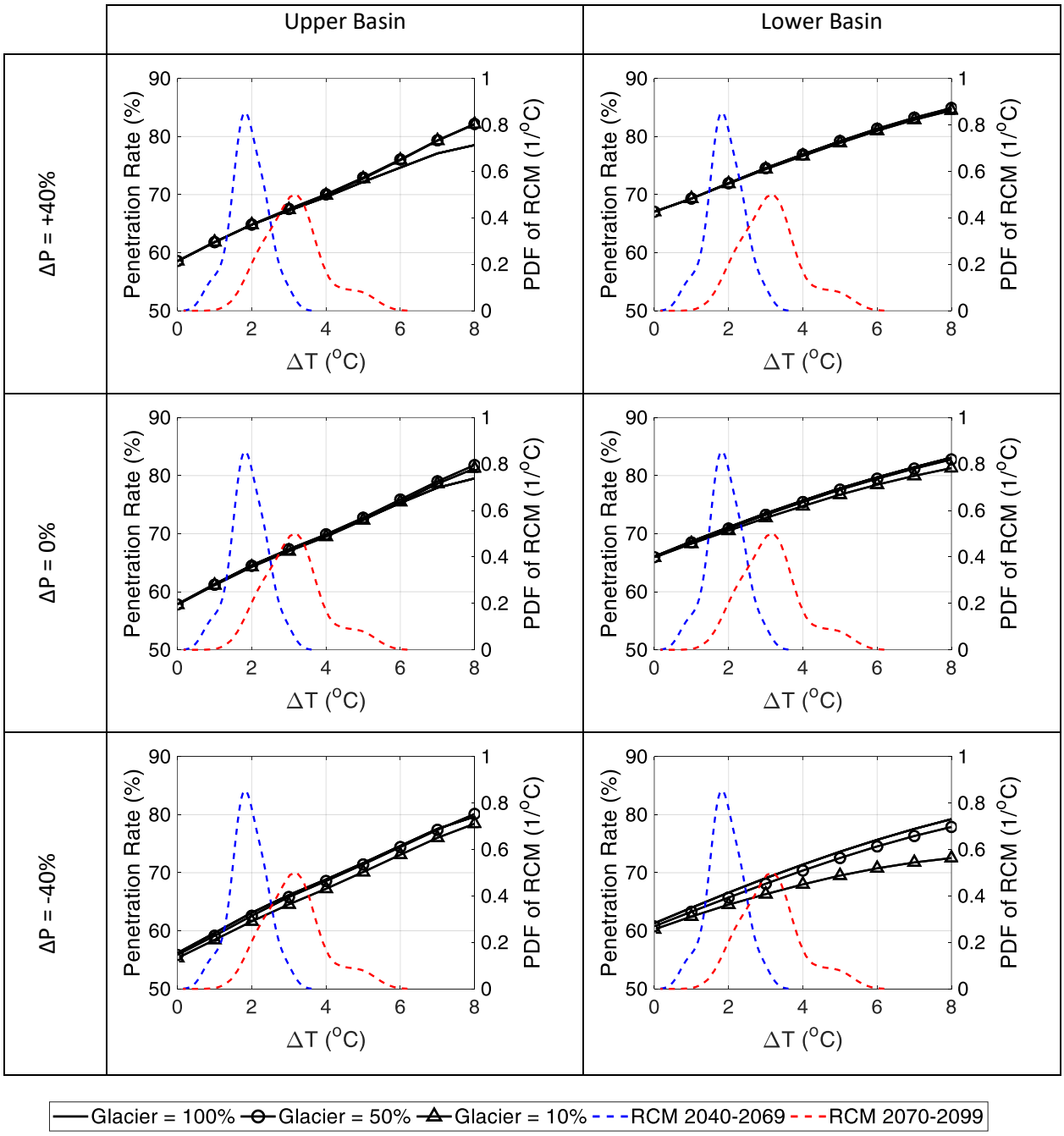

Figure B4. Same as Figure 8 but for the penetration rate metric.

References

Aguiar, F.C., Bentz, J., Silva, J.M.N., Fonseca, A.L., Swart, R., Santos, F.D., Penha-Lopes, G., 2018. Adaptation to climate change at local level in Europe: An overview. Environ. Sci. Policy 86, 38–63. https://doi.org/10.1016/J.ENVSCI.2018.04.010

Ahmad, M.I., Sinclair, C.D., Werritty, A., 1988. Log-logistic flood frequency analysis. J. Hydrol. 98, 205–224. https://doi.org/10.1016/0022-1694(88)90015-7

Albadi, M.H., El-Saadany, E.F., 2008. A summary of demand response in electricity markets. Electr. Power Syst. Res. 78, 1989–1996. https://doi.org/10.1016/J.EPSR.2008.04.002

Ashfaq, A., Kamali, Z.H., Agha, M.H., Arshid, H., 2017. Heat coupling of the pan-European vs. regional electrical grid with excess renewable energy. Energy 122, 363–377. https://doi.org/10.1016/j.energy.2017.01.084

Auffhammer, M., Baylis, P., Hausman, C.H., 2017. Climate change is projected to have severe impacts on the frequency and intensity of peak electricity demand across the United States. Proc. Natl. Acad. Sci. U. S. A. 114, 1886–1891. https://doi.org/10.1073/pnas.1613193114

Bagatini, M., Benevit, M.G., Beluco, A., Risso, A., 2017. Complementarity in Time between Hydro, Wind and Solar Energy Resources in the State of Rio Grande do Sul, in Southern Brazil. Energy Power Eng. 09, 515–526. https://doi.org/10.4236/epe.2017.99036

Barton, J.P., Infield, D.G., 2004. Energy Storage and Its Use With Intermittent Renewable Energy. IEEE Trans. Energy Convers. 19, 441–448. https://doi.org/10.1109/TEC.2003.822305

Bett, P.E., Thornton, H.E., 2016. The climatological relationships between wind and solar energy supply in Britain. Renew. Energy 87, 96–110. https://doi.org/10.1016/J.RENENE.2015.10.006

Biesbroek, G.R., Swart, R.J., Carter, T.R., Cowan, C., Henrichs, T., Mela, H., Morecroft, M.D., Rey, D., 2010. Europe adapts to climate change: Comparing National Adaptation Strategies. Glob. Environ. Chang. 20, 440–450. https://doi.org/10.1016/J.GLOENVCHA.2010.03.005

Blaabjerg, F., Guerrero, J.M., 2011. Smart grid and renewable energy systems, in: 2011 International Conference on Electrical Machines and Systems. IEEE, pp. 1–10. https://doi.org/10.1109/ICEMS.2011.6073290

Blaschke, T., Biberacher, M., Gadocha, S., Schardinger, I., 2013. 'Energy landscapes': Meeting energy demands and human aspirations. Biomass and Bioenergy 55, 3–16. https://doi.org/10.1016/j.biombioe.2012.11.022

Borga, M., Degli Esposti, S., Norbiato, D., 2006. Influence of errors in radar rainfall estimates on hydrological modeling prediction uncertainty. Water Resour. Res. 42. https://doi.org/10.1029/2005WR004559

Brown, C., Ghile, Y., Laverty, M., Li, K., 2012. Decision scaling: Linking bottom-up vulnerability analysis with climate projections in the water sector. Water Resour. Res. 48. https://doi.org/10.1029/2011WR011212

Burnett, D., Barbour, E., Harrison, G.P., 2014. The UK solar energy resource and the impact of climate change. Renew. Energy 71, 333–343. https://doi.org/10.1016/j.renene.2014.05.034

Çakir, U., Çomakli, K., Yüksel, F., 2012. The role of cogeneration systems in sustainability of energy. Energy Convers. Manag. 63, 196–202. https://doi.org/10.1016/j.enconman.2012.01.041

Chaudhary, P., Rizwan, M., 2018. Voltage regulation mitigation techniques in distribution system with high PV penetration: A review. Renew. Sustain. Energy Rev. 82, 3279–3287. https://doi.org/10.1016/J.RSER.2017.10.017

Christenson, M., Manz, H., Gyalistras, D., 2005. Climate warming impact on degree-days and building energy demand in Switzerland. https://doi.org/10.1016/j.enconman.2005.06.009

CODE2, 2015. European Cogeneration Roadmap.

Dirks, J.A., Gorrissen, W.J., Hathaway, J.H., Skorski, D.C., Scott, M.J., Pulsipher, T.C., Huang, M., Liu, Y., Rice, J.S., 2015. Impacts of climate change on energy consumption and peak demand in buildings: A detailed regional approach. Energy 79, 20–32. https://doi.org/10.1016/J.ENERGY.2014.08.081

Engeland, K., Borga, M., Creutin, J.-D., François, B., Ramos, M.-H., Vidal, J.-P., 2017. Space-time variability of climate variables and intermittent renewable electricity production – A review. Renew. Sustain. Energy Rev. 79, 600–617. https://doi.org/10.1016/j.rser.2017.05.046

European Commission, 2018. A Clean Planet for all A European strategic long-term vision for a prosperous, modern, competitive and climate neutral economy.

Ferreira, C., Gama, J., Matias, L., Botterud, A., Wang, J., 2010. A Survey on Wind Power Ramp Forecasting.

Finger, D., Heinrich, G., Gobiet, A., Bauder, A., 2012. Projections of future water resources and their uncertainty in a glacierized catchment in the Swiss Alps and the subsequent effects on hydropower production during the 21st century. Water Resour. Res. 48. https://doi.org/10.1029/2011WR010733

Fisher, S.M., Schoof, J.T., Lant, C.L., Therrell, M.D., 2013. The effects of geographical distribution on the reliability of wind energy. Appl. Geogr. 40, 83–89. https://doi.org/10.1016/J.APGEOG.2013.01.010

François, B., Borga, M., Anquetin, S., Creutin, J.D., Engeland, K., Favre, A.C., Hingray, B., Ramos, M.H., Raynaud, D., Renard, B., Sauquet, E., Sauterleute, J.F., Vidal, J.P., Warland, G., 2014a. Integrating hydropower and intermittent climate-related renewable energies: a call for

hydrology. Hydrol. Process. 28, 5465–5468. https://doi.org/10.1002/hyp.10274

François, B., Borga, M., Creutin, J.D., Hingray, B., Raynaud, D., Sauterleute, J.F., 2016a. Complementarity between solar and hydro power: Sensitivity study to climate characteristics in Northern-Italy. Renew. Energy 86, 543–553. https://doi.org/10.1016/j.renene.2015.08.044

François, B., Hingray, B., Borga, M., Zoccatelli, D., Brown, C., Creutin, J.-D., 2018. Impact of Climate Change on Combined Solar and Run-of-River Power in Northern Italy. Energies 11, 290. https://doi.org/10.3390/en11020290

François, B., Hingray, B., Hendrickx, F., Creutin, J.D., 2014b. Seasonal patterns of water storage as signatures of the climatological equilibrium between resource and demand. Hydrol. Earth Syst. Sci. 18, 3787–3800. https://doi.org/10.5194/hess-18-3787-2014

François, B., Hingray, B., Raynaud, D., Borga, M., Creutin, J.D., 2016b. Increasing climate-related-energy penetration by integrating run-of-the river hydropower to wind/solar mix. Renew. Energy 87, 686–696. https://doi.org/10.1016/j.renene.2015.10.064

François, B., Martino, S., Tøfte, L., Hingray, B., Mo, B., Creutin, J.-D., 2017a. Effects of Increased Wind Power Generation on Mid-Norway's Energy Balance under Climate Change: A Market Based Approach. Energies 10, 227. https://doi.org/10.3390/en10020227

François, B., Zoccatelli, D., Borga, M., 2017b. Assessing small hydro/solar power complementarity in ungauged mountainous areas: A crash test study for hydrological prediction methods. Energy. https://doi.org/10.1016/j.energy.2017.03.090

Frangopoulos, C.A., 2012. A method to determine the power to heat ratio, the cogenerated electricity and the primary energy savings of cogeneration systems after the European Directive. Energy 45, 52–61. https://doi.org/10.1016/J.ENERGY.2011.12.044

Gaudard, L., Avanzi, F., De Michele, C., 2018. Seasonal aspects of the energy-water nexus: The case of a run-of-the-river hydropower plant. Appl. Energy 210, 604–612. https://doi.org/10.1016/j.apenergy.2017.02.003

Gobiet, A., Kotlarski, S., Beniston, M., Heinrich, G., Rajczak, J., Stoffel, M., 2014. 21st century climate change in the European Alps—A review. Sci. Total Environ. 493, 1138–1151. https://doi.org/10.1016/j.scitotenv.2013.07.050

GSE, 2018. Rapporto Statistico Energia da Fonti Renovabili in Italia Anno 2016.

GSE, 2011. Statistical Report 2011.

Gu, W., Wang, J., Lu, S., Luo, Z., Wu, C., 2017. Optimal operation for integrated energy system considering thermal inertia of district heating network and buildings. Appl. Energy 199, 234–246. https://doi.org/10.1016/J.APENERGY.2017.05.004

Gvozdenac, D., Urošević, B.G., Menke, C., Urošević, D., Bangviwat, A., 2017. High efficiency cogeneration: CHP and non-CHP energy. Energy 135, 269–278. https://doi.org/10.1016/j.energy.2017.06.143

Handschy, M.A., Rose, S., Apt, J., 2017. Is it always windy somewhere? Occurrence of low-wind-power events over large areas. Renew. Energy 101, 1124–1130. https://doi.org/10.1016/J.RENENE.2016.10.004

Hänggi, P., Weingartner, R., 2012. Variations in Discharge Volumes for Hydropower Generation in Switzerland. Water Resour. Manag. 26, 1231–1252. https://doi.org/10.1007/s11269-011-9956-1

Hargreaves, G.., Samani, Z.., 1985. Reference Crop Evapotranspiration from Temperature. Appl. Eng. Agric. 1, 96–99. https://doi.org/10.13031/2013.26773

Hargreaves, G.., Samani, Z.., 1982. Estimating Potential Evapotranspiration. J. Irrig. Drain. Div. 108, 225–230.

Heide, D., Greiner, M., von Bremen, L., Hoffmann, C., 2011. Reduced storage and balancing needs in a fully renewable European power system with excess wind and solar power generation. Renew. Energy 36, 2515–2523. https://doi.org/10.1016/j.renene.2011.02.009

Heide, D., von Bremen, L., Greiner, M., Hoffmann, C., Speckmann, M., Bofinger, S., 2010. Seasonal optimal mix of wind and solar power in a future, highly renewable Europe. Renew. Energy 35, 2483–2489. https://doi.org/10.1016/j.renene.2010.03.012

Hekkenberg, M., Moll, H.C., Uiterkamp, A.J.M.S., 2009. Dynamic temperature dependence patterns in future energy demand models in the context of climate change. Energy 34, 1797–1806. https://doi.org/10.1016/j.energy.2009.07.037

Holmes, J.D., Moriarty, W.W., 1999. Application of the generalized Pareto distribution to extreme value analysis in wind engineering. J. Wind Eng. Ind. Aerodyn. 83, 1–10. https://doi.org/10.1016/S0167-6105(99)00056-2

Hosking, J.R.M., Wallis, J.R., 1997. Regional Frequency Analysis. Cambridge University Press, Cambridge. https://doi.org/10.1017/CBO9780511529443

Hosking, J.R.M., Wallis, J.R., 1987. Parameter and Quantile Estimation for the Generalized Pareto Distribution. Technometrics 29, 339–349. https://doi.org/10.1080/00401706.1987.10488243

Huertas-Hernando, D., Farahmand, H., Holttinen, H., Kiviluoma, J., Rinne, E., Söder, L., Milligan, M., Ibanez, E., Martínez, S.M., Gomez-Lazaro, E., Estanqueiro, A., Rodrigues, L., Carr, L., van Roon, S., Orths, A.G., Eriksen, P.B., Forcione, A., Menemenlis, N., 2017. Hydro power flexibility for power systems with variable renewable energy sources: an IEA Task 25 collaboration. Wiley Interdiscip. Rev. Energy Environ. 6, e220. https://doi.org/10.1002/wene.220

Huss, M., Jouvet, G., Farinotti, D., Bauder, A., 2010. Future high-mountain hydrology: a new parameterization of glacier retreat. Hydrol. Earth Syst. Sci. 14, 815–829. https://doi.org/10.5194/hess-14-815-2010

IEA, 2018a. CO2 emissions from fuel combustion: Highlights.

IEA, 2018b. Global Energy & CO2 Status Report.

IEA, 2018c. Renewables 2018: Analysis and forecast to 2023 (Executive summary).

IEA, 2016. World Energy Outlook 2016, World Energy Outlook. IEA, Paris. https://doi.org/10.1787/weo-2016-en

IEA, 2011. Harnessing Variable Renewables: A guide to the balancing challenge. International Renewable Energy Agency, France.

IPCC, 2018. Summary for Policymakers. In: Global warming of 1.5°C. An IPCC Special Report on the impacts of global warming of 1.5°C above pre-industrial levels and related global greenhouse gas emission pathways, in the context of strengthening the global response to. World Meteorological Organization, Geneva, Switzeralnd.

IPCC, 2014a. Climate Change 2014: Impacts, Adaptation, and Vulnerability. Part A: Global and Sectoral Aspects. Contribution of Working Group II to the Fifth Assessment Report of the Intergovernmental Panel on Climate Change, in: Field, C.B., Barros, V.R., Dokken, D.J., Mach, K.., Mastrandrea, M.., Bilir, T.., Chatterjee, M., Ebi, K.., Estrada, Y.., Genova, R.., Girma, B., Kissel, E.., Levy, A.., MacCracken, S., Mastrandrea, P.., White, L.. (Eds.), . Cambridge University Press, Cambridge, United Kingdom and New York, NY, USA.

IPCC, 2014b. Climate Change 2014: Mitigation of Climate Change. Contribution of Working Group III to the Fifth Assessment Report of the Intergovernmental Panel on Climate Change, in: Edenhofer, O., Pichs-Madruga, R., Sokona, Y., Farahani, E., Kadner, S., Seyboth, K., Adler, A., Baum, I., Brunner, S., Eickemeier, P., Kriemann, B., Savolainen, J., Schlömer, S., von Stechow, C., Zwickel, T., Minx, J.C. (Eds.), . Cambridge University Press, Cambridge, United Kingdom and New York, NY, USA.

Jakob Themeßl, M., Gobiet, A., Leuprecht, A., 2011. Empirical-statistical downscaling and error correction of daily precipitation from regional climate models. Int. J. Climatol. 31, 1530–1544. https://doi.org/10.1002/joc.2168

Jerez, Sonia, Tobin, Isabelle, Vautard, Robert, Montávez, J.P., López-Romero, J.M., Thais, F., Bartok, B., Christensen, O.B., Colette, A., Déqué, M., Nikulin, G., Kotlarski, Sven, van Meijgaard, E., Teichmann, C., Wild, Martin, Crook, J.A., Jones, L.A., Forster, P.M., Crook, R., Wild, M., Folini, D., Henschel, F., Fischer, N., Müller, B., Moss, R.H., Burnett, D., Barbour, E., Harrison, G.P., Panagea, I.S., Tsanis, I.K., Koutroulis, A.G., Grillakis, M.G., Wachsmuth, J., Tobin, I., Jacob, D., Pozo-Vázquez, D., Tovar-Pescador, J., Gámiz-Fortis, S.R., Esteban-Parra, M.J., Castro-Díez, Y., Jerez, S., Pašičko, R., Branković, Č., Šimić, Z., Patt, A., Pfenninger, S., Lilliestam, J., Jerez, S., Seneviratne, S.I., Luthi, D., Litschi, M., Schar, C., Zampieri, M., Jerez, S., Stegehuis, A., Gaetani, M., Soto, W. De, Klein, S.A., Beckman, W.A., Minemoto, T., Nagae, S., Takakura, H., Parretta, A., Sarno, A., Vicari, L.R., Wild, M., Schmucki, E., Allen, R.J., Norris, J.R., Wild, M., Vautard, R., Kotlarski, S., Wild, M., Wild, M., Hakuba, M.Z., Folini, D., Sanchez-Lorenzo, A., Wild, M., Lara-Fanego, V., Ruiz-Arias, J.A., Pozo-Vázquez, D., Santos-Alamillos, F.J., Tovar-Pescador, J., Radziemska, E., Mavromatakis, F., Tonui, J.K., Tripanagnostopoulos, Y., Chenni, R., Makhlouf, M., Kerbache, T., Bouzid, A., 2015. The

impact of climate change on photovoltaic power generation in Europe. Nat. Commun. 6, 10014. https://doi.org/10.1038/ncomms10014

Jurasz, J., Ciapała, B., 2017. Integrating photovoltaics into energy systems by using a run-off-river power plant with pondage to smooth energy exchange with the power gird. Appl. Energy 198, 21–35. https://doi.org/10.1016/j.apenergy.2017.04.042

Kahl, A., Dujardin, J., Lehning, M., 2019. The bright side of PV production in snow-covered mountains. Proc. Natl. Acad. Sci. U. S. A. 116, 1162–1167. https://doi.org/10.1073/pnas.1720808116

Kedia, D., Kedia, A., 2002. Energy Engineering Electrification of Remote Rural Communities in the Himalayas Through Solar-hydro Hybrid Power Projects Electrification of Remote Rural Communities in the Himalayas Through Solar-hydro Hybrid Power Projects. https://doi.org/10.1080/01998590209508899

Knoll, C., Kerschner, H., 2009. A glacier inventory for South Tyrol, Italy, based on airborne laser-scanner data. Ann. Glaciol. 50, 46–52. https://doi.org/10.3189/172756410790595903

Köhler, C., Steiner, A., Saint-Drenan, Y.-M., Ernst, D., Bergmann-Dick, A., Zirkelbach, M., Ben Bouallègue, Z., Metzinger, I., Ritter, B., 2017. Critical weather situations for renewable energies – Part B: Low stratus risk for solar power. Renew. Energy 101, 794–803. https://doi.org/10.1016/j.renene.2016.09.002

Kougias, I., Szabó, S., Monforti-Ferrario, F., Huld, T., Bódis, K., 2016. A methodology for optimization of the complementarity between small-hydropower plants and solar PV systems. Renew. Energy 87, 1023–1030. https://doi.org/10.1016/J.RENENE.2015.09.073

Laiti, L., Mallucci, S., Piccolroaz, S., Bellin, A., Zardi, D., Fiori, A., Nikulin, G., Majone, B., 2018. Testing the Hydrological Coherence of High-Resolution Gridded Precipitation and Temperature Data Sets. Water Resour. Res. 54, 1999–2016. https://doi.org/10.1002/2017WR021633

Leahy, P.G., McKeogh, E.J., 2013. Persistence of low wind speed conditions and implications for wind power variability. Wind Energy 16, 575–586. https://doi.org/10.1002/we.1509

Lin, B., Ouyang, X., 2014. Energy demand in China: Comparison of characteristics between the US and China in rapid urbanization stage. Energy Convers. Manag. 79, 128–139. https://doi.org/10.1016/j.enconman.2013.12.016

Lindelöf, D., 2017. Bayesian estimation of a building's base temperature for the calculation of heating degree-days. Energy Build. 134, 154–161. https://doi.org/10.1016/J.ENBUILD.2016.10.038

Lundström, L., Wallin, F., 2016. Heat demand profiles of energy conservation measures in buildings and their impact on a district heating system. Appl. Energy 161, 290–299. https://doi.org/10.1016/J.APENERGY.2015.10.024

Maran, S., Volonterio, M., Gaudard, L., 2014. Climate change impacts on hydropower in an

alpine catchment. Environ. Sci. Policy 43, 15–25. https://doi.org/10.1016/j.envsci.2013.12.001

Martins, E.S., Stedinger, J.R., 2000. Generalized maximum-likelihood generalized extreme-value quantile estimators for hydrologic data. Water Resour. Res. 36, 737–744. https://doi.org/10.1029/1999WR900330

Miara, A., Macknick, J.E., Vörösmarty, C.J., Tidwell, V.C., Newmark, R., Fekete, B., 2017. Climate and water resource change impacts and adaptation potential for US power supply. Nat. Clim. Chang. 7, 793–798. https://doi.org/10.1038/nclimate3417

Ming, B., Liu, P., Cheng, L., Zhou, Y., Wang, X., 2018. Optimal daily generation scheduling of large hydro–photovoltaic hybrid power plants. Energy Convers. Manag. 171, 528–540. https://doi.org/10.1016/J.ENCONMAN.2018.06.001

Monforti, F., Huld, T., Bódis, K., Vitali, L., D'Isidoro, M., Lacal-Arántegui, R., 2014. Assessing complementarity of wind and solar resources for energy production in Italy. A Monte Carlo approach. Renew. Energy 63, 576–586. https://doi.org/10.1016/j.renene.2013.10.028

Moore, R.J., 2007. The PDM rainfall-runoff model. Hydrol. Earth Syst. Sci. 11, 483–499. https://doi.org/10.5194/hess-11-483-2007

Moriarty, P., Honnery, D., 2016. Can renewable energy power the future? Energy Policy 93, 3–7. https://doi.org/10.1016/j.enpol.2016.02.051

Moriarty, P., Honnery, D., 2012. What is the global potential for renewable energy? Renew. Sustain. Energy Rev. 16, 244–252. https://doi.org/10.1016/j.rser.2011.07.151

Moser, D., Vettorato, D., Vaccaro, R., Del Buono, M., Sparber, W., 2014. The PV Potential of South Tyrol: An Intelligent Use of Space. Energy Procedia 57, 1392–1400. https://doi.org/10.1016/j.egypro.2014.10.130

Nash, J.E., Sutcliffe, J.V., 1970. River flow forecasting through conceptual models part I — A discussion of principles. J. Hydrol. 10, 282–290. https://doi.org/10.1016/0022-1694(70)90255-6

Nawri, N., Petersen, G.N., Bjornsson, H., Hahmann, A.N., Jónasson, K., Hasager, C.B., Clausen, N.-E., 2014. The wind energy potential of Iceland. Renew. Energy 69, 290–299. https://doi.org/10.1016/j.renene.2014.03.040

Norbiato, D., Borga, M., Degli Esposti, S., Gaume, E., Anquetin, S., 2008. Flash flood warning based on rainfall thresholds and soil moisture conditions: An assessment for gauged and ungauged basins. J. Hydrol. 362, 274–290. https://doi.org/10.1016/j.jhydrol.2008.08.023

Norbiato, D., Borga, M., Merz, R., Blöschl, G., Carton, A., 2009. Controls on event runoff coefficients in the eastern Italian Alps. J. Hydrol. 375, 312–325. https://doi.org/10.1016/j.jhydrol.2009.06.044

Orlanski, I., 1975. A rational subdivision of scales for atmospheric processes. Bull. Am. Meteorol. Soc. 56, 527–530.

Palensky, P., Kupzog, F., 2013. Smart Grids. Annu. Rev. Environ. Resour. 38, 201–226. https://doi.org/10.1146/annurev-environ-031312-102947

Patro, E.R., De Michele, C., Avanzi, F., 2018. Future perspectives of run-of-the-river hydropower and the impact of glaciers' shrinkage: The case of Italian Alps. Appl. Energy 231, 699–713. https://doi.org/10.1016/J.APENERGY.2018.09.063

Patuzzi, F., Prando, D., Vakalis, S., Rizzo, A.M., Chiaramonti, D., Tirler, W., Mimmo, T., Gasparella, A., Baratieri, M., 2016. Small-scale biomass gasification CHP systems: Comparative performance assessment and monitoring experiences in South Tyrol (Italy). Energy 112, 285–293. https://doi.org/10.1016/j.energy.2016.06.077

Pelland, S., Remund, J., Kleissl, J., Oozeki, T., De Brabandere, K., 2013. Photovoltaic and Solar Forecasting [WWW Document]. URL http://www.iea-pvps.org/index.php?id=278 (accessed 9.28.19).

Pellicciotti, F., Carenzo, M., Bordoy, R., Stoffel, M., 2014. Changes in glaciers in the Swiss Alps and impact on basin hydrology: Current state of the art and future research. Sci. Total Environ. 493, 1152–1170. https://doi.org/10.1016/j.scitotenv.2014.04.022

Perpiñan, O., Lorenzo, E., Castro, M.A., 2007. On the calculation of energy produced by a PV grid-connected system. Prog. Photovoltaics Res. Appl. 15, 265–274. https://doi.org/10.1002/pip.728

Piria, R., Junge, J., 2013. Norway's Key Role in the European Energy Transition.

Prina, M.G., Cozzini, M., Garegnani, G., Manzolini, G., Moser, D., Filippi Oberegger, U., Pernetti, R., Vaccaro, R., Sparber, W., 2018. Multi-objective optimization algorithm coupled to EnergyPLAN software: The EPLANopt model. Energy 149, 213–221. https://doi.org/10.1016/j.energy.2018.02.050

Raj, N.T., Iniyan, S., Goic, R., 2011. A review of renewable energy based cogeneration technologies. Renew. Sustain. Energy Rev. 15, 3640–3648. https://doi.org/10.1016/j.rser.2011.06.003

Rashid, M.H., Putrus, G., Bentley, E., 2016. Integration of distributed renewable energy systems into the smart grid. Electr. Renew. Energy Syst. 487–518. https://doi.org/10.1016/B978-0-12-804448-3.00020-7

Rasul, G., Sharma, B., 2016. The nexus approach to water–energy–food security: an option for adaptation to climate change. Clim. Policy 16, 682–702. https://doi.org/10.1080/14693062.2015.1029865

Raynaud, D., Hingray, B., François, B., Creutin, J.D., 2018. Energy droughts from variable renewable energy sources in European climates. Renew. Energy 125, 578–589. https://doi.org/10.1016/J.RENENE.2018.02.130

Renné, D.S., 2014. Emerging Meteorological Requirements to Support High Penetrations of Variable Renewable Energy Sources: Solar Energy, in: Weather Matters for Energy.

Springer New York, New York, NY, pp. 257–273. https://doi.org/10.1007/978-1-4614-9221-4_12

Rieger, D., Steiner, A., Bachmann, V., Gasch, P., Förstner, J., Deetz, K., Vogel, B., Vogel, H., 2017. Impact of the 4 April 2014 Saharan dust outbreak on the photovoltaic power generation in Germany. Atmos. Chem. Phys. 17, 13391–13415. https://doi.org/10.5194/acp-17-13391-2017

Romanchenko, D., Kensby, J., Odenberger, M., Johnsson, F., 2018. Thermal energy storage in district heating: Centralised storage vs. storage in thermal inertia of buildings. Energy Convers. Manag. 162, 26–38. https://doi.org/10.1016/J.ENCONMAN.2018.01.068

Romero Rodríguez, L., Salmerón Lissén, J.M., Sánchez Ramos, J., Rodríguez Jara, E.Á., Álvarez Domínguez, S., 2016. Analysis of the economic feasibility and reduction of a building's energy consumption and emissions when integrating hybrid solar thermal/PV/micro-CHP systems. Appl. Energy 165, 828–838. https://doi.org/10.1016/J.APENERGY.2015.12.080

Ruosteenoja, K., Räisänen, P., 2013. Seasonal Changes in Solar Radiation and Relative Humidity in Europe in Response to Global Warming*. J. Clim. 26, 2467–2481. https://doi.org/10.1175/JCLI-D-12-00007.1

Schaefli, B., 2015. Projecting hydropower production under future climates: a guide for decision-makers and modelers to interpret and design climate change impact assessments. Wiley Interdiscip. Rev. Water 2, 271–289. https://doi.org/10.1002/wat2.1083

Schaefli, B., Hingray, B., Musy, A., 2007. Climate change and hydropower production in the Swiss Alps: quantification of potential impacts and related modelling uncertainties. Hydrol. Earth Syst. Sci. 11, 1191–1205. https://doi.org/10.5194/hess-11-1191-2007

Schaefli, B., Manso, P., Fischer, M., Huss, M., Farinotti, D., 2019. The role of glacier retreat for Swiss hydropower production. Renew. Energy. https://doi.org/10.1016/j.renene.2018.07.104

Scott, C.A., 2011. The water-energy-climate nexus: Resources and policy outlook for aquifers in Mexico. Water Resour. Res. 47. https://doi.org/10.1029/2011WR010805

Scott, C.A., Pierce, S.A., Pasqualetti, M.J., Jones, A.L., Montz, B.E., Hoover, J.H., 2011. Policy and institutional dimensions of the water–energy nexus. Energy Policy 39, 6622–6630. https://doi.org/10.1016/j.enpol.2011.08.013

Seibert, J., Vis, M.J.P., Kohn, I., Weiler, M., Stahl, K., 2018. Technical note: Representing glacier geometry changes in a semi-distributed hydrological model. Hydrol. Earth Syst. Sci. 22, 2211–2224. https://doi.org/10.5194/hess-22-2211-2018

Shen, P., 2017. Impacts of climate change on U.S. building energy use by using downscaled hourly future weather data. Energy Build. 134, 61–70. https://doi.org/10.1016/J.ENBUILD.2016.09.028

Siano, P., 2014. Demand response and smart grids—A survey. Renew. Sustain. Energy Rev. 30,

461–478. https://doi.org/10.1016/j.rser.2013.10.022

Silvestro, F., Parodi, A., Campo, L., Ferraris, L., 2018. Analysis of the streamflow extremes and long-term water balance in the Liguria region of Italy using a cloud-permitting grid spacing reanalysis dataset. Hydrol. Earth Syst. Sci. 22, 5403–5426. https://doi.org/10.5194/hess-22-5403-2018

Singh, V.P., Guo, H., 1995. Parameter estimation for 3-parameter generalized pareto distribution by the principle of maximum entropy (POME). Hydrol. Sci. J. 40, 165–181. https://doi.org/10.1080/02626669509491402

Söder, L., Lund, P.D., Koduvere, H., Bolkesjø, T.F., Rossebø, G.H., Rosenlund-Soysal, E., Skytte, K., Katz, J., Blumberga, D., 2018. A review of demand side flexibility potential in Northern Europe. Renew. Sustain. Energy Rev. 91, 654–664. https://doi.org/10.1016/j.rser.2018.03.104

Staffell, I., Pfenninger, S., 2018. The increasing impact of weather on electricity supply and demand. Energy 145, 65–78. https://doi.org/10.1016/J.ENERGY.2017.12.051

Stainforth, D.A., Downing, T.E., Washington, R., Lopez, A., New, M., 2007. Issues in the interpretation of climate model ensembles to inform decisions. Philos. Trans. A. Math. Phys. Eng. Sci. 365, 2163–77. https://doi.org/10.1098/rsta.2007.2073

Themeßl, M.J., Gobiet, A., Heinrich, G., 2012. Empirical-statistical downscaling and error correction of regional climate models and its impact on the climate change signal. Clim. Change 112, 449–468. https://doi.org/10.1007/s10584-011-0224-4

Tobin, I., Jerez, S., Vautard, R., Thais, F., van Meijgaard, E., Prein, A., Déqué, M., Kotlarski, S., Maule, C.F., Nikulin, G., Noël, T., Teichmann, C., 2016. Climate change impacts on the power generation potential of a European mid-century wind farms scenario. Environ. Res. Lett. 11, 034013. https://doi.org/10.1088/1748-9326/11/3/034013

Troccoli, A., Dubus, L., Haupt, S.E. (Eds.), 2014. Weather Matters for Energy. Springer New York, New York, NY. https://doi.org/10.1007/978-1-4614-9221-4

Turner, S.W.D., Voisin, N., Fazio, J., Hua, D., Jourabchi, M., 2019. Compound climate events transform electrical power shortfall risk in the Pacific Northwest. Nat. Commun. 10, 8. https://doi.org/10.1038/s41467-018-07894-4

Ueckerdt, F., Pietzcker, R., Scholz, Y., Stetter, D., Giannousakis, A., Luderer, G., 2017. Decarbonizing global power supply under region-specific consideration of challenges and options of integrating variable renewables in the REMIND model. Energy Econ. 64, 665–684. https://doi.org/10.1016/j.eneco.2016.05.012

United Nations, 2015. Adoption of Paris Agreement. Paris.

Urry, J., 2015. Climate Change and Society, in: Why the Social Sciences Matter. Palgrave Macmillan UK, London, pp. 45–59. https://doi.org/10.1057/9781137269928_4

van der Linden, P., Mitchell, J.F.B., 2009. ENSEMBLES: Climate Change and its Impacts:

Summary of research and results from the ENSEMBLES project. Met Office Hadley Centre, FitzRoy Road, Exeter EX1 3PB, UK.

Vicuna, S., Leonardson, R., Hanemann, M.W., Dale, L.L., Dracup, J.A., 2008. Climate change impacts on high elevation hydropower generation in California's Sierra Nevada: a case study in the Upper American River. Clim. Change 87, 123–137. https://doi.org/10.1007/s10584-007-9365-x

Virasjoki, V., Siddiqui, A.S., Zakeri, B., Salo, A., 2018. Market Power With Combined Heat and Power Production in the Nordic Energy System. IEEE Trans. Power Syst. 33, 5263–5275. https://doi.org/10.1109/TPWRS.2018.2811959

von Bremen, L., 2010. Large-Scale Variability of Weather Dependent Renewable Energy Sources. Springer, Dordrecht, pp. 189–206. https://doi.org/10.1007/978-90-481-3692-6_13

Wang, H., Chen, Q., 2014. Impact of climate change heating and cooling energy use in buildings in the United States. Energy Build. 82, 428–436. https://doi.org/10.1016/j.enbuild.2014.07.034

Wang, H., Yin, W., Abdollahi, E., Lahdelma, R., Jiao, W., 2015. Modelling and optimization of CHP based district heating system with renewable energy production and energy storage. Appl. Energy 159, 401–421. https://doi.org/10.1016/j.apenergy.2015.09.020

Wood, A.J., Wollenberg, B.F., Sheblé, G.B., 1984. Power generation, operation, and control.

Zaramella, M., Borga, M., Zoccatelli, D., Carturan, L., 2018. TOPMELT 1.0: A topography-based distribution function approach to snowmelt simulation for hydrological modelling at basin scale. Geosci. Model Dev. Discuss. 1–18. https://doi.org/10.5194/gmd-2018-202

List of Publication

List of scientific papers

Puspitarini, H.D., François, B. Zaramella, M., Brown, C., Borga, M. 2019. The impact of glacier shrinkage on energy production from hydropower-solar complementarity in alpine river basins. Science of Total Environment. Conditionally accepted.

Puspitarini, H.D., François, B. Zaramella, M., Baratieri, M., Brown, C., Borga, M. 2019. Complementary between Combined Heat and Power systems, solar PV, and hydropower at a district level: Application to the North Eastern Alps. Manuscript in preparation

Puspitarini, H.D., François, B., Borga, M. 2019. Statistical analysis of energy supply droughts from renewable energy sources across an Alpine transect. Manuscript in preparation

Perez-Ciria, T., **Puspitarini, H.D.**, François, B., Borga, M., et al. 2019. M Multi-temporal scale analysis of complementarity between hydro and solar power along an alpine transect. Manuscript in preparation.

Mondino, E., Barendrecht, M., **Puspitarini, H.D.**, Ghoreishi, M., Zhou, H., Wei, J., Tian, F., et al. 2019. Socio-Hydrological Modelling of Cooperation and Conflicts in the Transboundary River Nile. Manuscript in preparation

List of abstracts

Puspitarini, H.D., François, Borga, M. (2019). Intensity-duration-frequency analysis of energy supply droughts from renewable energy sources across an Alpine transect. To be presented in AGU 2019, San Francisco, USA.

Zuecco, G., Penna, D., Marchina, C., Amin, A., Gelmini, Y, **Puspitarini, H.D.**, Borga, M. 2019. Understanding hydrological processes in small Alpine and pre-Alpine catchments: the case of Rio Vauz and Ressi, Northern Italy. To be presented in AGU 2019, San Francisco, USA.

Mondino, E., Barendrecht, M., **Puspitarini, H.D.**, Ghoreishi, M., Zhou, H., Wei, J., Tian, F. 2019. Socio-Hydrological Modelling of Cooperation and Conflicts in the Transboundary River Nile. To be presented in AGU 2019, San Francisco, USA.

Puspitarini, H. D., François, B., Zaramella, M., Brown, C., Borga, M. 2019. Complementarity between Combined Heat and Power systems, solar PV, and hydropower at a district level: Application to the North Eastern Alps. Abstract EGU2019-10466, Vol. 21. Presented at EGU 2019, Vienna, Austria

Puspitarini, H. D., Zoccatelli, D., Creutin, J.D., Zaramella, M., Borga, M. 2018. Water-Energy-Climate Nexus: Does glacier shrinkage matter? Abstract EGU2018-1171. Presented at EGU 2018, Vienna, Austria

Puspitarini, H. D., François, B., Zoccatelli, D., Brown, C., Creutin, J.D., Zaramella, M., Borga, M. 2017. Assessing climate change impact on complementarity between solar and hydro power in areas affected by glacier shrinkage. Abstract EGU2017-13511-2, Vol. 2. Presented at EGU 2017, Vienna, Austria.